APPROVED FOR PUBLIC RELEASE; DISTRIBUTION UNLIMITED

AFTAC Project No. VT/1705

EVALUATION OF DETECTION AND DISCRIMINATION CAPABILITY OF THE ALASKAN LONG PERIOD ARRAY

AD 745197

SPECIAL REPORT NO. 4
EXTENDED ARRAY EVALUATION PROGRAM

Prepared by
Leo N. Heiting, Gary D. McNeely, and Alan C. Strauss

T. W. Harley, Program Manager
Area Code,703, 836-3882 Ext. 300

TEXAS INSTRUMENTS INCORPORATED
Services Group
P.O. Box 5621
Dallas, Texas 75222

Contract No. F33657-71-C-0843
Amount of Contract: $511,580
Beginning 1 April 1971
Ending 31 March 1972

Prepared for

AIR FORCE TECHNICAL APPLICATIONS CENTER
Alexandria, VA 22313

Sponsored by

ADVANCED RESEARCH PROJECTS AGENCY
Nuclear Monitoring Research Office
ARPA Order No. 1714
ARPA Program Code No. 1F10

DDC
JUN 29 1972
C

Reproduced by
NATIONAL TECHNICAL INFORMATION SERVICE
U S Department of Commerce
Springfield VA 22151

30 April 1972

Acknowledgement: This research was supported by the Advanced Research Projects Agency, Nuclear Monitoring Research Office, under Project VELA-UNIFORM, and accomplished under the technical direction of the Air Force Technical Applications Center under Contract No. F33657-71-C-0843.

UNCLASSIFIED
Security Classification

DOCUMENT CONTROL DATA - R & D
(Security classification of title, body of abstract and indexing annotation must be entered when the overall report is classified)

1. ORIGINATING ACTIVITY (Corporate author)
Texas Instruments Incorporated
Services Group
P.O. Box 5621, Dallas, Texas 75222

2a. REPORT SECURITY CLASSIFICATION
UNCLASSIFIED

2b. GROUP

3. REPORT TITLE
Evaluation of Detection and Discrimination Capability of the Alaskan Long Period Array, Special Report No. 4, Extended Array Evaluation Program

4. DESCRIPTIVE NOTES (Type of report and inclusive dates)
Special

5. AUTHOR(S) (First name, middle initial, last name)
Leo N. Heiting, Gary D. McNeely, and Alan C. Strauss

6. REPORT DATE
30 April 1972

7a. TOTAL NO. OF PAGES
109

7b. NO. OF REFS
7

8a. CONTRACT OR GRANT NO.
Contract No. F33657-71-C-0843

b. PROJECT NO.
AFTAC Project No. VT/1705

c.

d.

9a. ORIGINATOR'S REPORT NUMBER(S)
Special Report No. 4

9b. OTHER REPORT NO(S) (Any other numbers that may be assigned this report)

10. DISTRIBUTION STATEMENT
APPROVED FOR PUBLIC RELEASE; DISTRIBUTION UNLIMITED

11. SUPPLEMENTARY NOTES

12. SPONSORING MILITARY ACTIVITY
Advanced Research Projects Agency
Nuclear Monitoring Research Office
Arlington, Virginia 22209

13. ABSTRACT

This report describes the continued evaluation of the 19-element Alaskan Long Period Array (ALPA), which was conducted by Texas Instruments Incorporated, at the Seismic Array Analysis Center over the period 1 April 1971 to 31 March 1972.

The major areas of study in the evaluation were:

- Signal analysis - signal similarity, beamsteer signal attenuation
- Noise analysis - spectral shape and levels, time variability
- Two component processing gains
- Matched filter processing gains - master waveform and chirp matched filters
- ALPA detection and discrimination capability using S-waves
- Surface wave detection threshold at ALPA as a function of m_b
- Performance of standard discriminants at ALPA-M_s vs. m_b, AL, and AR

More than 120 events, primarily from the Sino-Soviet area, were processed in the course of this evaluation. Where applicable, earlier ALPA evaluation results are discussed in conjunction with the present results.

DD FORM 1473

I

109

UNCLASSIFIED
Security Classification

14. KEY WORDS	LINK A ROLE	LINK A WT	LINK B ROLE	LINK B WT	LINK C ROLE	LINK C WT
Seismic signal analysis						
Seismic noise analysis						
Matched filter						
Chirp filter						
Seismic event detection						
Seismic event discrimination						

II

AFTAC Project No. VT/1705

EVALUATION OF DETECTION AND DISCRIMINATION CAPABILITY OF THE ALASKAN LONG PERIOD ARRAY

SPECIAL REPORT NO. 4
EXTENDED ARRAY EVALUATION PROGRAM

Prepared by
Leo N. Heiting, Gary D. McNeely, and Alan C. Strauss

T. W. Harley, Program Manager
Area Code 703, 836-3882 Ext. 300

TEXAS INSTRUMENTS INCORPORATED
Services Group
P.O. Box 5621
Dallas, Texas 75222

Contract No. F33657-71-C-0843
Amount of Contract: $511,580
Beginning 1 April 1971
Ending 31 March 1972

Prepared for

AIR FORCE TECHNICAL APPLICATIONS CENTER
Alexandria, VA 22313

Sponsored by

ADVANCED RESEARCH PROJECTS AGENCY
Nuclear Monitoring Research Office
ARPA Order No. 1714
ARPA Program Code No. 1F10

30 April 1972

Acknowledgement: This research was supported by the Advanced Research Projects Agency, Nuclear Monitoring Research Office, under Project VELA-UNIFORM, and accomplished under the technical direction of the Air Force Technical Applications Center under Contract No. F33657-71-C-0843.

ABSTRACT

This report describes the continued evaluation of the 19-element Alaskan Long Period Array (ALPA), which was conducted by Texas Instruments, Incorporated, at the Seismic Array Analysis Center over the period 1 April 1971 through 31 March 1972.

The major areas of study in the evaluation were:

- Signal analysis - signal similarity, beamsteer signal attenuation
- Noise analysis - spectral shape and levels, time variability
- Two component processing gains
- Matched filter processing gains - master waveform and chirp matched filters
- ALPA detection and discrimination capability using S-waves
- Surface wave detection threshold at ALPA as a function of m_b
- Performance of standard discriminants at ALPA - M_s vs. m_b, AL, and AR

More than 120 events, primarily from the Sino-Soviet area, were processed in the course of this evaluation. Where applicable, earlier ALPA evaluation results are discussed in conjunction with the present results.

Neither the Advanced Research Projects Agency nor the Air Force Technical Applications Center will be responsible for information contained herein which has been supplied by other organizations or contractors, and this document is subject to later revision as may be necessary. The views and conclusions presented ate those of the authors and should not be interpreted as necessarily representing the official policies, either expressed or implied, of the Advanced Research Projects Agency, the Air Force Technical Applications Center, or the US Government.

TABLE OF CONTENTS

TABLE OF CONTENTS
(continued)

LIST OF FIGURES

LIST OF FIGURES
(continued)

LIST OF TABLES

SECTION I
INTRODUCTION

This report presents the results of an evaluation of the full nineteen site Alaskan Long Period Array (ALPA). It extends an analysis performed on a nine-site ALPA subarray, which has been reported earlier in Final Report for Long Period Array Processing Development, (Harley 1971). The evaluation focuses on determination of optimum techniques for the extraction of those long-period signals which may be useful in classifying events, and on the utility of classification parameters obtained at ALPA. Specific areas of investigation include:

- Signal Analysis
- Noise Analysis
- Analysis of Two Component Processing
- Matched Filter Performances
- Analysis of S-Wave Processing
- Seismic Event Detection Threshold
- Behavior of Seismic Discriminants

When applicable, results from the evaluation of the limited array are compared to full array results.

The data base is described and preliminary comments on the data processing methods are made in Section II. Sections III through IX discuss details of the specific areas of study. Section X summarizes results and conclusions and suggests areas of further analysis utilizing the ALPA array.

SECTION II

DATA BASE AND GENERAL COMMENTS ON ANALYSIS METHODS EMPLOYED

Results presented in this report are based mainly on seismic events recorded during the time interval after the full nineteen element array became available; June, 1971 through the end of 1971. A few events of special interest which occurred prior to this time period are also included. Significant parameters for each of these 117 events are listed in Table II-1. Each event is named by a three part designator consisting of a three letter abbreviation for the region, the Julian date, and the hour (GMT) of occurrence. Parameters listed include the exact event time, latitude and longitude, epicentral distance and great circle azimuth from ALPA, body wave magnitude (m_b); ALPA surface wave magnitudes computed from both Rayleigh and Love wave energy, AL and AR discriminant values (see Section IX), and depth if known. Also listed are comments for each event giving the data source (L for LASA Bulletin, N for NORSAR Bulletin, or C for National Earthquake Information Center data), and whether the event was detected (D) or not detected (ND). Also designated by the letter E in the comments section of Table II-1 are the events which are presumed to be explosions.

In all processing discussed in following paragraphs, the raw data from the triaxial seismometers at each site at ALPA have been rotated by means of a transformation of coordinates to form three mutually perpendicular components of ground motion, one vertical and two horizontal. Of the horizontal components, one lies in the direction of the great circle azimuth to the event in question (radial component) and the second lies perpendicular to this (transverse component). Therefore the Love wave energy from a seismic event will occur on the transverse component trace and the Rayleigh wave energy will occur on the vertical and radial traces.

TABLE II-1

LIST OF EVENTS USED FOR EVALUATION
(PAGE 1 OF 7)

Event Name	Date (1971)	Time (hr-min-sec)	Lat. °N / Lon. °E	Δ° / AZ°	m_b	$(M_s)_R$	$(M_s)_L$	AL	AR	Depth	Comments
EKZ*145*04AL	5/25	04-02-58	49.8/78.2	59.6/-32.5	5.2	≤2.7	-	-	-	0	ND (4) C, E
EKZ*115*03AL	4/25	03-32-58	49.8/78.1	59.7/-32.5	5.9	3.6	3.4	10	11	0	D (2) C, E
URL*082*06AL	3/23	06-59-56	61.3/56.5	52.2/-14.5	5.6	3.4	3.4	16	21	0	D (5) C, E
EKZ*081*04AL	3/22	04-32-58	49.7/78.2	59.7/-32.6	5.8	3.6	3.6	14	14	0	D (4) C, E
EKZ*170*04QC	6/19	04-03-58	50.0/77.7	59.6/-32.1	5.5	3.0	≤3.4	6	6	0	D (6) C, E
EKZ*157*04QC	6/06	04-02-57	50.0/77.8	59.5/-32.2	5.5	3.2	≤2.9	7	11	0	D (4) C, E
SIN*184*04AL	7/03	04-26-22	41.3/79.3	67.4/-36.6	4.9	3.6	3.8	130	130	17	D (14) C
KUR*182*21AL	7/01	21-57-32	44.0/148.0	40.4/-89.4	3.9	-	-	-	-	33	ND (11) L
KUR*190*16AL	7/09	16-44-16	43.5/147.7	40.9/-89.5	4.5	4.2	4.6	1800	1300	46	D (8) C
WRS*190*14AL	7/09	14-51-08	61.0/37.0	53.7/ -2.8	3.8	-	-	-	-	33	ND (12) L
SAK*182*14AL	7/01	14-03-27	47.0/143.0	40.1/-82.2	4.9	≤2.4	2.9	17	9	33	D (10) L
HIN*182*14AL	7/01	14-37-26	36.7/68.3	74.3/-29.3	4.6	3.4	3.5	130	86	33	D (12) C
WRS*184*17QC	7/03	17-30-17	54.0/44.0	60.4/ -7.9	3.9	-	-	-	-	33	ND (10) L
KUR*185*15QD	7/04	15-29-22	43.7/147.5	40.8/-89.2	4.4	3.2	3.6	230	180	33	D (8) C
HOK*185*19QC	7/04	19-23-54	41.0/147.0	43.3/-91.0	3.5	≤2.6	2.8	490	370	33	D (11) L
KAM*193*02AL	7/12	02-12-30	53.1/160.0	28.3/-89.8	4.9	3.3	3.5	190	130	33	D (10) C
EKZ*192*05AL	7/11	05-10-37	52.0/76.0	58.0/-30.1	3.7	<2.8	-	-	-	33	ND (12) L
KUR*191*02AL	7/10	02-04-28	51.0/153.0	32.8/-86.5	3.6	-	-	-	-	33	ND (12) L

TABLE II-1

LIST OF EVENTS USED FOR EVALUATION
(PAGE 2 OF 7)

Event Name	Date (1971)	Time (hr-min-sec)	Lat./Lon. $^{o}N / ^{o}E$	Δ^{o}/AZ^{o}	m_b	$(M_s)_R$	$(M_s)_L$	AL	AR	Depth	Comments
KUR*191*03AL	7/10	03-05-01	43.6/147.7	40.8/-89.4	4.8	3.6	4.1	290	240	36	D(12)C
KUR*191*14AL	7/10	14-29-02	44.0/149.0	40.0/-90.3	4.3	3.4	3.8	370	320	33	D(12)L
URL*191*16QC	7/10	16-59-59	62.4/55.2	51.2/-13.4	5.3	<2.9	≤2.9	-	-	0	ND(10)C, E
KUR*203*22QC	7/22	22-56-05	44.0/149.0	40.0/-90.3	4.3	4.2	3.8	420	240	33	D(14)L
HOK*203*16AL	7/22	16-04-16	41.0/147.0	43.3/-91.0	3.6	-	-	-	-	33	ND(8)L
WRS*202*15TD	7/21	15-49-27	52.0/54.0	61.6/-15.0	3.8	-	-	-	-	33	ND(5)L
KUR*202*23AL	7/21	23-50-14	47.0/147.0	38.4/-85.6	3.8	-	-	-	-	33	ND(14)L
BAL*201*15AL	7/20	15-25-34	52.0/118.0	45.9/-58.8	4.0	2.9	2.8	200	210	33	D(15)L
KAM*201*05AL	7/20	05-33-24	56.0/161.0	25.9/-86.1	3.7	-	-	-	-	33	ND(15)L
SWR*200*20AL	7/19	20-41-20	49.0/39.0	65.6/-4.9	3.8	3.2	≤3.0	390	760	33	D(13)L
KUR*199*12QC	7/18	12-32-38	51.0/157.0	31.1/-90.0	4.3	2.3	2.5	37	31	33	D(13)L
KUR*213*02AL	8/1	02-06-07	50.4/156.8	31.7/90.6	5.6	4.5	4.5	300	210	20	D(14)C
KUR*206*00AL	7/25	00-41-26	50.0/154.0	33.1/-88.5	4.1	2.5	2.5	65	76	33	D(13)L
KAM*206*01AL	7/25	01/23/19	55.0/163.0	25.8/-89.6	4.0	-	-	-	-	33	ND(14)L
KAM*206*03AL	7/25	03-45-05	52.6/160.7	28.4/-91.2	4.9	3.7	4.2	570	180	33	D(16)C
KAM*206*08AL	7/25	08-12-34	53.0/160.0	28.4/-90.0	3.7	2.5	3.0	580	270	33	D(16)L

TABLE II-1

LIST OF EVENTS USED FOR EVALUATION
(PAGE 3 OF 7)

Event Name	Date (1971)	Time (hr-min-sec)	Lat./Lon. ^{o}N / ^{o}E	Δ^{o}/AZ^{o}	m_b	$(M_s)_R$	$(M_s)_L$	AL	AR	Depth	Comments
KUR*206*08AL	7/25	08-35-19	44.0/147.0	40.8/-88.5	4.0	-	-	-	-	33	ND(12)L
KUR*205*04AL	7/24	04-19-41	45.0/147.0	40.0/-87.5	3.6	-	-	-	-	33	ND(13)L
SWR*205*11AL	7/24	11-11-42	48.0/28.0	66.7/3.1	3.5	-	-	-	-	33	ND(13)L
TAD*205*11AL	7/24	11-43-39	39.5/73.2	70.5/-32.4	5.6	4.3	4.4	99	100	33	D(15)C
KAM*204*08AL	7/23	08-01-23	52.7/160.7	28.3/-91.1	4.8	3.6	4.2	650	220	33	D(17)C
KUR*204*12AL	7/23	12/45/12	46.0/150.0	37.9/-89.3	3.7	-	-	-	-	33	ND(14)L
SIN*221*01AL	8/9	01-03-17	42.1/83.4	65.6/-39.4	4.2	3.3	3.0	150	190	33	D(12)C
SIN*219*15AL	8/7	15-21-53	36.1/77.7	72.7/-37.1	4.8	4.9	4.4	450	310	33	D(10)C
KAM*217*01AL	8/5	01-05-57	50.0/156.8	32.0/-91.1	3.7	-	-	-	-	33	ND(13)L
KUR*216*08AL	8/4	08-58-16	41.8/141.5	44.9/-85.4	3.7	2.8	2.7	260	280	33	D(9)L
KYU*214*13AL	8/2	13-59-41	33.0/130.9	56.8/-82.2	3.6	-	-	-	-	33	ND(17)L
KUR*214*02QC	8/2	02-57-24	50.8/158.1	30.8/-91.3	3.6	-	-	-	-	33	ND(16)L
IRA*221*02QE	8/9	02-54-37	36.2/52.7	77.3/-16.8	5.2	5.1	4.9	1700	2100	27	D(17)C
UKR*238*15QC	8/26	15-17-22	45.4/36.7	69.3/-3.3	4.1	$\leq$2.7	-	-	-	12	ND(10)L
KUR*230*23AL	8/18	23-27-16	43.1/145.8	42.0/-88.2	3.6	$\leq$2.9	4.1	520	360	33	D(6)L
KUR*226*14AL	8/14	14-47-57	48.0/153.0	35.1/-89.9	3.8	$\leq$2.5	$\leq$2.5	150	130	33	D(12)L
KUR*225*06AL	8/13	06-15-57	46.0/151.0	37.5/-90.2	4.1	2.4	2.3	37	44	33	D(13)L

TABLE II-1

LIST OF EVENTS USED FOR EVALUATION
(PAGE 4 OF 7)

Event Name	Date (1971)	Time (hr-min-sec)	Lat./Lon. $^{o}N/^{o}E$	Δ^{o}/AZ^{o}	m_b	$(M_s)_R$	$(M_s)_L$	AL	AR	Depth	Comments
KUR*224*22AL	8/12	22-55-28	47.0/150.0	37.1/-88.3	3.9	-	-	-	-	33	ND(13)L
KAM*225*00AL	8/13	00-34-44	49.0/156.0	33.1/-91.5	3.7	-	-	-	-	33	ND(13)L
SIN*237*06QC	8/25	06-15-23	40.5/77.2	68.6/-35.2	4.4	2.7	2.9	80	55	15	D(11)L
IRA*237*00QC	8/25	00-30-45	28.2/52.3	85.3/-17.6	4.1	≤2.9	≤2.9	160	180	33	D(15)C
CRS*236*16QC	8/24	16-33-23	52.2/91.4	54.1/-40.5	5.2	4.7	4.8	920	720	33	D(15)C
KUR*234*02AL	8/22	02-46-19	43.6/144.1	42.3/-86.2	4.1	≤2.6	-	-	-	33	ND(12)L
NRS*233*19AL	8/21	19-34-23	81.9/118.9	26.4/-18.4	4.6	3.9	3.3	200	490	33	D(13)C
KUR*233*04AL	8/21	04-21-46	40.9/143.2	45.0/-87.7	3.8	-	-	-	-	33	ND(12)L
TIB*302*17AL	10/29	17-16-52	34.0/86.0	72.4/-44.5	5.0	3.7	3.6	93	100	-	D(14)N
IRA*288*14AL	10/15	14-19-32	37.0/55.0	76.2/-18.5	4.7	5.1	3.6	180	310	39	D(16)C
CAU*288*17AL	10/15	17-08-06	41.0/49.0	73.0/-13.1	4.9	3.7	3.3	40	100	33	D(14)C
TAD*259*10AL	9/16	10-59-27	40.0/68.0	71.1/-28.2	4.2	≤3.0	-	-	-	-	ND(12)N
CHI*258*11AL	9/15	11-22-43	34.0/101.0	67.6/-56.7	4.2	≤3.0	-	-	-	-	ND(15)N
TUR*251*22AL	9/8	22-35-16	41.0/44.0	73.4/-9.2	4.8	4.1	3.7	250	550	33	D(15)C
TIB*278*05AL	10/5	05-29-48	33.0/93.0	71.2/-50.6	4.2	3.0	≤2.9	120	110	-	D(14)N
CHI*283*05AL	10/10	05-53-55	34.0/95.0	69.6/-51.8	4.4	3.5	3.5	270	160	-	D(11)N
CAU*283*09AL	10/10	09-05-45	43.0/44.0	71.4/-9.0	4.0	2.8	2.8	200	170	-	D(12)L

TABLE II-1

LIST OF EVENTS USED FOR EVALUATION

(PAGE 5 OF 7)

Event Name	Date (1971)	Time (hr-min-sec)	Lat./Lon. $^{o}N/^{o}E$	Δ^{o}/AZ^{o}	m_b	$(M_s)_R$	$(M_s)_L$	AL	AR	Depth	Comments
EKZ*282*06AL	10/9	06-02-57	50.0/78.0	59.5/-32.3	5.4	≤2.9	≤3.1	15	12	0	D(10)C, E
SIN*281*09AL	10/8	09-20-15	41.0/79.0	67.7/-36.4	4.4	3.1	≤2.9	100	96	-	D(16)L
CHR*266*21RT	9/23	21-08-00	53.0/120.0	44.3/-59.4	4.2	3.7	2.9	120	120	-	D(14)L
CAU*262*06AL	9/19	06-44-40	43.0/47.0	71.2/-11.3	4.4	≤2.5	≤2.7	-	-	-	ND(16)L
CAU*263*08AL	9/20	08-03-00	43.0/33.0	71.8/-1.0	4.2	≤3.2	-	-	-	-	ND(16)L
WRS*262*11AL	9/19	11-00-07	58.0/41.0	56.6/-5.5	4.5	≤2.7	≤2.9	-	-	33	ND(16)C
WRS*277*10AL	10/4	10-00-42	62.0/47.0	52.3/-8.7	5.1	3.0	≤2.8	13	16	13	D(17)C, E
TAD*274*16AL	10/1	16-27-48	39.0/70.0	71.7/-30.1	4.9	3.7	4.0	220	170	36	D(15)C
KAZ*273*12AL	9/30	12-43-45	50.0/88.0	57.0/-39.3	4.5	3.7	3.2	150	180	-	D(16)N
NVZ*270*05AL	9/27	05-59-55	73.0/55.0	40.9/-9.9	6.4	4.6	4.4	21	42	0	D(18)C, E
KGZ*301*14AL	10/28	13-30-57	41.9/72.4	68.4/-31.1	5.5	4.8	4.7	580	480	22	D(13)C
SAK*270*19AL	9/27	19-01-45	46.4/141.1	41.3/-81.2	5.9	5.6	5.8	2400	890	21	D(19)C
SAK*251*11AL	9/8	11-48-23	46.4/141.1	41.3/-81.2	5.9	6.0	6.2	6100	2700	6	D(19)C
SAK*251*16AL	9/8	16-59-53	46.3/140.9	41.5/-81.1	5.9	5.8	5.9	3500	1700	16	D(18)C
SAK*248*18AL	9/5	18-35-25	46.5/141.2	41.2/-81.2	7.1	6.4	6.1	18000	7500	9	D(18)C
HOK*214*07AL	8/2	07-24-57	41.4/143.5	44.4/-87.5	6.6	6.1	6.7	6400	3500	51	D(18)C
ERS*256*14AL	9/13	14-26-00	52.0/134.0	39.8/-70.3	3.7	2.7	2.7	330	230	-	D(15)L
EKZ*294*06AL	10/21	06-02-57	50.0/78.0	59.5/-32.3	5.6	3.1	3.0	8	8	0	D(14)C, E

TABLE II-1

LIST OF EVENTS USED FOR EVALUATION
(PAGE 6 OF 7)

Event Name	Date (1971)	Time (hr-min-sec)	Lat./Lon. °N / °E	Δ° / AZ°	m_b	$(M_s)_R$	$(M_s)_L$	AL	AR	Depth	Comments
WRS*295*05AL	10/22	05-00-00	52.0/55.0	61.5/-15.7	5.3	≤2.7	≤2.8	7	6	6	D(16)C, E
WKZ*356*06R2	12/22	06-59-56	47.9/48.2	66.2/-11.6	6.0	3.5	3.2	4	8	0	D(9)C, E
EKZ*364*06R2	12/30	06-20-57	49.7/78.1	59.8/-32.5	5.8	3.5	3.3	8	10	0	D(17)C, E
EKZ*333*06N2	11/29	06-02-57	50.0/78.0	59.5/-32.3	5.5	3.1	3.1	8	8	0	D(14)C
SAK*249*03AL	9/6	02-59-39	46.7/141.2E	39.7/-80.0	5.4	-	-	-	-	33	C
SAK*249*07AL	9/6	06-45-59	46.4/141.1E	40.5/-81.0	5.7	-	-	-	-	16	C
SAK*249*13AL	9/6	13-37-11	46.7/141.4	39.7/-80.0	6.1	-	-	-	-	29	C
SOL*221*12AL	8/9	12-12-02	5.9S/154.3	82.3/-132.0	6.0	-	-	-	-	63	C
SOL*230*10	9/18	10-40-31	6.1S/154.5	82.7/-132.0	5.2	-	-	-	-	54	C
SOL*277*01AL	10/4	01-30-34	5.8S/154.2	82.6/-132.0	5.7	-	-	-	-	74	C
HOK*177*08AL	6/26	08-56-24	40.0/142.0	46.0/-87.6	4.9	3.5	3.4	67	79	49	(10)
SIN*170*17AL	6/19	17-23-03	41.5/79.3	67.2/-36.5	5.2	4.6	4.9	790	460	33	(10)C
SIN*170*21AL	6/19	21-08-46	41.5/79.4	67.2/-36.6	4.7	3.4	3.4	59	90	33	(4)C
KAM*168*08AL	6/17	08-20-47	54.0/161.0	27.3/-89.4	4.1	2.8	2.9	-	-		(7)
KUR*168*09AL	6/17	09-32-05	44.4/148.9	39.7/-89.8	4.9	2.9	3.3	34	24	33	(7)C
SIN*168*15AL	6/17	15-20-12	41.3/79.4	67.3/-36.6	4.9	3.3	3.3	46	31	33	(9)C
SIN*167*13AL	6/16	13-46-51	41.3/79.3	67.4/-36.6	5.1	3.5	3.6	47	39	33	(4)C

TABLE II-1

LIST OF EVENTS USED FOR EVALUATION
(PAGE 7 OF 7)

Event Name	Date (1971)	Time (hr-min-sec)	Lat. °N / Lon. °E	Δ°/AZ°	m_b	$(M_s)_R$	$(M_s)_L$	AL	AR	Depth	Comments
KUR*167*09AL	6/16	09-05-29	48.0/154.0	34.7/-90.8	4.1	2.7	2.8	-	-	-	(4)
MON*167*03AL	6/16	03-16-30	49.0/92.0	56.9/-42.6	3.9	3.2	3.1	-	-	-	(5)
KUR*181*09AL	6/30	09-31-20	50.0/158.0	31.5/-92.2	3.8	≤2.5	2.8	300	-	-	(9)
SIN*181*13AL	6/30	13-36-00	39.0/79.0	70.0/-37.1	4.6	3.4	3.3	89	100	-	(12)
CAU*179*19AL	6/28	19-53-46	42.0/43.0	72.0/-8.6	4.6	3.3	3.2	-	-	-	(13)C
KUR*180*15AL	6/29	15-11-33	45.3/151.7	38.0/-91.5	4.8	3.6	3.5	-	-	50	(12)C
CHI*156*10AL	6/5	10-21-28	37.3/113.7	59.0/-64.0	4.7	3.9	4.3	230	200	33	(11)C
KAM*166*14AL	6/15	14-04-09	52.8/160.8	29.0/-90.0	5.1	4.2	4.2	340	240	55	(10)C
KAM*162*04AL	6/11	04-24-03	51.4/159.3	30.2/-92.0	4.8	3.7	4.0	470	220	33	(4)C
SIN*166*23AL	6/15	23-07-01	41.0/80.0	67.5/-37.2	4.6	3.5	-	-	-	-	(5)L
SIN*166*47AL	6/15	23-17-34	41.6/79.2	67.5/-37.2	4.9	3.5	-	-	-	33	(5)C
SIN*166*07AL	6/15	07-39-37	39.0/80.0	69.4/-37.9	5.9	4.9	4.9	180	170	33	(10)C
CHI*161*19AL	6/10	19-28-15	40.0/116.0	56.7/-65.6	4.0	3.2	3.5	-	-	-	(11)
KAM*163*07AL	6/12	07-25-00	52.0/159.0	29.6/-90.5	3.5	2.6	2.9	600	510	-	(6)L

Whenever beamsteering is performed on an event, a beamsteer trace is formed for each component of motion (transverse, vertical, and radial) using all available sites. The number of sites available for beamsteering each event is given in parenthesis in the comments section of Table II-1. Each beam was aimed in the direction of the great circle azimuth to the event; the velocities used were 4.0 km/sec for the Love Waves, 3.5 km/sec for the Rayleigh Waves, and appropriate distance-dependent velocities for the Shear Waves.

The configuration of the ALPA array is shown in Figure II-1. Analytical methods relating to specific areas of study are described in the following sections.

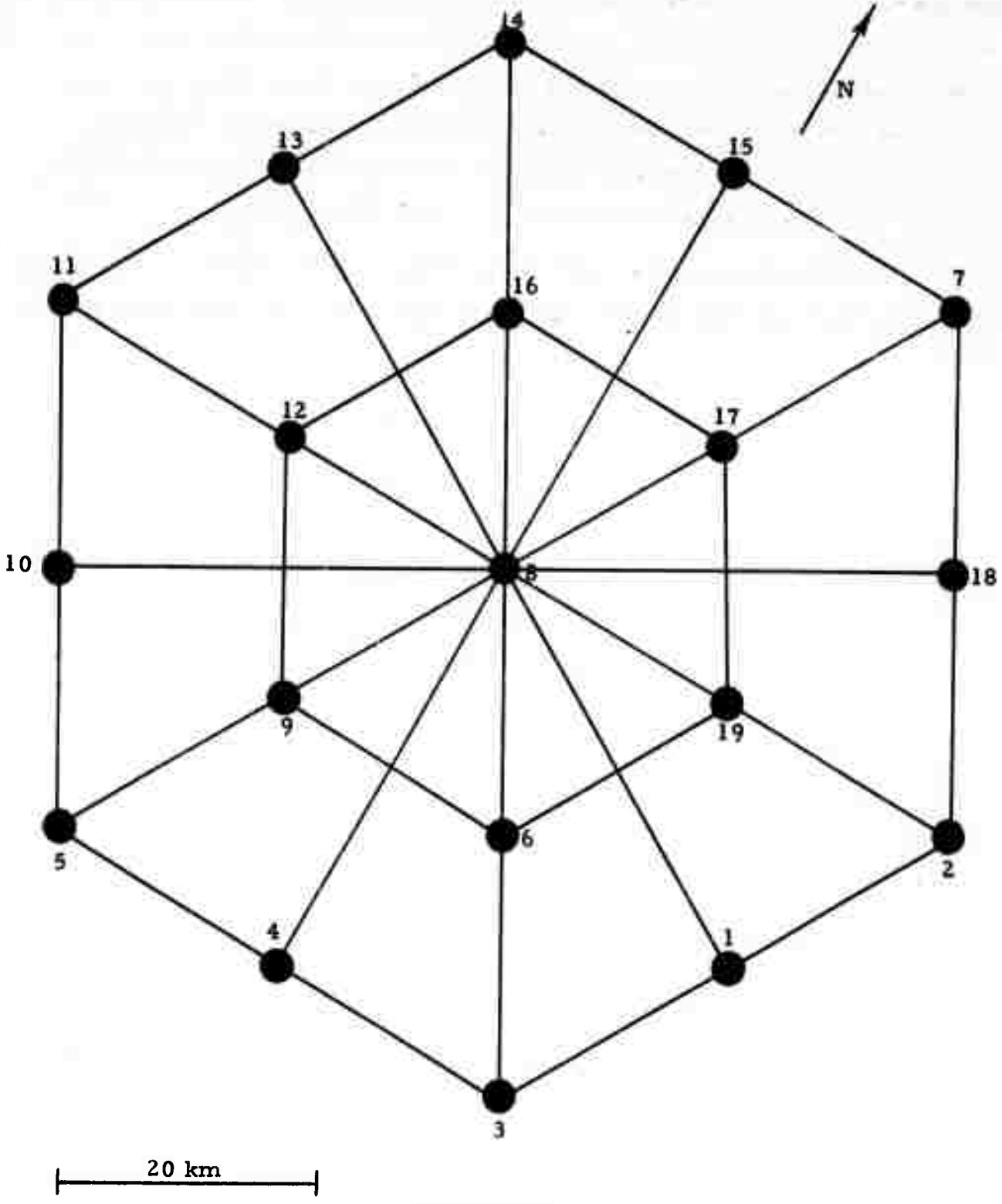

FIGURE II-1

ALPA ARRAY CONFIGURATION

SECTION III

SIGNAL ANALYSIS

The signal analysis presented here was undertaken to examine the following characteristics of ALPA, using the full 19-element array:

- Site-to-site signal similarity
- Signal attenuation for the 19-element array versus a 7-element subarray

A. SITE-TO-SITE SIGNAL SIMILARITY

The signal similarity between sites was determined in terms of the correlation coefficient between a reference site (site 8, at the center of the array) and each of the remaining 18 sites, computed over a time gate containing a large event. The correlation coefficient ρ is defined in the following manner (Harley 1967).

$$\rho = \frac{\Phi_{ij}(\Delta)}{\Phi_{ii}(0)\,\Phi_{jj}(0)}$$

where

$\Phi_{ij}(t)$ is the crosscorrelation between sites i and j at lag t;
Δ is the lag at which $\Phi_{ij}(t)$ is a maximum; and
$\Phi_{ii}(0)$ and $\Phi_{jj}(0)$ are the zero lag autocorrelation values for sites i and j.

Identical signals on the i-th and j-th sensors yield the maximum ρ value of unity; in practice, ρ values greater than 0.85 indicate good signal similarity.

Axis rotation was performed to obtain transverse, vertical, and radial components of ground motion, and correlation coefficients were computed for

each component. Data from all sites were first time-aligned using the great circle signal azimuth and the appropriate mode velocity. This was done to reduce the number of lags for which the crosscorrelation functions must be computed in order to locate their maxima. The lags at which the correlation coefficient maxima occur are then lags with respect to proper beamsteer time alignment. Maxima occurring at appreciable lag values are evidence of moveout anomalies which will cause beamsteer signal attenuation if not taken into account. This method is the same one used in a signal similarity study of the 9-site limited array, the results of which were reported earlier (Harley 1971).

The values of correlation coefficient computations for 14 events ranging in m_b from 4.6 to 7.1 are presented in Tables III-1 through III-3 (one table for each of the transverse, vertical, and radial components). Also presented in each table are the average correlation coefficient for each site, the average correlation coefficient for each event, and a typical zero-to-peak value of ground motion at the reference site for each event. No evidence of moveout anomalies was found; therefore, lag data are omitted. Note that this observation shows that a plane-wave nondispersive signal model is adequate for array beamforming.

In the case of the LQ transverse component the average correlation coefficient is greater than 0.85 for all the large events. The somewhat lower values for the small events occurred because the signal-to-noise ratio was too small to get a clear estimate of signal similarity.

Noise corruption does not appear to be a sufficient explanation for the anomalously low correlation coefficient values for the transverse component of the NRS*233*19 event. To test whether the reference site might be causing the low values, correlation coefficients were also computed using site 6 as the reference site. The results were substantially unchanged.

In the case of the LR-vertical and LR-radial ρ values, overall correlation coefficients are somewhat lower than for the LQ-transverse component. Correlation coefficients for most of the larger events are still above 0.80 with

TABLE III-1
CORRELATION COEFFICIENTS FOR LQ-TRANSVERSE COMPONENT

Event	Sites																		Event Avg
	1	2	3	4	5	6	7	9	10	11	12	13	14	15	16	17	18	19	
KUR*213*02AL (1350 mμ)	.940	.948			.929	.962	.925	.981	.954	.974	.987	.957	.915	.945	.980	.982		.980	.957
KAM*206*03AL (790 mμ)	.927	.918	.868	.904	.932	.950	.919	.963	.977	.947	.979	.915	.882	.899	.946	.964		.929	.932
TAD*s05*11AL (277 mμ)	.933	.779	.905	.835	.711	.931		.874	.778	.826	.873	.921	.915	.803	.931	.864		.883	.860
CRS*236*16QC (60 mμ)	.927	.834	.878	.786	.664	.932	.646	.882	.780	.855	.860	.944	.904	.834	.949	.866		.687	.836
NRS*233*19AL (113 mμ)	.706	.412	.489	.366	.502	.623		.418	.203	.641		.591	.365	.474	.514	.484		.758	.503
KGZ*301*14AL (890 mμ)	.953		.921		.545	.931	.740		.697			.946	.938	.851	.897		.792	.948	.847
SAK*270*19AL (23,500 mμ)	.926	.923	.881			.945	.876	.959	.945	.979	.989	.933	.864	.895	.958	.941	.969	.966	.934
SAK*251*11AL (70,500 mμ)	.926	.927	.899	.936	.905	.950	.887	.971	.955	.980	.981	.950	.873	.913	.959	.948	.919	.957	.935
SAK*251*16AL (24,800 mμ)	.924	.930	.902	.946	.920	.946	.883	.976	.955	.980	.981	.955	.870	.914	.958	.949		.952	.938
SAK*248*18AL (675,000 mμ)	.882	.889	.879	.898	.866	.925	.892	.927	.913	.931	.946	.904	.899	.900	.935	.911		.917	.907
HOK*214*07AL (169,000 mμ)	.910	.878	.837	.876	.921	.923	.920	.934	.924	.927	.960	.837	.850	.854	.938	.949		.883	.901
SAK*249*03AL (1220 mμ)	.970	.974		.973			.975	.987	.976	.976		.969	.969	.950		.972		.914	.967
SAK*249*07AL (2650 mμ)	.978	.980	.965	.967	.964	.977	.968	.984	.973	.984		.959	.964	.970	.989	.972		.947	.971
SAK*249*13AL (5450 mμ)	.944	.937	.912	.926	.902	.960	.962	.973	.958	.979		.971	.964	.971	.979	.959		.952	.953
Site Avg*	.918	.871	.861	.856	.813	.920	.883	.910	.856	.921	.951	.911	.869	.870	.918	.905	.893	.905	

* Without NRS*233*19AL

TABLE III-2

CORRELATION COEFFICIENTS FOR LR-VERTICAL COMPONENT

Event	Sites																		Event Avg
	1	2	3	4	5	6	7	9	10	11	12	13	14	15	16	17	18	19	
KUR*213*02AL (1110 mμ)	.903	.921			.905	.914	.942	.939	.920	.966	.974	.953	.928	.913	.947	.949		.976	.937
KAM*206*03AL (266 mμ)	.571	.620	.462	.589	.678	.749	.615	.866	.841	.602	.832	.483	.317	.372	.691	.804		.843	.644
TAD*205*11AL (209 mμ)	.888	.645	.935	.868	.769	.944		.891	.774	.763	.878	.913	.917	.808	.944	.830		.860	.852
CRS*236*16QC (63 mμ)	.893	.644	.854	.789	.630	.928	.342	.832	.717	.780	.838	.878	.892	.704	.912	.795		.728	.774
NRS*233*19AL (370 mμ)	.958	.911	.913	.910	.952	.930		.884	.885	.944		.896	.885	.912	.901	.865		.958	.914
KGZ*301*14AL (820 mμ)	.915		.941		.702	.948	.660		.729			.926	.902	.807	.769		.668	.912	.823
SAK*270*19AL (8500 mμ)	.762	.724	.714			.888	.823	.893	.948	.920	.943	.878	.682	.743	.924	.924	.879	.936	.849
SAK*251*11AL (25400 mμ)	.859	.846	.859	.811	.868	.928	.843	.910	.960	.936	.941	.896	.757	.791	.932	.932	.719	.954	.875
SAK*251*16AL (15100 mμ)	.893	.873	.895	.860	.907	.932	.846	.924	.966	.940	.950	.916	.813	.822	.941	.934		.962	.904
SAK*248*18AL (254000 mμ)	.711	.630	.716	.669	.719	.811	.590	.828	.820	.760	.802	.682	.506	.482	.737	.752		.788	.706
HOK*214*07AL (359000 mμ)	.951	.952	.918	.925	.922	.955	.925	.976	.961	.948	.970	.932	.926	.891	.964	.971		.970	.944
SAK*249*03AL (625 mμ)	.914	.861		.901			.932	.959	.984	.956		.937	.896	.858		.970		.906	.923
SAK*249*07AL (1450 mμ)	.890	.799	.825	.798	.848	.929	.908	.943	.960	.895		.888	.784	.854	.912	.940		.820	.875
SAK*249*13AL (1500 mμ)	.730	.625	.568	.648	.843	.903	.702	.913	.920	.802		.661	.342	.363	.792	.843		.872	.720
Site Avg	.845	.773	.800	.797	.812	.904	.761	.904	.884	.862	.903	.837	.753	.737	.874	.885	.755	.891	

TABLE III-3

CORRELATION COEFFICIENTS FOR LR-RADIAL COMPONENT

Event	Sites																		Event Avg
	1	2	3	4	5	6	7	9	10	11	12	13	14	15	16	17	18	19	
KUR*213*02AL (865 mμ)	.904	.897			.910	.948	.934	.953	.886	.889	.982	.915	.876	.916	.938	.948		.930	.922
KAM*206*03AL (226 mμ)	.478	.413	.338	.563	.636	.674	.641	.672	.731	.535	.834	.512	.423	.426	.697	.798		.654	.590
TAD*205*11AL (226 mμ)	.862	.746	.829	.752	.659	.905		.858	.740	.768	.865	.814	.880	.784	.921	.824	.	.838	.815
CRS*236*16QC (72 mμ)	.822	.721	.676	.615	.476	.827	.331	.805	.670	.760	.740	.813	.721	.604	.845	.744		.787	.703
NRS*233*19AL (196 mμ)	.914	.923	.934	.925	.931	.939		.917	.932	.906		.942	.916	.947	.936	.944		.954	.930
KGZ*301*14AL (510 mμ)	.837		.782		.574	.940	.587		.712			.864	.756	.671	.702		.529	.873	.736
SAK*270*19AL (14100 mμ)	.743	.629	.668			.855	.693	.823	.886	.726	.743	.746	.515	.711	.835	.815	.904	.662	.747
SAK*251*11AL (23500 mμ)	.806	.683	.745	.763	.874	.873	.752	.854	.888	.762	.937	.817	.650	.750	.873	.834	.432	.744	.780
SAK*251*16AL (13600 mμ)	.832	.750	.776	.798	.896	.890	.830	.869	.905	.811	.966	.867	.771	.829	.903	.872		.794	.845
SAK*248*18 AL (265000 mμ)	.739	.593	.664	.579	.722	.804	.578	.755	.814	.618	.865	.703	.394	.540	.741	.753		.615	.675
HOK*214*07AL (350000 mμ)	.930	.941	.876	.861	.897	.932	.904	.949	.934	.939	.972	.923	.901	.888	.953	.956		.934	.923
SAK*249*03AL (575 mμ)	.895	.789		.847			.852	.884	.953	.825		.902	.793	.826		.880		.773	.852
SAK*249*07AL (1100 mμ)	.810	.652	.794	.768	.889	.883	.734	.862	.958	.795		.814	.695	.788	.892	.856		.633	.801
SAK*249*13AL (1800 mμ)	.512		.406	.313	.684	.750	.484	.614	.844	.472		.702	.471	.430	.678	.637			.571
Site Avg	.792	.728	.707	.708	.762	.863	.693	.822	.847	.754	.878	.810	.697	.722	.814	.836	.622	.784	

the exception of events SAK*248*18 and SAK*249*13, which appear to yield anomalously low correlation coefficients. It also appears that the correlation coefficients between site 8 and sites 14 and 15 are consistently low for the Sakhalin Island (designated SAK) events. No explanation has been found for this phenomenon; however, it is possible that the site 14 and 15 system responses may be somewhat different from the rest during the day 248 to day 270 time period.

In the case of the KAM*206*03 event, there appears to be a substantial difference in waveform across the array. The vertical and radial component correlation coefficients are generally better on the southwest side of the array (Figure II -1) than elsewhere. Correlation coefficients were also computed for this event using site 6 as the reference site. With this change, correlation coefficient values were above 0.70 in the southwest part of the array (sites 1-9) and were low elsewhere.

Overall, correlation coefficients for the full array are somewhat lower than those obtained for the nine-site limited array. This difference indicates that array processing signal loss for the full array might be expected to be somewhat greater for the full array than for the limited array. Some of the difference for the smaller events may be due to the fact that the reference site (8) for the full array study is noisier than the reference site (6) used in most of the limited array study.

B. BEAMSTEER SIGNAL ATTENUATION

A study was made to examine beamsteer signal attenuation by the full array and to compare the full array in this respect to a seven-element subarray. The seven-element subarray used was the hexagonal array formed from sites 1, 3, 4, 6, 8, 9, and 19 (Figure II -1). Fifteen events ranging in m_b from 4.6 to 7.1 were used in the study. The events used are listed in Table III-4. Two beams were formed for each event, one from the full array and the other from the subarray. For each event, peak-to-peak signal amplitudes were measured

TABLE III-4

SMALL ARRAY AND FULL ARRAY BEAM SIGNAL ATTENUATION

Event Name	Signal Attenuation Relative to Reference Site (dB)					
	Small Array			Full Array		
	T	V	R	T	V	R
KUR*213*02	0.7	0.2	0.2	1.0	0.6	0.3
KAM*206*03	1.6	0.8	-1.1	1.2	3.0	0.0
TAD*205*11	1.6	-0.3	0.0	2.9	0.9	0.9
SAK*249*03	0.0	0.2	0.6	0.4	1.8	1.8
IRA*221*02	1.0	1.1	0.2	1.5	2.1	1.0
CRS*236*16	1.6	1.2	-0.3	1.8	1.2	1.3
NRS*233*19	2.4	1.6	0.1	3.1	2.1	2.1
SAK*249*07	2.2	1.4	2.0	1.2	2.9	2.7
HOK*214*07	0.3	1.1	1.0	1.0	2.1	2.2
KGZ*301*14	0.2	1.3	0.1	1.6	2.9	1.7
SAK*249*13	1.8	2.6	3.4	1.2	3.6	4.9
SAK*248*18	1.9	0.5	1.2	1.6	2.3	1.7
SAK*251*11	1.6	1.5	0.6	1.1	2.1	1.8
SAK*251*16	1.5	0.4	0.9	1.0	1.3	1.4
SAK*270*19	1.8	1.2	0.7	1.2	2.2	2.0
AVERAGE	1.3	1.0	0.6	1.4	2.1	1.7

at three corresponding points in the reference site waveform, the seven-site beam, and the full array beam. Three ratios of the reference waveform amplitude to the beam amplitude were computed for each beam and averaged. The value of this averaged ratio (in dB) was used as the signal attenuation figure for the beam in question. The results of these measurements for the transverse (T), vertical (V), and radial (R) components are presented in Table III-4.

The observed signal attenuation results are generally consistent with the observed correlation coefficient values. In the case of the vertical component, event NRS*233*19 yielded the lowest correlation coefficients, and it also exhibits the most signal attenuation. In the case of the vertical component data, the consistency is somewhat less; the event which exhibits the greatest attenuation on the full array beam, SAK*249*13, has a low site average correlation coefficient, but not the lowest observed.

Radial component data is also generally consistent; the event with the lowest average correlation coefficient is also the most severely attenuated. Event KAM*206*03 appears to be anomalous. The average correlation coefficient is the second lowest observed (0.59), but there is no perceptible signal attenuation on the full array beam.

The average beam attenuation for the transverse component is approximately the same for both the small array and the full array, about 1.4 dB. For the vertical and radial components the full array beam causes about two dB attenuation, as opposed to about one dB for the small array beam. The slightly higher Rayleigh wave attenuation is consistent with the lower observed correlation coefficients. Differences among components are small, however, and probably not physically significant; it appears reasonable to say that full array and partial array surface wave beamforming signal losses average about two dB and one dB, respectively.

SECTION IV
NOISE ANALYSIS

Analysis of one-hour ALPA noise samples, recorded at approximately ten-day intervals, has continued during 1971. The analysis was directed to an understanding of the ambient noise field as recorded by the full nineteen-site array. The principal tools used were spectral analysis and high-resolution frequency-wavenumber analysis.

Figure IV-1 gives average ALPA noise power density spectra for data recorded during the winters of 1970 and 1971. During the winter of 1970, high noise levels were observed frequently at ALPA at periods greater than twenty seconds (Long [illegible]od Array Processing Development Reports (Harley 1971) and (Texas Instruments, Inc. 1970). This noise was highly variable and incoherent from site-to-site. It was particularly bothersome since it fell in that part of the spectrum containing normal long-period signals. During late 1970 and early 1971 steps were taken at the array to alleviate this difficulty. Figure IV-1 illustrates the efficacy of these measures. Four different noise samples were selected randomly from each of the winters of 1970 and 1971. For each of these samples single-site power density spectra were computed, and the resultant spectra were averaged over the individual sites. These average spectra were averaged further over the four samples of each winter and the resultant average spectra are given in the figure. Since only nine sites located in the southern half of ALPA were available during 1970, the 1971 computations also were made with these same nine sites. The spectral levels at periods greater than twenty seconds are about ten dB lower for the 1971 data than for the 1970 data. This suggests that the remedial steps taken were quite effective.

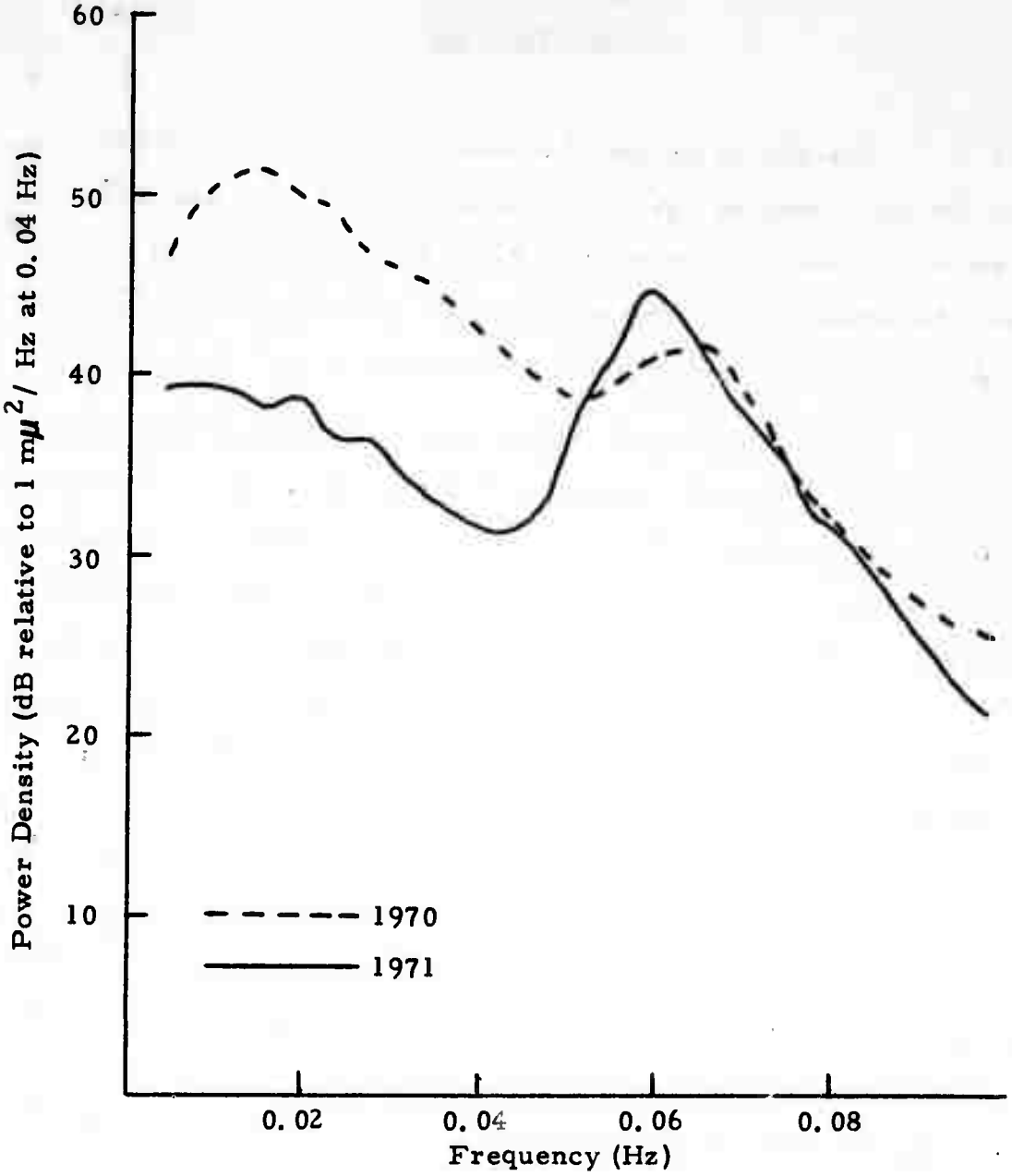

ALPA NOISE POWER DENSITY SPECTRA AVERAGED OVER FIRST NINE SITES AND FOUR WINTER NOISE SAMPLES FOR 1970 AND 1971

FIGURE IV-1

Figures IV-2, 3, and 4 illustrate the RMS noise levels observed at ALPA during 1971. Corresponding values for NORSAR are included for comparison. For each noise sample the RMS value of the noise at each site in the 0.025 to 0.055 Hz band was computed over a one hour time gate. This is the standard bandpass used for signal extraction at ALPA. The RMS values were averaged over all functioning sites of the array and the resultant averages are shown in the figures. The three figures give data for the vertical, east-west, and north-south components respectively. During the period day 240 to day 320 ALPA experienced occasional days with high RMS noise levels. From day 320 to 360, however, the noise levels were slightly above normal summer levels. The winter time increase at NORSAR appeared to begin at a later date in the year, but persisted through the end of the year.

A different mechanism dominates the cold weather increases at ALPA than at NORSAR. Although Figure IV-1 indicates that the high long-period noise levels observed at ALPA during 1970 have been substantially reduced, occasional high noise levels still occur. The noise levels during the period day 240 to day 320 in Figures IV-2, 3, and 4 appear only at a few sites and are not correlatable to microseismic activity. At NORSAR, on the other hand, the increases at the end of 1971 are relatable to increased microseismic levels. This is evidenced by Figure IV-5 which illustrates the spectral levels in the fifteen to twenty second band at ALPA and NORSAR. Microseisms at ALPA show some tendency to be higher in winter, but the trend at NORSAR is much more pronounced.

The directions to the sources of ALPA microseisms are shown in Figure IV-6. In this figure the source direction of the peak microseismic noise, measured from frequency-wavenumber spectra, is indicated by an arrowhead. When a clearly discernible secondary peak was present, its source direction is indicated by a circle. On days when an azimuthal continuum of energy was present, the range of source azimuths for this energy is indicated by a line. The spectral levels of the total microseismic energy are shown at the bottom of the figure.

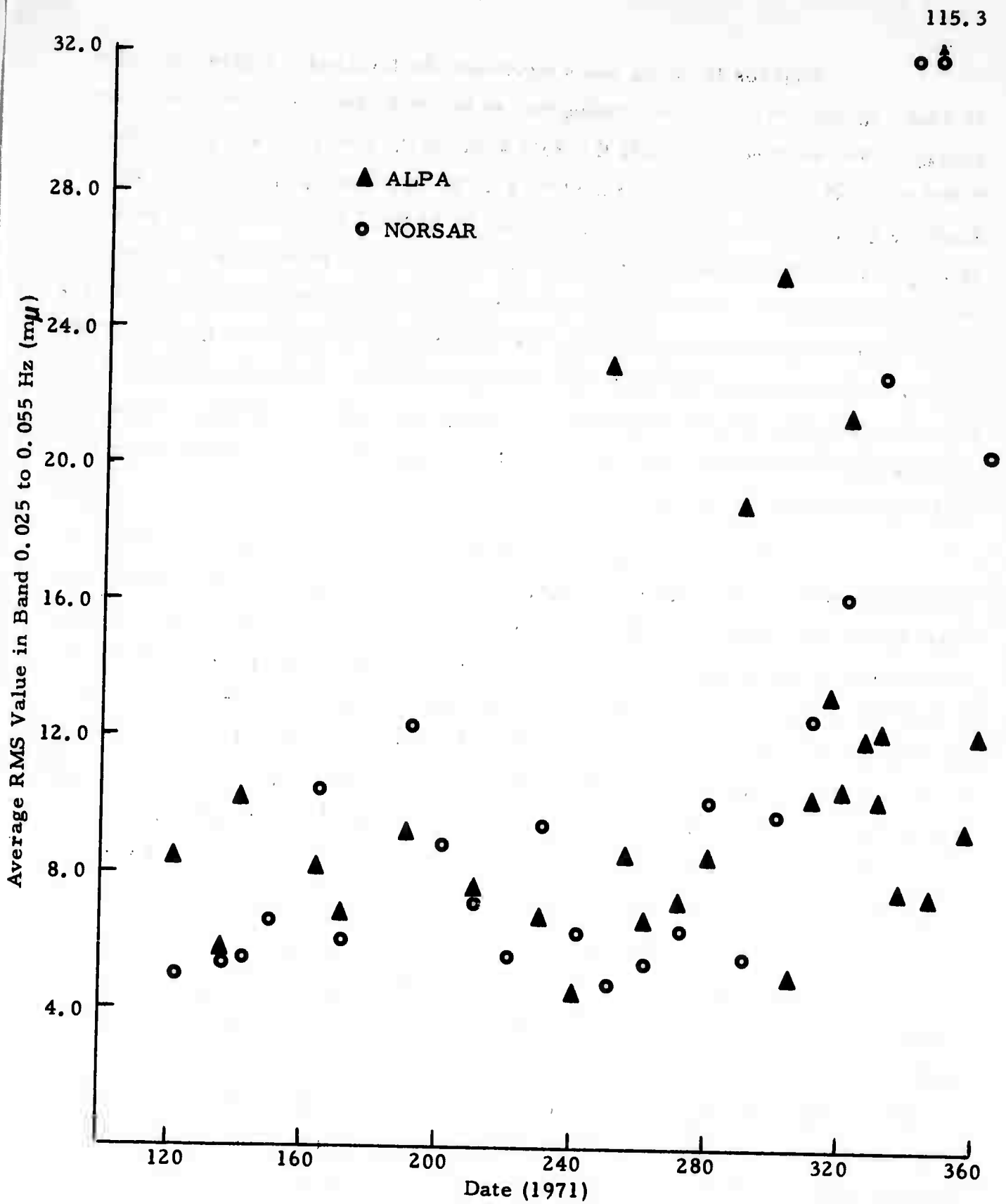

AVERAGE RMS NOISE LEVELS AT ALPA AND NORSAR IN 0.025 TO 0.055 Hz BAND (VERTICAL COMPONENT)

FIGURE IV-2

IV-4

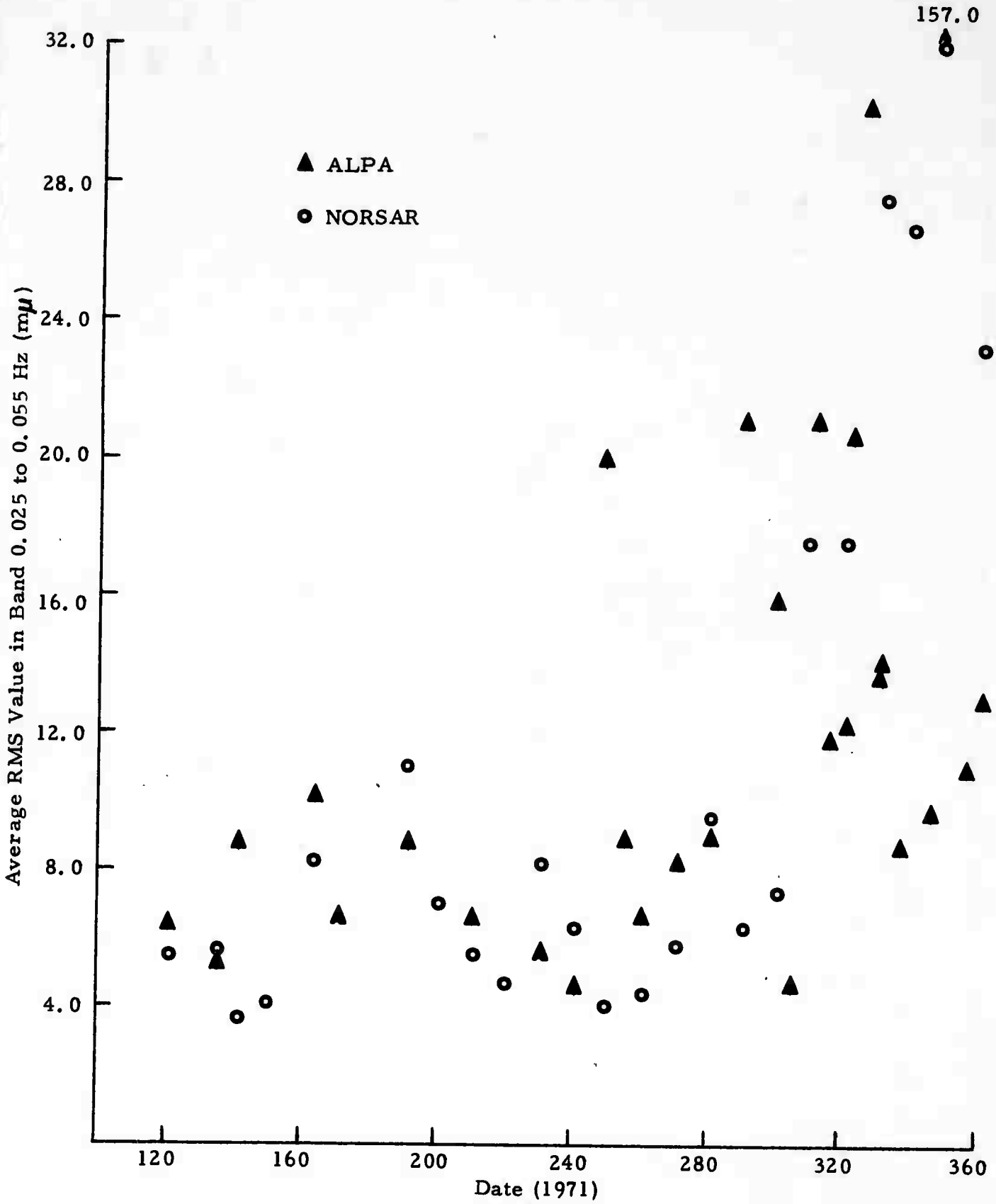

AVERAGE RMS NOISE LEVELS AT ALPA AND NORSAR IN 0.025 TO 0.055 Hz BAND (EAST-WEST COMPONENT)

FIGURE IV-3

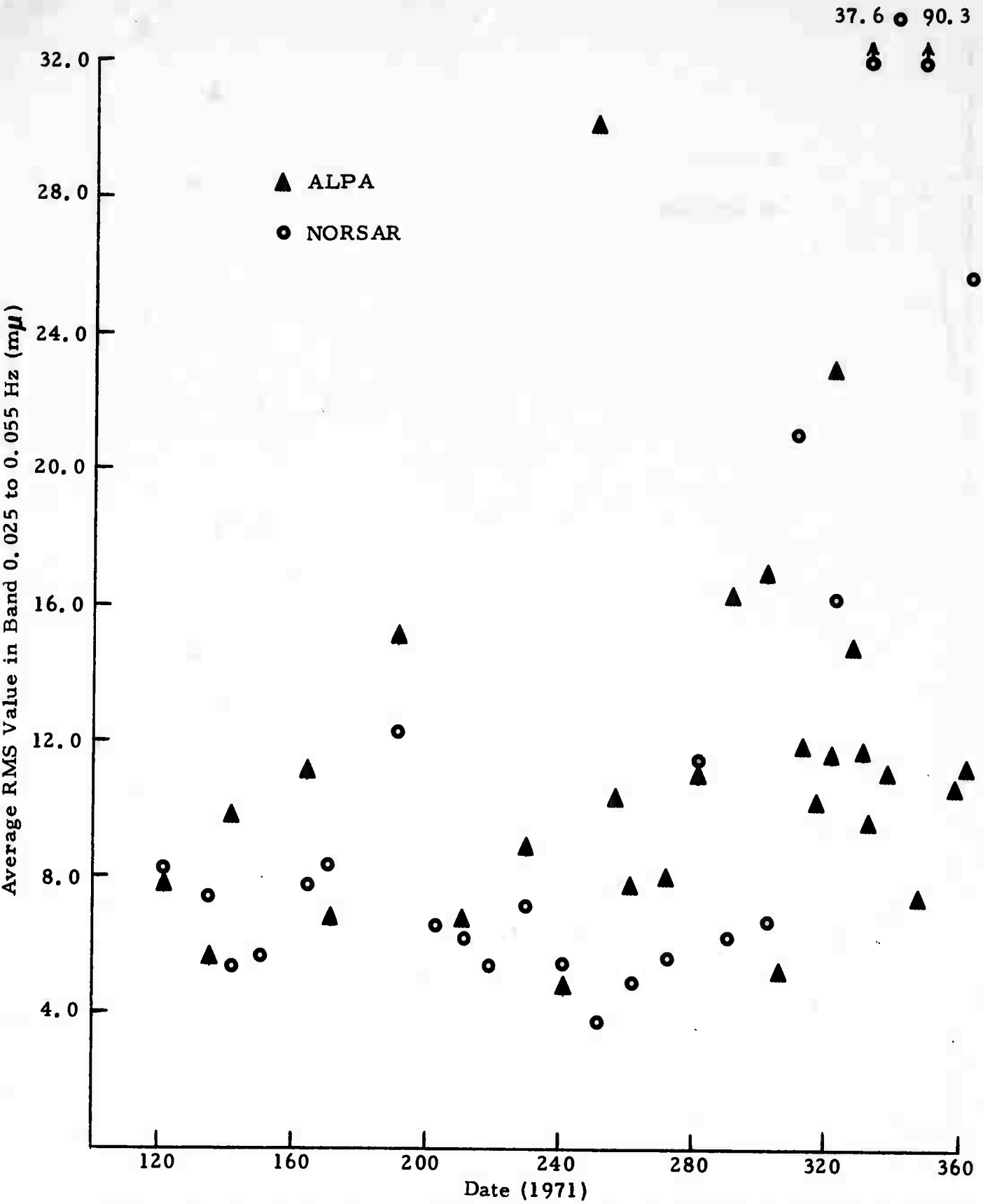

AVERAGE RMS NOISE LEVELS AT ALPA AND NORSAR IN 0.025 TO 0.055 Hz BAND (NORTH-SOUTH COMPONENT)

FIGURE IV-4

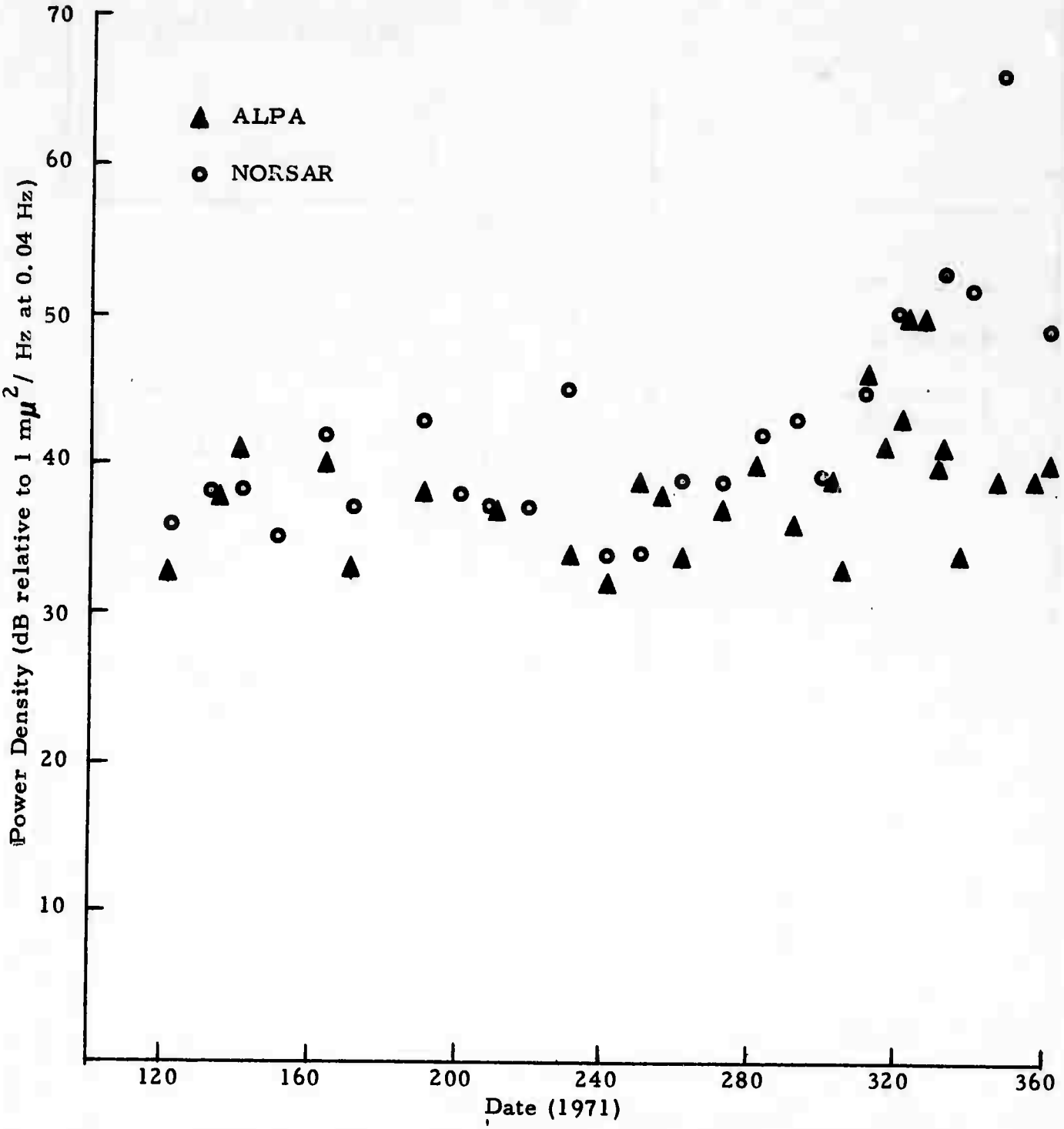

PEAK POWER DENSITY LEVELS IN 15 TO 20 SECOND BAND AT ALPA AND NORSAR

FIGURE IV-5

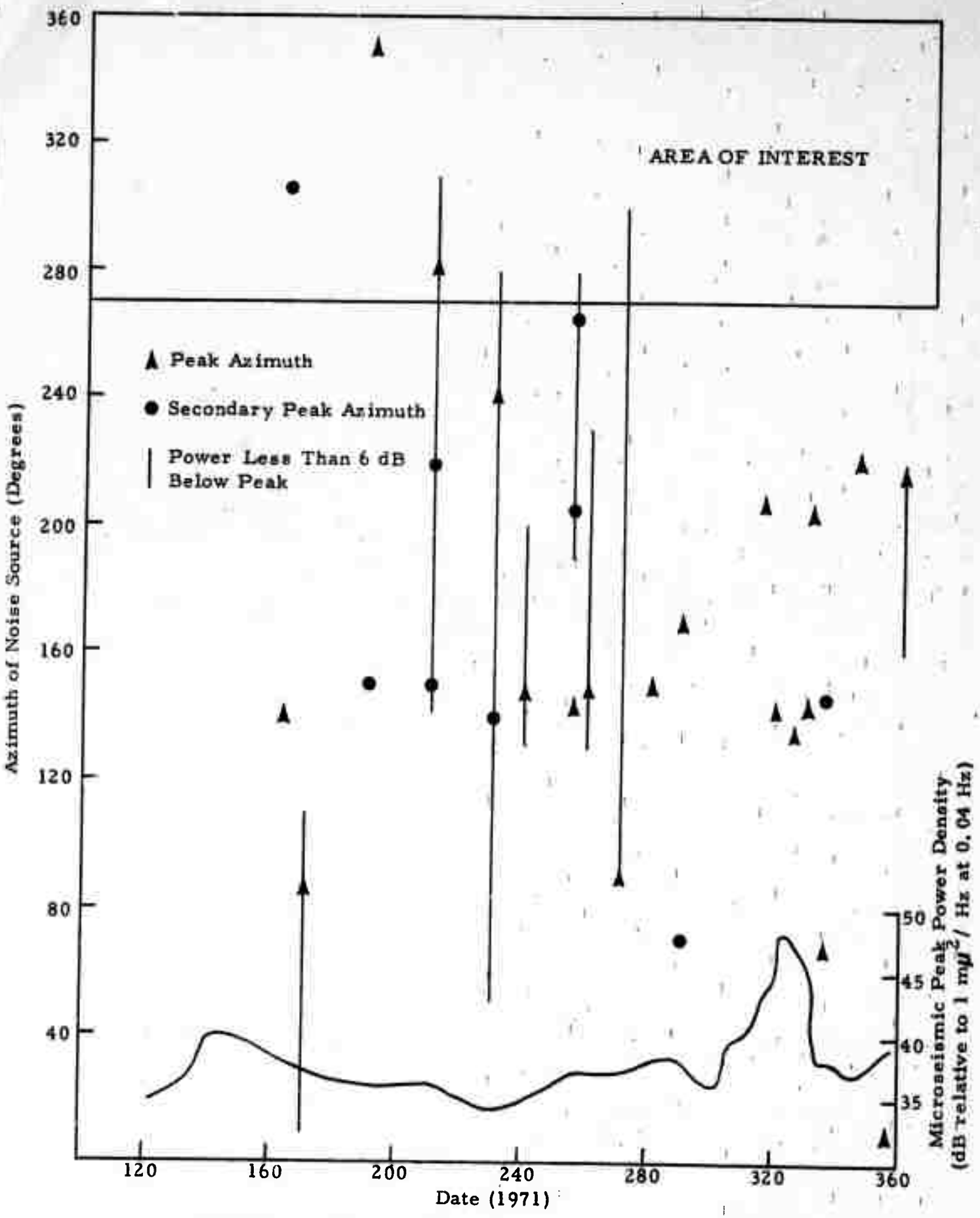

VERTICAL COMPONENT NOISE SOURCE AZIMUTHS

FIGURE IV-6

IV-8

The predominant source direction during 1971 was in the vicinity of 140°, which coincides with the western Canadian and United States coastlines. Only rarely do the sources fall in the range of azimuths to the area of interest (270° to 360°). The figure also suggests that the noise tends to have an isotropic distribution of sources only on fairly quiet days, but this is possibly an artifact of the way in which the data are presented. This is suggested by the following considerations. Continua are indicated only when their levels are six dB or less below the peak value of the frequency-wavenumber spectra. On days when strong point sources are present the residual isotropic noise, if it exists, tends to be masked. Thus it is possible that there is a low level isotropic component at all times, but this only becomes evident on days when the more directional components are relatively weak. The important observation, however, is that strong directional sources rarely coincide with directions to the area of interest.

The efficacy of beamsteering the nine-sites located in the southern half of ALPA has been reported previously in the Long Period Final Report (Harley, 1971). It is of interest to compare the performance of this subarray with that of the full array. In addition, it has been observed that sites 6, 12, 13, 14, 15, 16, and 17 typically have lower noise levels in the signal processing band than do the other sites of the array. Thus the performance of an array composed of these sites is also of interest. Vertical component weighted beamsteers were formed for a suite of the 1971 noise samples. In each case three beams were formed; one using the nine sites available during 1970, one using the full array, and one using the optimal seven sites listed above. Surface wave velocities and a 340° source azimuth were used in forming the beams. Note that on any particular day only the well recorded sites of the array or subarray were used in forming the beams. The output measure in each case was the RMS value of the noise in the 0.025 to 0.055 Hz bandpass.

These results are presented in Figure IV-7. As expected the full array beams always result in lower noise levels than do the subarray beams. Comparison of the nine-site subarray beams with the optimal seven-site beams does not indicate a marked preference for either one. The high output level of the nine-site beam on day 250 results from the fact that of the eight sites used in the beam, only three had normal noise levels. The remaining five sites showed abnormally high noise levels at periods greater than twenty seconds. The sites used in the seven-site beam tended to have lower noise levels. As a result both the seven-site and the full array beams showed lower output noise levels. The poor performance of the seven-site beam on day 281 results from the fact that only three of the seven sites were available for processing.

The ratio of nine-site array to full array output noise, averaged over the fifteen samples is 1.33, suggesting a difference in surface-wave detectability of 0.12 M_s units. In the most extreme case (day 250) the ratio is 1.71, corresponding to 0.23 M_s units. The theoretical result for nine vs. nineteen sites, assuming $\sqrt{n}$ noise suppression, suggests a difference of 0.16 M_s units. As discussed in section III beamsteer signal degradation will be slightly more severe with nineteen sites than with nine. Thus it would appear that on the average the nineteen-site array will provide no more than 0.1 M_s units of increased detectability over the nine-site array.

In summary it appears that the anomalous long-period noise problem observed during 1970 has been apparently alleviated. During 1971 high long-period noise appeared occasionally on a few sites, particularly during the period day 240 to day 320. In the period day 320 to day 360, the ALPA noise levels were only slightly above those observed during the summer. Only rarely do the sources of microseisms at ALPA coincide with directions to the area of interest. The RMS value of beamsteered noise in the band 0.025 to 0.055 Hz ranges from 1.5 to 3.0 mμ. If some seven-site subset rather than the full array is used in forming the beams it appears that the average increase in output noise will be less than a factor of 1.5.

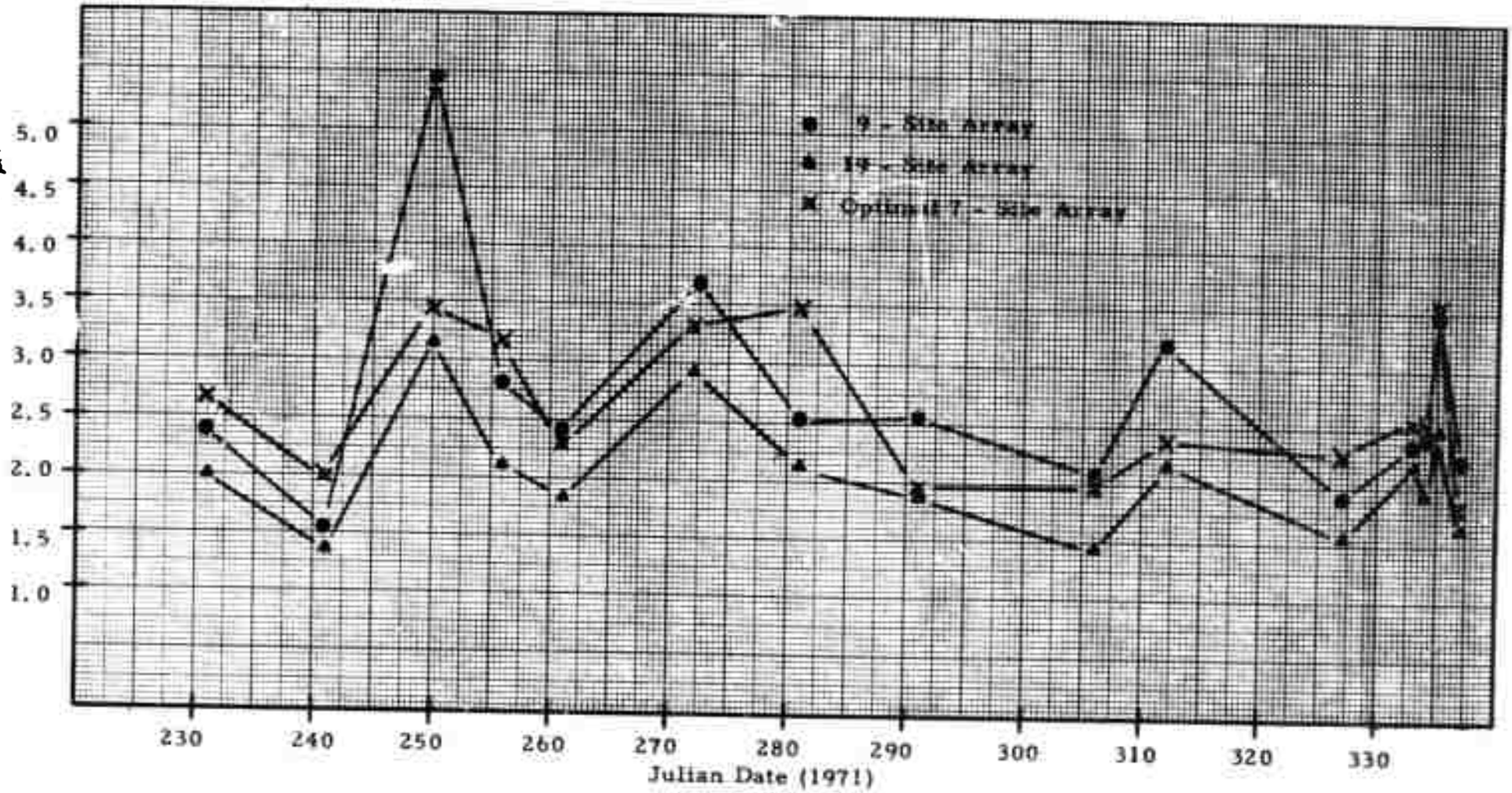

NOISE OUTPUT OF BANDPASSED BEAMSTEER PROCESSORS

FIGURE IV-7

SECTION V

TWO-COMPONENT PROCESSING GAINS

It appears possible that after beamsteering and bandpass filtering the vertical and radial components of the Rayleigh wave, additional signal-to-noise ratio (SNR) enhancement can be realized by properly combining the outputs of the two beams. Recognizing that in theory the vertical and radial components of the fundamental mode Rayleigh wave are related at each frequency by an appropriate scalar and a ninety-degree phase shift, a simple means of accomplishing this involves scaling the two beams, delaying the radial component by ninety degrees, and summing. It has been observed empirically that the use of frequency independent scale factors of 0.5 for both components results in acceptable signal preservation (Harley 1971). Proceeding in this manner, if the noise in the two beam outputs is completely incoherent one would expect a noise suppression of 3 dB from the two-component processor. If the noise is to some extent coherent, then the processing gain is less predictable. In view of the situation at ALPA, however, greater gains might be expected occasionally. The azimuths to most sources of interest lie in the northwest quadrant, that is, between 270° and 0°. Coherent noise sources are largely confined to southerly directions. The predominant source azimuth for noise is near 140°. Thus the noise tends to come from the back azimuth and the coherent Rayleigh-wave noise on the signal-oriented radial component will lag that noise on the vertical component by ninety degrees. After delaying the radial component by ninety degrees to align the two-component signal, the two components of this noise will be exactly 180° out of phase and should tend to cancel.

In practice only about 2 dB SNR gains have been observed with this technique at ALPA (Harley 1971). Further experimentation with the technique has been conducted in an effort to refine these results. Fifty-three of the events listed in Table II-1 were processed using this technique.

The results will be discussed first with regard to the theoretical considerations mentioned above. For 25 of the events the RMS value of the noise in the band 0.025 to 0.055 Hz was computed for both the vertical and radial components and averaged. The ratio of this average to the corresponding RMS value of the two-component output noise was then computed. The average of this ratio over the 25 cases is a measure of expected noise suppression and proved to be 1.9 dB. The largest ratio observed in any of these cases was 3.9 dB. These results indicate that the theoretical suppression of 3.0 dB for random noise is not realized on the average, and that additional gains stemming from the back azimuth theory are almost never observed. There are two probable reasons for the latter result. Microseismic energy which one would expect to be coherent occurs largely at frequencies above the band considered here. Secondly, beam-steering the vertical and radial components will in all likelihood reduce any coherence that existed between those two components of noise at any given site.

The ratio of the peak signal value in the two-component output to the average of the vertical and radial peak signal values was also examined. This ratio averaged over sixteen large events was found to be 1.01. This suggests that when the signal amplitudes are similar on the two components, they are preserved by the processor. When there is a noticeable difference between the peaks on the two components, the processor yields a peak value somewhere between those two peaks.

Combining these results it would appear that the two-component processor will yield an average SNR gain of about two dB and only on very rare occasions will this range as high as four dB. It is important to note, however, that the comparison here is between the processor output SNR and the average of the SNR's on the two input components. In the practical case where the processor output is compared to the input component having the highest SNR, the processor gain would be expected to be less.

Two-component signal-to-noise ratios, defined as the ratio (in dB) of the peak value of the signal to the RMS value of the preceding noise, were computed

from the two-component bandpassed output trace for the 34 events which were detected. The SNR gain from two-component processing was then computed for these events by subtracting from the two-component SNR in dB the SNR of the better of the LR vertical or LR radial bandpassed trace. The bandpass was 0.025-0.055 Hz. The results of this computation are presented in Table VI-9. The following observations concern these results.

- The SNR gain observed was quite variable, and surprisingly low values occurred fairly frequently. This probably is the result of several factors. In many cases the noise and/or the signal had significantly different levels on the vertical component than on the radial component. As a result one of the two was a high SNR component in comparison with the other. The processor output compared quite favorably with the poorer component, but the valid comparison is with the better of the two input components. (This is the comparison presented in Table VI-9.) In such cases the processor output was little better than, or even inferior to, the high SNR component. A second reason for the variability stems from the fact that some of the events were fairly small, and presumed measurements of the signal were really measurements of signal plus noise. When the processor attenuated the noise, it appeared that signal attenuation had occurred. Thus the measured SNR improvement for such events was biased low.

- The average SNR gain for the events listed was 0.8 dB. In view of the bias mentioned above it is likely that this value is slightly lower than the true expected value of gain. It is not likely, however, that the true value of SNR gain is appreciably greater than one dB. As

noted above, when the processor output SNR is compared to the average SNR of the two components only 1.9 dB of improvement is observed on the average. Here, where the comparison is with the better of the two components a lesser value will result. Thus it appears that the true average SNR gain is between one and two dB.

- On occasion somewhat higher values of SNR gain do occur. (The largest value in Table VI-9 is 3.4 dB.)

To summarize, it appears that, on the average, the SNR of the less noisy of the vertical and radial components can be improved by two dB or less. Occasionally the improvement is somewhat higher, but it appears unlikely that it will ever be greater than four dB.

SECTION VI
MATCHED FILTER RESULTS

A. INTRODUCTION

Matched filtering as a method of SNR improvement was examined using both master events and chirp waveforms. SNR improvement results for 65 events which were detected in chirp filter output traces and 56 events which were detected in master waveform matched filter output traces are discussed below. These results are compared to results obtained earlier using the initial nine-site array (Harley 1971). All events were bandpass-filtered before matched filtering using a 0.025-0.055 Hz bandpass. True signal-to-noise ratios (SNR's) were used in the present study to obtain matched filter results. Each SNR was calculated as the ratio of the peak value of the signal to the RMS value of the noise in a gate ahead of the signal. The SNR improvement of a matched filtered beam over the corresponding bandpassed beam is then the difference in dB between the SNR's for the two beams. Processing was done in the same manner for each of the three components of each waveform—Transverse (T), Vertical (V), and Radial (R).

B. MASTER WAVEFORM MATCHED FILTER RESULTS

1. Routine Processing Results

A suite of 21 master events has been selected to evaluate master waveform matched filtering. The selection criteria were good SNR, shallow focus, and location in an area of interest. The approximate locations of the master events are shown in Figure VI-1 and Table VI-1 gives the name and pertinent data for the event corresponding to each numbered location in the figure. Slashes are used within event names in Table VI-1 to designate events occurring in 1970 and reported earlier (Harley 1971); the asterisks are used in naming those events occurring in 1971 and listed in Table II-1.

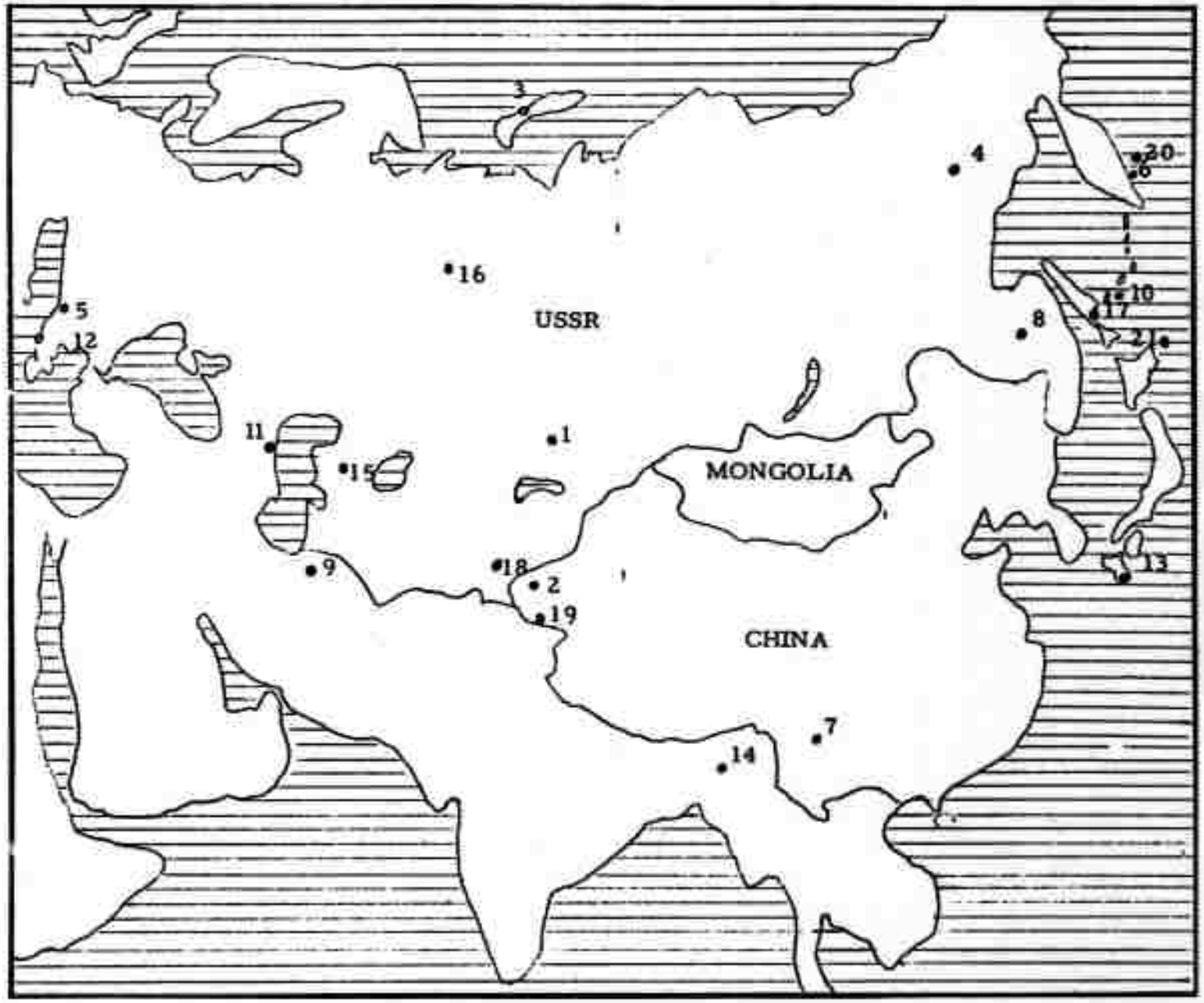

FIGURE VI-1

MASTER EVENT LOCATIONS

TABLE VI-1

MASTER WAVEFORM EVENT DATA

Event Name	Date M/D/Y	Time (hr-min-sec)	Lat. (^{o}N)	Lon. (^{o}E)	Depth (km)	m_b	Location number Fig. V-1
KAZ/249/04	9/06/70	04-02-57	49.8	78.1	0	5.6	1
CHI/210/05	7/29/70	05-50-56	39.9	77.8	13	5.2	2
CRS/287/05	10/14/70	05-59-57	73.3	55.1	0	6.7	3
SIB/156/10	6/05/70	10-31-54	63.4	146.2	33	5.5	4
ALB/231/02	8/19/70	02-01-53	41.4	19.8	33	5.2	5
KAM/242/00	8/30/70	00-38-40	52.1	159.6	33	5.2	6
CHI/212/13	7/31/70	13-10-47	28.6	103.6	25	5.5	7
ERS/241/14	8/29/70	14-59-23	51.1	135.3	33	5.4	8
IRA/242/16	8/30/70	16-17-31	37.4	56.0	33	5.1	9
KUR/219/01	8/07/70	01-43-19	43.8	148.3	33	5.0	10
CAU/137/06	5/17/70	06-49-06	43.0	46.9	33	5.0	11
GRC/184/00	7/03/70	00-41-01	38.7	20.4	33	5.1	12
KYU/206/22	7/25/70	22-41-11	32.2	131.7	34	6.1	13
BUR/210/10	7/29/70	10-16-19	26.0	95.4	59	6.5	14
WKZ/357/07	12/21/70	07-00-57	43.8	54.8	0	6.1	15
URL*082*06	3/21/71	06-59-56	61.3	56.5	0	5.6	16
SAK*251*16	9/06/71	16-59-53	48.0	143.0	16	5.9	17
TAD*205*11	7/22/71	11-43-39	39.5	73.2	33	5.6	18
SIN*219*15	8/05/71	15-21-53	36.1	77.7	33	4.8	19
KAM*206*03	7/23/71	03-45-05	52.6	160.7	33	4.5	20
KUR*190*16	7/07/71	16-44-16	43.5	147.7	46	4.5	21

The master events were matched filtered against themselves; the time of occurrence of the peak in the output waveform was used along with the event origin time and distance from ALPA in order to arrive at an effective "velocity of propagation" of the matched filter output peak for that master event. This velocity was in turn used to calculate an expected time of occurrence of the matched filter output peak for each test event filtered with that master waveform. The maximum deviation in seconds from the expected peak occurrence time (considering all three components) is listed in Table VI-2 for each test event. Better than 90% of the peaks for events detected by master waveform matched filtering fell within a time gate of $\pm$170 seconds from the expected arrival time. This percentage could be increased if adjustment were made in cases of those master waveforms for which the computed arrival time shows a consistent bias with respect to the actual arrival time (e.g., the KAZ/249/04 master event data).

The SNR improvements obtained from master waveform matched filtering of 56 events are also given in Table VI-2, along with the master-test event separation distance in kilometers for each event. Exact comparisons between the present results and earlier reported results (Harley 1971) are impossible because different bandpasses were used. However, in the comments on the present results which follow, certain general similarities and differences in the two sets of results will be noted.

There is substantial variation in the SNR improvement from event to event (Table VI-2), even for events which are close to the master event. For example, in the case of the KAZ/249/04 master, more than five dB difference in LR vertical component SNR improvement was found between two events within thirty kilometers of the master event. Similar event-to-event variations were observed in the earlier results.

In the present results there is a general tendency toward larger SNR improvement for the LR vertical component than for the LR radial component, as was observed in the earlier study. Overall, SNR improvement for the LR vertical component averages 3.5 dB as opposed to 2.7 dB for the LR-radial

TABLE VI-2

MASTER WAVEFORM MATCHED FILTER IMPROVEMENTS
(PAGE 1 OF 4)

Event Designation	Master/Test Event Separation (km)	Max. Time Delay (sec.)	dB SNR Improvement Over the Equivalent Bandpass Filter (0.025 - 0.055 Hz)			SNR Improvement of 2-Component Matched Filter Over Conventional Matched Filter (LR-V or LR-R)
			T	V	R	
KUR/219/01	←(Master)					
KUR*191*03AL	53	+18	1.0	4.8	2.3	--
KUR*190*16AL	59	+13	1.5	4.1	2.5	--
KUR*191*14AL	60	+41	0.0	3.7	4.9	--
KUR*203*22QC	60	+63	-0.2	5.3	3.8	--
KUR*185*15QD	65	+27	0.1	4.6	2.3	--
KUR*230*23AL	216	-49	0.0	ND*	ND	ND
KUR*225*06AL	324	-12	ND	2.6	ND	0.0
HOK*185*19QC	329	-53	2.4	2.0	-0.9	--
HOK*214*07AL	474	+28	4.2	1.6	2.8	-0.6
KUR*226*14AL	591	-88	ND	ND	-0.2	--
KUR*216*08AL	597	+13	ND	0.6	4.8	-0.4
Average Improvements for KUR/219/01 Master			1.1	3.3	2.6	-0.5
KAM/242/00	←(Master)					
KAM*206*03AL	93	+121	4.4	-1.2	-0.2	-0.2
KAM*204*08AL	100	+125	4.6	2.4	4.4	0.6
KAM*206*08AL	104	-37	4.2	2.8	3.4	0.4
KAM*193*02AL	114	-18	4.9	2.2	3.4	--
KUR*199*12QC	217	+40	1.0	0.6	0.8	--
KUR*213*02AL	271	-55	4.6	7.0	6.6	0.2
KUR*206*00AL	455	-38	ND	5.6	6.8	0.8
Average Improvements for KAM/242/00 Master			4.0	2.8	3.6	0.4

* ND = Not detected

TABLE VI-2

MASTER WAVEFORM MATCHED FILTER IMPROVEMENTS
(PAGE 2 OF 4)

Event Designation	Master/Test Event Separation (km)	Max. Time Delay (sec.)	dB SNR Improvement Over the Equivalent Bandpass Filter (0.025 - 0.055 Hz) T	V	R	SNR Improvement of 2-Component Matched Filter Over Conventional Matched Filter (LR-V or LR-R)
CHI/210/05	← (Master)					
SIN*237*06QC	84	+55	0.8	3.2	1.6	2.6
SIN*281*09AL	159	+11	ND	5.4	3.4	1.8
SIN*184*04AL	201	-13	4.0	7.9	6.2	--
TAD*205*11AL	396	+14	3.4	5.8	4.8	2.0
SIN*219*15AL	422	-127	7.0	3.6	-0.4	2.2
SIN*221*01AL	529	+83	0.0	-3.6	-0.6	1.8
HIN*182*14AL	901	-35	-1.2	1.1	-1.0	--
TIB*302*17AL	979	+178	-1.8	-0.8	-0.6	0.0
Average Improvements for CHI/210/05 Master			1.7	2.8	1.7	1.7
CAU/137/06	← (Master)					
CAU*283*09AL	236	-77	ND	3.6	4.0	-0.4
CAU*288*17AL	282	-72	-5.8	3.6	2.2	-1.0
TUR*251*22AL	327	-172	0.8	4.4	4.0	-0.6
SWR*200*20AL	902	+167	ND	1.3	2.6	--
Average Improvements for CAU/137/06 Master			-2.5	3.2	3.2	-0.7
IRA/242/16	← (Master)					
IRA/288/14AL	99	+34	2.0	3.8	0.4	-1.0
IRA/221/02QE	322	+197	2.0	6.8	4.6	-1.0
IRA/237/00QC	1079	+147	ND	5.2	ND	-0.6
Average Improvements for IRA/242/16 Master			2.0	5.3	2.5	-0.9

TABLE VI-2

MASTER WAVEFORM MATCHED FILTER IMPROVEMENTS
(PAGE 3 OF 4)

Event Designation	Master/ Test Event Separation (km)	Max. Time Delay (sec.)	dB SNR Improvement Over the Equivalent Bandpass Filter (0.025 - 0.055 Hz)			SNR Improvement of 2-Component Matched Filter Over Conventional Matched Filter (LR-V or LR-R)
			T	V	R	
KAZ/249/04	← (Master)					
EKZ*115*03AL	0	+3	6.4	3.2	2.4	--
EKZ*364*06R2	11	+52	4.0	4.2	4.6	1.0
EKZ*081*04AL	13	+57	-0.8	6.2	ND	--
EKZ*282*06AL	23	+61	ND	2.0	1.0	0.8
EKZ*294*06AL	23	+53	ND	5.2	4.0	0.0
EKZ*333*06N2	30	+108	ND	1.0	-1.4	--
EKZ*157*04QC	31	-105	-2.4	5.0	-1.2	--
EKZ*170*04QC	49	+155	-0.7	1.2	-0.2	--
KAZ*273*12AL	708	+35	ND	-0.6	-1.2	0.8
CRS*236*16QC	966	+80	1.4	0.4	0.0	0.8
Average Improvements for KAZ/249/04 Master			1.3	2.8	0.9	0.7
CHI/212/13	← (Master)					
CHI*283*05AL	1013	-31	-1.6	ND	ND	--
TIB*278*05AL	1123	-92	2.2	ND	ND	--
Average Improvements for CHI/212/13 Master			0.3	--	--	--
CRS/287/06	← (Master)					
NVZ*270*05AL	33	+47	5.0	7.8	6.8	0.2
TAD*205*11	← (Master)					
KGZ*301*14AL	275	--	-3.6	5.4	3.4	3.4
TAD*274*16AL	280	--	1.2	1.2	3.0	2.8
Average Improvements for TAD*205*11 Master			2.4	3.3	3.2	3.1

TABLE VI-2

MASTER WAVEFORM MATCHED FILTER IMPROVEMENTS
(PAGE 4 OF 4)

Event Designation	Master/Test Event Separation (km)	Max. Time Delay (sec.)	dB SNR Improvement Over the Equivalent Bandpass Filter (0.025 - 0.055 Hz)			SNR Improvement of 2-Component Matched Filter Over Conventional Matched Filter (LR-V or LR-R)
			T	V	R	
SAK*251*16	← (Master)					
SAK*182*14AL	111	-113	1.0	3.0	6.3	--
SAK*248*18AL	35	+15	7.4	4.4	4.4	1.4
SAK*251*11AL	25	+9	6.8	4.8	7.0	1.4
SAK*270*19AL	25	-13	5.4	5.4	4.8	-0.2
Average Improvements for SAK*251*16 Master			5.2	4.4	5.6	0.9
ERS/241/14	← (Master)					
ERS*256*14AL	134	+34	5.0	4.4	2.4	-0.4
CHR*266*21RT	1064	+52	1.0	5.0	ND	-3.0
Average Improvements for ERS/241/14 Master			3.0	4.7	--	-1.7
WKZ/357/07	← (Master)					
WKZ*356*06RZ	684	-220	1.6	5.6	3.0	0.8
WRS*295*05AL	911	-22	ND	3.8	ND	-1.6
Average Improvements for WKZ/357/07 Master			--	4.7	--	-0.4
Average Master Waveform Improvements			2.1	3.5	2.7	0.5

component. An exception to this tendency was found in both studies in the case of events processed with the Kamchatka master event (KAM/242/00). In the present study the LR radial component averages about 0.8 dB greater improvement than the LR vertical component (3.6 dB vs 2.8 dB). This fact adds to the evidence of apparently anomalous behavior of the LR vertical and LR radial components of signals from this region, and also was noted in the two-component processing study discussed previously.

Matched filtering the LQ transverse components of the events of the present study yielded a generally smaller SNR improvement than either the LR vertical or LR radial components, particularly in the case of events from the Asian continent. Overall SNR improvement for the LQ-transverse component averaged only 2.1 dB. The Kamchatka (KAM/242/00) and Sakhalin Island (SAK*251*16) matched filters yielded better results however, achieving average improvements of 4.0 and 5.2 dB, respectively. Love wave amplitudes from the Sakhalin Island events were substantially larger than the Rayleigh wave amplitudes for those events. It is likely that the master event and at least some of the test events were on the same fault.

One of the differences observed between present results and the earlier results is the greater region-to-region consistency of the present average SNR improvements, especially for the four regions for which the greatest number of events were processed; Kurile Islands (KUR/219/01), Eask Kazakh (KAZ/249/04), Sinkiang (CHI/210/05), and Kamchatka (KAM/242/00). Average SNR improvement results were within 0.5 dB in the present study, and were identical for three of the four regions. Differences in average SNR improvement among these regions of more than five dB were observed in the earlier study. One possible explanation for this fact is that in the present study the greater number of events in the suite of test events for each master tended to smooth out the relatively large event-to-event variation in SNR improvement.

Another difference between present and earlier results is the generally lower SNR improvements in the present study. Earlier master waveform

matched filter improvements exceeded five dB in 27% or more of the cases studied; the five dB SNR improvement figure was exceeded in only 17% of the present cases. This difference comes mainly from the following sources.

- The earlier SNR improvement calculations used measurements of signal peaks only, with the assumption that for all events both bandpass and matched filters affected the RMS noise equally. However, as shown later, some of the master waveform matched filters were observed to yield larger RMS noise outputs than the equivalent bandpass filter. Thus the previous estimates probably were biased high.
- Test events of the present study were generally smaller than events of the earlier study. A given amount of corrupting noise in the filtered signal outputs will tend to reduce measured SNR ratio improvements more for small test events than for large ones.
- Some of the master-test event separation distances were significantly larger in the present study, which would tend to result in poorer matching between the master and test event.

In Figure VI-2 master waveform matched filter improvements for the LR vertical signal component are plotted as a function of master-test event separation. Although there is considerable scatter, the trend is toward decreasing improvement for greater distances.

Examples of the difference in effect on RMS noise between a master waveform matched filter and a bandpass filter are given in Table VI-3. Noise samples preceding nine test events were filtered with the KAZ/249/04 master waveform matched filter and the 0.025-0.055 Hz bandpass filter. The ratio of the RMS noise output from the master waveform filter to the RMS noise

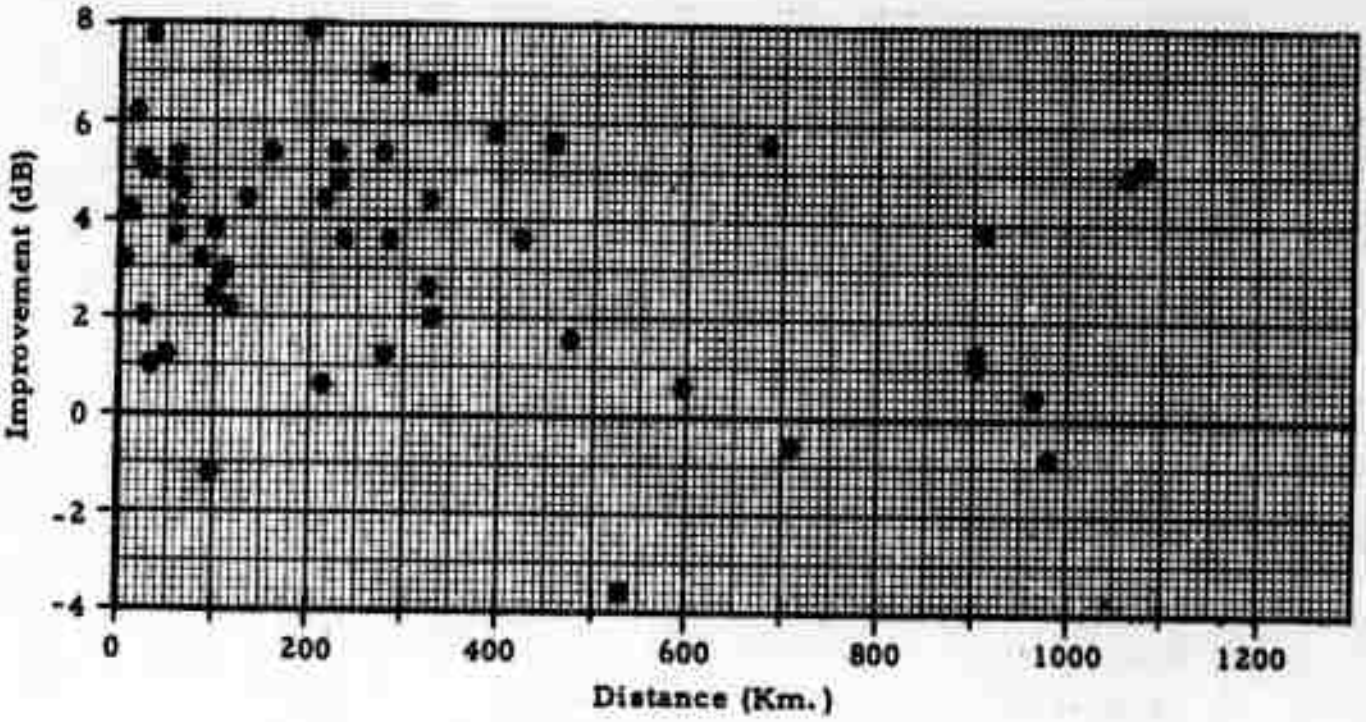

FIGURE VI-2

MASTER WAVEFORM MATCHED FILTER IMPROVEMENT VS. MASTER/TEST EVENT SEPARATION

TABLE VI-3

RATIO OF
MASTER WAVEFORM MATCHED FILTER RMS NOISE OUTPUT
TO BANDPASS FILTER RMS NOISE OUTPUT IN dB

Events Which Noise Sample Precedes:	(Matched Filter RMS Noise Out/ Bandpass Filter Noise Out) dB		
	T	V	R
EKZ*115*03	4.6	3.0	-0.1
EKZ*364*06	-4.2	1.8	-3.4
EKZ*081*04	-1.6	1.0	-1.8
EKZ*282*06	--	1.0	-1.4
EKZ*294*06	-3.2	1.2	-2.0
EKZ*157*04	-3.2	0.8	--
EKZ*170*04	-3.6	3.4	-2.0
KAZ*273*12	--	1.4	-1.8
CRS*236*16	-4.6	0.8	-3.4

output from the bandpass filter was computed from each noise sample and converted to dB. These dB values are shown in Table VI-3. Positive values indicate greater RMS noise in the matched filter output, which must be made up for by an increase in the peak signal out of the matched filter in order to show a net SNR gain over the bandpass filter. In the case of the LR vertical component data in Table VI-3, the master waveform matched filters showed an average of 1.6 dB higher RMS output noise level than the bandpass filter. Table VI-3 also shows evidence of a significant variation from sample to sample in the relative effect of the matched filter and bandpass filter on the RMS noise. This variability is a result of the effect of the spectral shape of the matched filter on the differing spectral contents of the various noise samples.

2. Investigation of the Performance of Different Master Waveforms on Events from the Same Region

An implicit assumption in the discussion of the master waveform matched filtering results given in Table VI-2 is that the master waveform selected for each region is nearly optimum for events from that region. In order to explore this assumption, events from two regions, already processed with one master, were processed with a second master waveform from the same region. In each case the second master waveform was chosen from the suite of events processed with the first matched waveform. It was selected insofar as possible on the basis of an anomalously low SNR improvement when processed with the first master waveform; the assumption being that the poor performance was due to a significant difference in waveform. The first alternate matched filter chosen was the event KAM*206*03, from the suite of events processed with the KAM/242/00 master waveform. The second was the event SIN*219*15, from the suite of events processed with the CHI/210/05 matched filter. The results of processing each suite of events with two masters are given in Table VI-4. The figures given represent true SNR improvement in dB.

In the case of the suite of Sinkiang events (CHI/210/05 and SIN*219*15 masters), the CHI/210/05 master performs better than the SIN*219*15 master

TABLE VI-4

MATCHED FILTER IMPROVEMENTS FOR TWO SUITES OF EVENTS PROCESSED WITH ALTERNATE MASTER WAVEFORMS

MASTER EVENT / TEST EVENT	Separation	CHI/210/05 T	CHI/210/05 V	CHI/210/05 R	Separation	SIN*219*15 T	SIN*219*15 V	SIN*219*15 R
SIN*237*06	84	0.8	3.2	1.6	491	0.0	2.2	-0.4
SIN*184*04	201	4.0	7.9	6.2	594	6.4	6.6	2.8
TAD*205*11	396	3.4	5.6	4.8	546	0.6	1.6	1.8
SIN*221*01	529	0.0	-3.6	0.6	828	-2.2	-1.0	-3.8
HIN*182*14	901	-1.1	1.0	-1.0	843	-2.0	0.2	1.4
Average		1.4	2.8	2.4		0.6	1.9	0.4
MASTER EVENT / TEST EVENT	**Separation**	**KAM/242/00**			**Separation**	**KAM*206*03**		
KAM*204*08	100	4.6	2.4	4.4	11	4.6	5.0	4.2
KAM*206*08	104	4.2	2.8	3.4	65	4.4	4.2	4.0
KAM*193*02	114	4.9	2.2	3.4	73	4.7	2.1	2.3
KUR*199*12	217	1.1	0.6	-0.8	310	-1.0	-5.8	1.5
KUR*213*02	271	4.6	7.0	6.6	364	2.8	-1.0	7.0
KUR*206*00	455	-	5.6	6.8	547	-	-1.4	0.0
Average		3.9	3.4	4.0		3.1	0.5	3.2

in four out of five cases for each component. The greatest average gain in SNR improvement, two dB, occurs on the radial component.

The results for the KAM/242/00 and KAM*206*03 masters show a case where more than one master waveform is needed in order to process optimally all events from a region. In the case of the vertical component, the KAM/242/00 master outperforms the KAM*206*03 master by an average of 1.3 dB on three events; on the remaining three events the relative performance of the two masters is reversed, and the difference in performance for these three events averages 7.1 dB. Overall, the KAM/242/00 master outperforms the KAM*206*03 master by an average of 0.8 dB on the transverse and radial component, and by 2.9 dB on the vertical component.

Results of this study suggest that it may often be worthwhile to try several master events from a given region in order to find the best master event for that region. Results for the Kamchatka region show that in some cases two or more master events may be needed to achieve the maximum possible master waveform matched filter SNR gains for all events from the region.

3. Effect of Filter Length on Master Waveform Matched Filter Performance

In theory, the optimum length for a master waveform matched filter is the full length of the observed wave train. However, if effects such as multipathing cause dissimilarities among later portions of the wave trains of events from the same region, the optimum filter length may be less than the full event length. Lengths for the master waveforms listed in Table VI-1 were selected by comparing the master event waveforms with the waveforms for a large test event, where available, and selecting the portion of the waveform where the events showed good agreement.

To examine the effect of length on filter performance analytically, master events KAM*206*03 and KUR*190*16 each were divided into six matched filters of increasing length. Each of these matched filters then was applied to a suite

of test events. The lengths in seconds of each set of six matched filters, designated by the suffixes A through F, are given in Table VI-5. The two master waveforms and the segments into which they were divided are shown in Figures VI-3 and VI-4. All of the matched filters began at the same point. SNR improvements resulting from application of these matched filters are shown in Tables VI-6 through VI-8.

In the case of the KUR*190*16 event matched filter B (the second shortest matched filter) gave the best average results for the Love wave energy. Matched filter A is too short, and F is too long. Filters C, D, and E are about as good as B. For the Rayleigh waves matched filters B through F gave essentially the same results but filter A was too short. For both waves there is very little difference between the optimum filter length found by this test and the filter length which would have been chosen visually as containing most of the significant energy in the master waveform. For the Rayleigh component, there is 0.4dB or less difference in SNR improvement performance for filter lengths ranging from 494 through 1022 seconds.

The shortest matched filters chosen showed best SNR improvement performance overall in the case of the KAM*206*03 event. The difference in performance between the best matched filter for the transverse component (matched filter A) and the one which would have been chosen visually (matched filter D) is less than one dB. The difference is more pronounced in the case of the LR vertical and radial components, however. The filter which would have been chosen visually (matched filter E) exhibits more than 2.5 dB poorer performance than filter A.

These results indicate that the choice of matched filter length can affect the improvement significantly (as much as three or four dB). Note that this variability with filter length is on the same order as the average improvement obtained by master waveform matched filtering. Thus it appears that the matched filter length must be varied if optimum results are to be obtained. We plan to study this more thoroughly in the future; it is possible that many of our

TABLE VI-5

WAVEFORM LENGTHS - MASTER WAVEFORM LENGTH STUDY

Waveform Designation	Length (seconds)	
	Love (T)	Rayleigh (V, R)
KUR*190*16A	274	368
KUR*190*16B	464	494
KUR*190*16C	632	690
KUR*190*16D	730	802
KUR*190*16E	800	908
KUR*190*16F	1010	1022
KAM*206*03A	246	230
KAM*206*03B	356	386
KAM*206*03C	456	452
KAM*206*03D	574	590
KAM*206*03E	678	882
KAM*206*03F	1000	1020

TABLE VI-6

SNR IMPROVEMENT—MASTER WAVEFORM LENGTH STUDY

(TRANSVERSE COMPONENT)

(MASTER WAVEFORM KUR*190*16)

TEST EVENT:	A	B	C	D	E	F
KUR*185*15	-1.0	3.0	2.6	2.2	1.6	1.0
KUR*191*03	-1.0	3.8	3.4	2.8	2.6	0.2
KUR*191*14	-0.4	2.0	2.0	2.0	2.0	1.2
KUR*203*22	-2.0	5.3	5.0	4.4	4.3	4.8
HOK*214*07	-2.4	3.6	4.2	4.4	4.6	4.0
Average	-1.4	3.5	3.4	3.2	3.0	2.2

(MASTER WAVEFORM KAM*206*03)

TEST EVENT:	A	B	C	D	E	F
KAM*193*02	4.2	4.8	4.8	4.8	4.8	1.4
KUR*199*12	1.2	0.8	-0.8	-1.2	-1.0	-0.6
KUR*213*02	4.0	3.6	2.8	2.2	2.4	2.4
KAM*206*08	4.6	4.0	4.4	4.2	4.2	4.0
KAM*204*08	4.8	5.0	5.0	4.4	4.6	4.6
Average	3.8	3.6	3.2	2.9	3.0	2.4

TABLE VI-7

SNR IMPROVEMENTS—MASTER WAVEFORM LENGTH STUDY

(VERTICAL COMPONENT)

(MASTER WAVEFORM KUR*190*16)

TEST EVENT:	A	B	C	D	E	F
KUR*185*15	4.0	7.2	8.0	8.6	7.8	7.8
KUR*191*03	6.0	6.8	5.8	6.6	6.8	6.8
KUR*191*14	1.4	5.2	5.8	6.0	5.8	5.4
KUR*203*22	3.2	4.0	5.6	5.6	6.0	5.8
HOK*214*07	4.4	6.0	4.8	3.8	3.6	3.8
Average	3.8	5.8	6.0	6.1	6.0	5.9

(MASTER WAVEFORM KAM*206*03)

TEST EVENT:	A	B	C	D	E	F
KAM*193*02	3.0	3.8	3.4	2.8	2.2	2.0
KUR*199*12	-3.0	-5.6	-6.4	-5.8	-5.8	-5.6
KUR*213*02	7.0	-0.4	0.4	-1.0	-1.0	-2.2
KAM*206*08	4.4	5.6	5.8	4.8	4.2	3.8
KAM*204*08	6.4	5.4	6.0	5.0	5.0	5.4
Average	3.6	1.8	1.8	1.2	0.9	0.7

TABLE VI-8

SNR IMPROVEMENTS—MASTER WAVEFORM LENGTH STUDY

(RADIAL COMPONENT)

(MASTER WAVEFORM KUR*190*16)

TEST EVENT:	A	B	C	D	E	F
KUR*185*15	2.6	5.6	6.0	6.4	6.0	6.0
KUR*191*03	1.8	4.2	3.4	4.4	4.6	4.4
KUR*191*14	2.2	5.0	5.4	5.4	5.4	5.4
KUR*203*22	2.2	4.4	5.2	5.6	6.2	6.4
HOK*214*07	6.0	6.6	6.4	5.6	5.4	5.6
Average	3.0	5.2	5.3	5.5	5.5	5.6

(MASTER WAVEFORM KAM*206*03)

TEST EVENT:	A	B	C	D	E	F
KAM*193*02	3.6	3.6	3.4	3.0	2.4	1.0
KUR*199*12	-0.4	-0.6	-0.6	0.2	0.4	0.4
KUR*213*02	8.0	-0.2	0.8	-1.6	-1.2	-1.0
KUR*206*08	2.8	6.2	5.6	4.6	4.0	2.6
KAM*204*08	6.4	4.8	5.4	3.8	4.2	4.6
Average	5.1	2.8	2.9	2.0	2.0	1.5

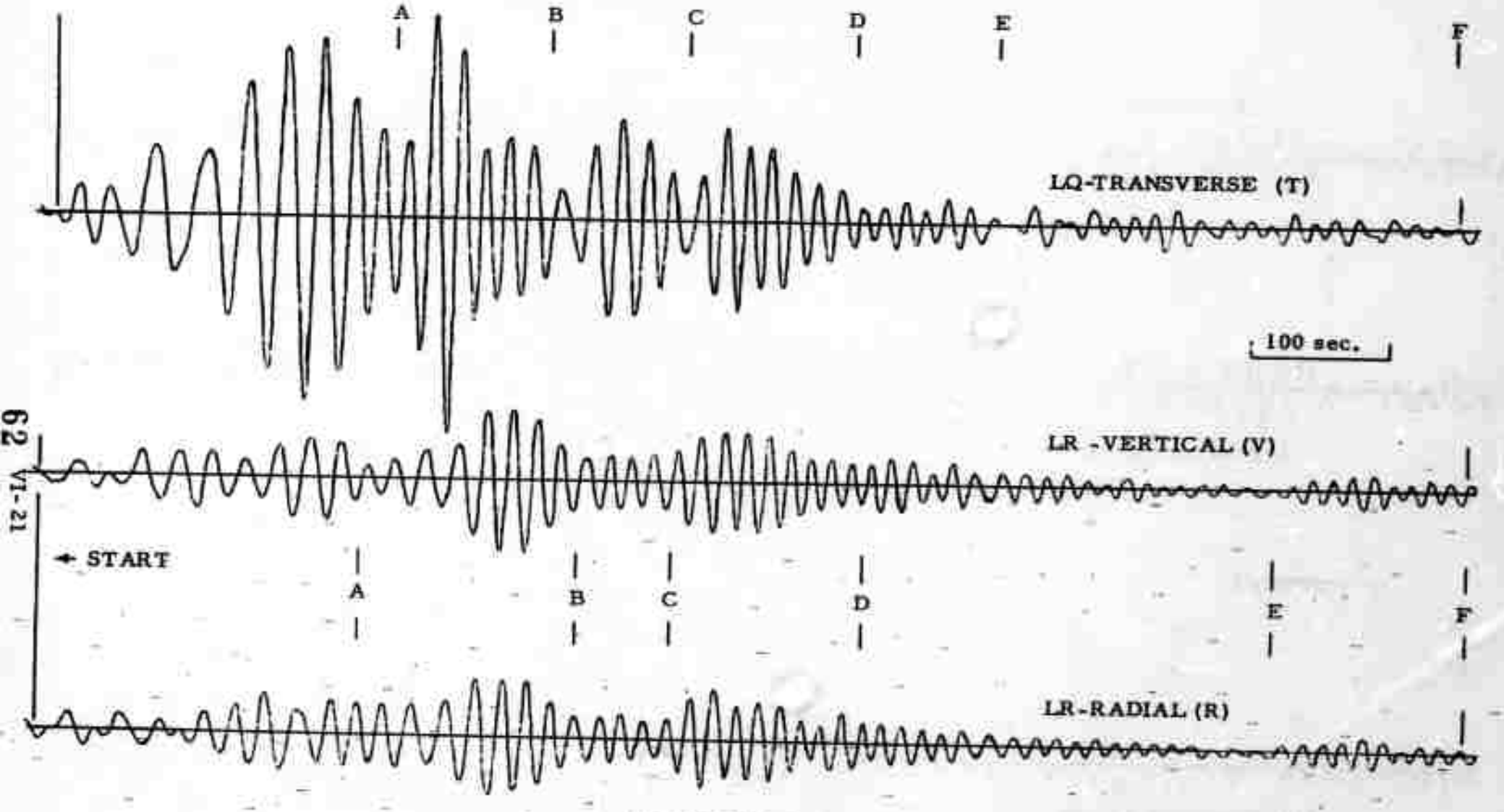

FIGURE VI-4

MASTER WAVEFORM LENGTHS (KAM#206#03)

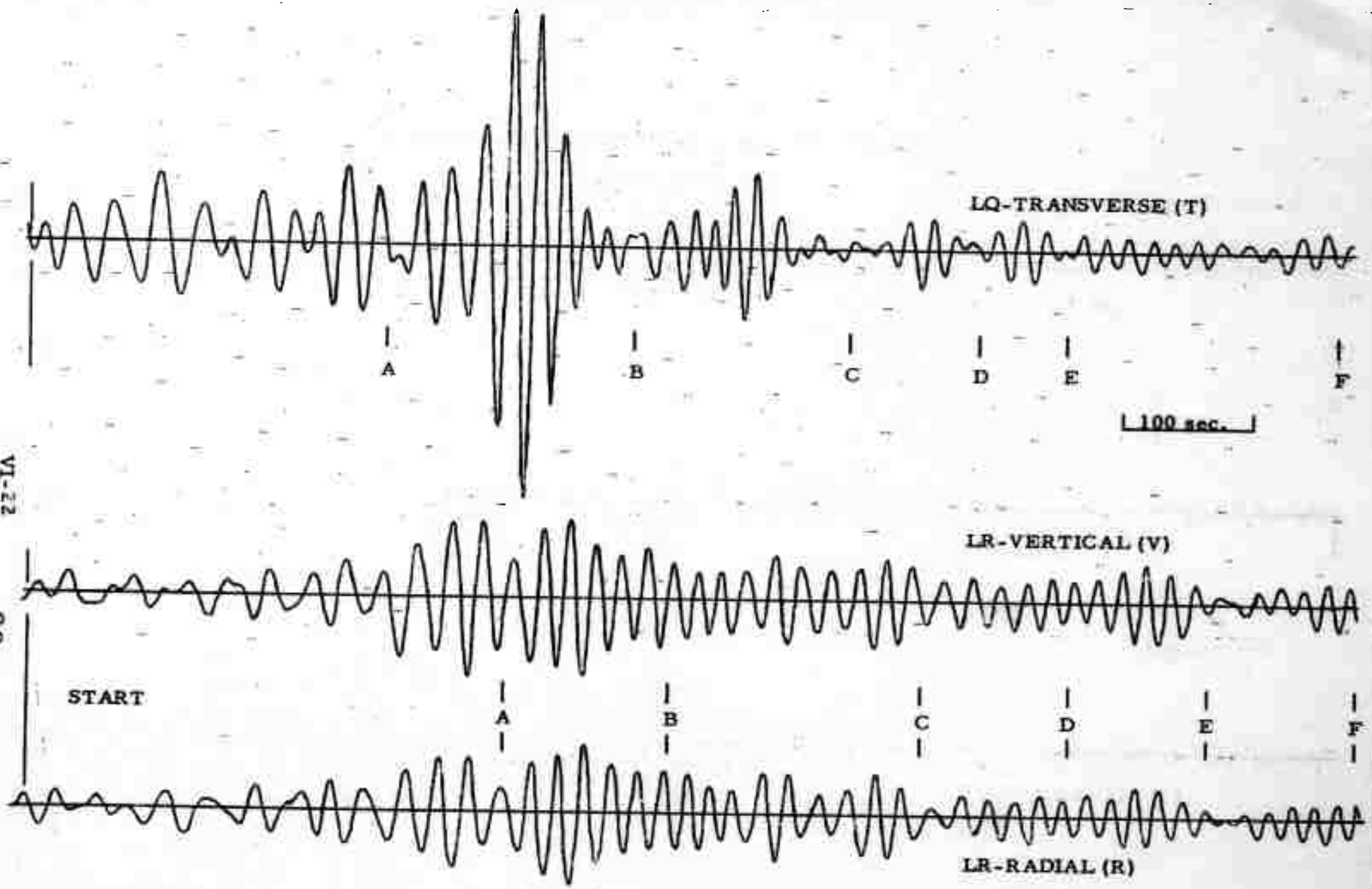

FIGURE VI-3

MASTER WAVEFORM LENGTHS (KUR#190#14)

low SNR improvements can be explained on the basis of incorrect matched filter length.

C. CHIRP FILTER RESULTS

1. Routine Processing Results

Linear chirp matched filters were applied to the beamsteer signal outputs of 65 events, many of which were used in the master waveform matched filter evaluation above. The method of chirp filter design and application has been described earlier (Harley 1971). As before, chirp filter lengths were selected for each region by applying several different length chirps to the region's master event and selecting the length which gave the greatest SNR improvement. To each test event from a given region five chirps were applied with lengths centered about the empirically determined optimum length and differing in length by increments of ± 50 seconds. The improvement for the test event was then measured from the best among these.

Table VI-9 presents the chirp SNR ratio improvements in dB for these 65 events. The average result shows somewhat more variability from region to region than the master waveform results above; however, in the case of the LR vertical component data for the four regions with the greatest number of events, there is a maximum variation of only one dB. For the LR vertical and LR radial components, chirp improvements average slightly better overall than master waveform improvements. The chirp filters and master waveform filters perform about equally well on the transverse component data. Chirp filter improvements exceeded five dB in the same percentage of cases as did master waveform improvements: 17 percent.

The general conclusion concerning relative merits of chirp filtering and master waveform filtering are the same as reached in the earlier study; with the possible exception of Love wave energy for some regions, it appears that chirp filtering is as effective as master waveform processing in SNR improvement.

TABLE VI-9

CHIRP FILTER IMPROVEMENTS AND TWO COMPONENT SIGNAL PROCESSING IMPROVEMENTS

(PAGE 1 OF 4)

Event Designation	Region	dB SNR Improvement Over the Equivalent Bandpass Filter (0.025-0.055 Hz)			SNR Improvement of 2-Component Matched Filter Over Conventional/Matched Filter (LR-V or LR-R)	SNR Improvement of the 2-Component Beam over the Conventional Beam (LR-V or LR-R)
		T	V	R		
KUR*191*03AL	Kurile Islands	1.0	5.1	3.0	--	--
KUR*190*16AL	"	1.2	4.4	3.0	--	--
KUR*191*14AL	"	1.0	4.9	4.7	--	--
KUR*203*22QC	"	-0.5	3.8	2.1	--	--
KUR*185*15QD	"	0.4	5.1	2.4	--	--
KUR*230*23AL	"	0.0	ND*	ND	--	--
KUR*225*06AL	"	ND	2.2	ND	-0.2	-0.8
HOK*185*19QC	"	-0.8	2.7	1.6	--	--
HOK*214*07AL	"	3.6	4.2	2.6	2.2	3.4
KUR*226*14AL	"	ND	ND	2.0	--	--
KUR*216*08AL	"	ND	2.2	0.6	2.2	2.8
HOK*177*08AL	"	3.1	6.0	6.1	--	--
KUR*168*09AL	"	1.4	3.1	1.8	--	--
Average Improvements for Kurile Is. Region		1.0	4.0	2.7	1.4	1.8
KAM*206*03AL	Kamchatka	2.4	3.0	0.8	0.0	-0.6
KAM*204*08AL	"	2.0	3.0	0.4	-1.0	0.4
KAM*206*08AL	"	1.6	2.2	3.6	-0.6	-0.6
KAM*193*02AL	"	5.0	3.4	3.2	--	--
KUR*199*12QC	"	1.4	3.0	3.0	--	--
KUR*213*02AL	"	3.2	4.8	4.6	0.0	0.6
KUR*206*00AL	"	ND	3.4	3.4	-0.6	-0.4
KAM*168*08AL	"	2.3	4.0	5.0	--	--
Average Improvements for Kamchatka Region		2.6	3.4	3.0	-0.4	-0.1

*ND= Not Detected

TABLE VI-9

CHIRP FILTER IMPROVEMENTS AND TWO COMPONENT SIGNAL PROCESSING IMPROVEMENTS
(PAGE 2 OF 4)

Event Designation	Region	dB SNR Improvement Over the Equivalent Bandpass Filter (0.025-0.055 Hz) T	V	R	SNR Improvement of 2-Component Matched Filter Over Conventional/Matched Filter (LR-V or LR-R)	SNR Improvement of the 2-Component Beam over the Conventional Beam (LR-V or LR-R)
SIN*237*06QC	Sinkiang	1.0	2.0	0.6	2.0	--
SIN*281*09AL	"	ND	3.8	4.2	2.4	2.0
SIN*184*04AL	"	-0.6	5.1	2.6	--	--
TAD*205*11AL	"	-1.2	6.6	3.0	0.4	2.6
SIN*219*15AL	"	1.8	5.0	2.2	0.6	1.2
SIN*221*01AL	"	2.4	-0.6	-0.8	-0.4	0.0
HIN*182*14AL	"	-1.1	-1.6	0.0	--	--
TIB*302*17AL	"	0.2	2.6	0.6	0.8	0.0
SIN*170*17AL	"	3.2	5.5	2.9	--	--
SIN*170*21AL	"	-2.3	3.4	4.7	--	--
SIN*168*15AL	"	4.7	1.7	1.5	--	--
SIN*167*13AL	"	2.2	2.1	3.0	--	--
Average Improvements for Sinkigan Region		0.9	3.0	2.0	1.0	1.2
CAU*283*09AL	Caucasus	ND	2.2	ND	0.0	-1.4
CAU*288*17AL	"	-1.8	3.0	1.8	-0.4	0.2
TUR*251*22AL	"	-0.9	6.2	6.2	0.4	0.0
SWR*200*20AL	"	ND	2.3	1.9	--	--
Average Improvements for Caucasus Region		-1.4	3.4	3.3	-0.3	-0.4
IRA*228*14AL	Iran	4.8	5.8	2.4	-0.4	0.6
IRA*221*02QE	"	6.4	6.4	7.8	-0.2	0.2
IRA*237*00QC	"	ND	4.8	ND	0.4	2.2
Average Improvements for Iran Region		5.6	5.7	5.1	-0.1	1.0

TABLE VI-9

CHIRP FILTER IMPROVEMENTS AND TWO COMPONENT SIGNAL PROCESSING IMPROVEMENTS
(PAGE 3 OF 4)

Event Designation	Region	dB SNR Improvement Over the Equivalent Bandpass Filter (0.025-0.055 Hz) T	V	R	SNR Improvement of 2-Component Matched Filter Over Conventional/Matched Filter (LR-V or LR-R)	SNR Improvement of the 2-Component Beam over the Conventional Beam (LR-V or LR-R)
EKZ*115*03AL	E. Kazakh	-2.8	2.5	2.5	--	--
EKZ*364*06R2	"	3.0	1.8	5.0	2.8	1.8
EKZ*081*04AL	"	1.2	5.1	1.1	--	--
EKZ*282*06AL	"	ND	2.2	4.0	2.2	--
EKZ*294*06	"	2.0	5.1	6.4	2.3	1.4
EKZ*333*06NZ	"	ND	8.4	2.0	--	--
EKZ*157*04QC	"	ND	4.1	ND	--	--
EKZ*170*04QC	"	1.7	1.0	0.5	--	--
KAZ*273*12AL	"	0.0	1.8	0.4	0.2	0.8
CRS*236*16QC	"	0.0	3.0	2.4	0.6	1.2
Average Improvements for E. Kazakh Region		0.7	3.5	2.7	1.6	1.3
CHI*283*05AL	China	0.0	ND	ND	--	--
TIB*278*05AL	"	ND	0.6	ND	--	--
URL*082*04AL	Ural Mts.	2.0	2.6	3.3	--	--
NVZ*270*05AL	Novaya Zemlya	1.8	6.8	5.4	0.4	1.0
KGZ*301*14AL	Tadzhik	2.0	7.8	4.0	3.0	2.6
TAD*274*16AL	"	1.4	3.8	5.2	2.2	1.6
Average Improvements for Tadzhik Region		1.7	5.8	4.6	2.6	2.1

TABLE VI-9

CHIRP FILTER IMPROVEMENTS AND TWO COMPONENT SIGNAL PROCESSING IMPROVEMENTS
(PAGE 4 OF 4)

Event Designation	Region	dB SNR Improvement Over the Equivalent Bandpass Filter (0.025-0.055 Hz)			SNR Improvement of 2-Component Matched Filter Over Conventional/Matched Filter (LR-V or LR-R)	SNR Improvement of the 2-Component Beam over the Conventional Beam (LR-V or LR-R)
		T	V	R		
SAK*251*16AL	Sakhalin Is.	7.4	7.4	6.4	1.8	2.0
SAK*182*14AL	"	2.7	2.4	2.9	--	--
SAK*248*18AL	"	6.8	4.2	4.2	2.0	1.8
SAK*251*11AL	"	6.4	6.6	5.8	1.4	1.5
SAK*270*19AL	"	5.2	5.2	3.8	-0.4	-0.4
Average Improvements for Sakhalin Is. Region		5.7	5.8	4.7	1.2	1.2
ERS*256*14AL	E. Russia	5.0	2.0	0.6	-0.2	-1.6
CHR*266*21RT	China/Russia Border	0.8	5.2	2.4	-1.4	-1.4
Average Improvements for E. Russia Region		2.9	3.6	1.5	-0.8	-1.5
WKZ*356*06R2	W. Kazakh	ND	5.2	1.4	0.4	0.2
NRS*233*19AL	N. Russia	3.4	4.8	4.6	1.6	1.6
Average Chirp Filter Improvements		2.0	3.9	3.0	0.7	0.8

2. Optimum (Experimental) Chirp Filter Length vs Distance

Plots of best chirp filter length vs distance are presented in Figure VI-5 through VI-7 for the transverse, vertical, and radial components, respectively. The chirp lengths are the best chirp lengths determined as described above. The distances are great circle distances in kilometers between the event epicenters and the ALPA array. For each component, 75 percent or more of these lengths fall within ±100 seconds (as indicated by the dashed lines in Figures VI-5 through VI-7) of a least squares straight line fitted to each set of data. This fact implies that the equation for the least squares line can be used to obtain a good first estimate of the best chirp length to use for routine chirp filter processing of an event from any given epicentral distance. Also included in Figure VI-6 and VI-7 is the curve for the predicted duration of 40 to 18 second (0.025 to 0.055 Hz) Rayleigh wave energy, obtained from an average group velocity curve (Harley 1971). The predicted event durations agree reasonably well with the optimum chirp filter lengths actually observed.

3. Effective Chirp Filter Travel Time vs Distance

Using origin times and observed times of occurrence of the filter output peak for chirp filtered events, plots of travel time vs distance were constructed for transverse and vertical component traces. These plots are presented in Figures VI-8 and VI-9. In the case of the transverse component data, 84 percent of the chirp peaks fell within ±120 seconds of the least squares straight line fit to the chirp travel time data. For the LR vertical data, 92 percent of the peaks fell within ±120 seconds of the least squares straight line. These figures indicate that the chirp peak arrival time can be predicted with accuracy. Reducing the time gate to be searched for peak occurrences reduces the event detection threshold, since the probability of occurrence of a random noise peak which might be mistaken for the event is reduced. Also included in Tables VI-8 and VI-9 are the travel time curves for 25-second (chirp filter center frequency) energy, obtained from an average group velocity curve for continental travelpaths

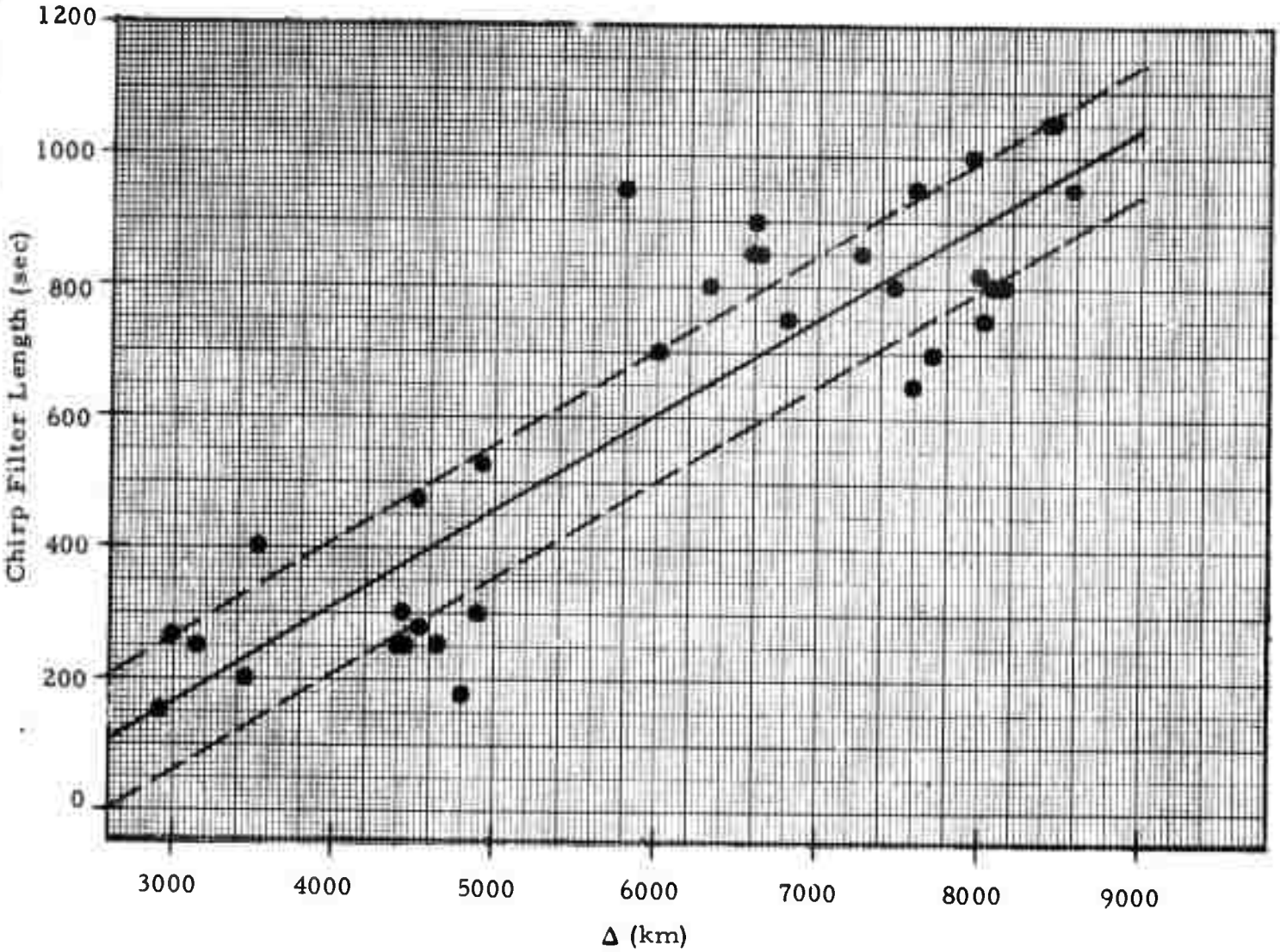

FIGURE VI-5

CHIRP LENGTH VS. DISTANCE-TRANSVERSE COMPONENT

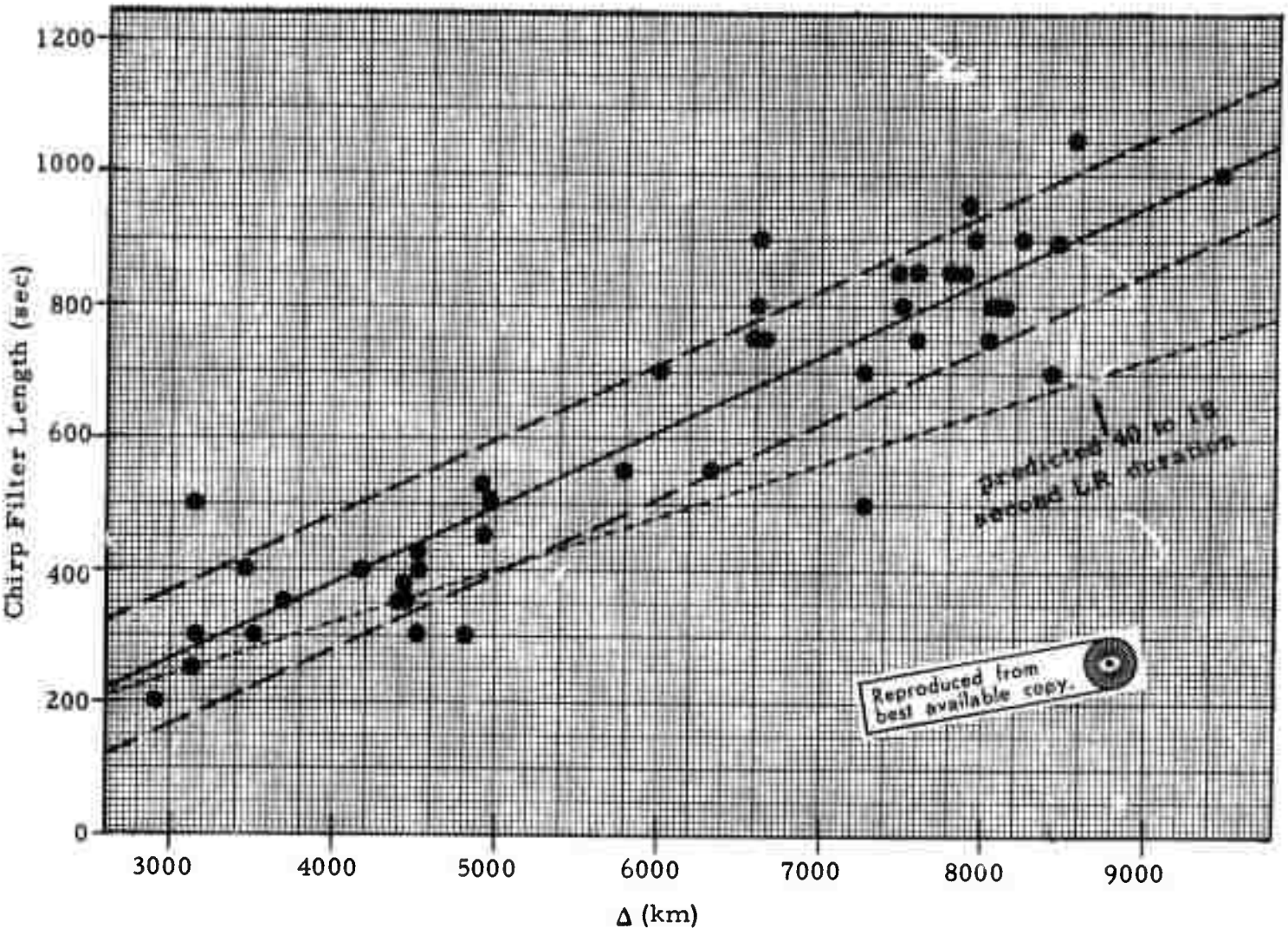

FIGURE VI-6

CHIRP LENGTH VS. DISTANCE-VERTICAL COMPONENT

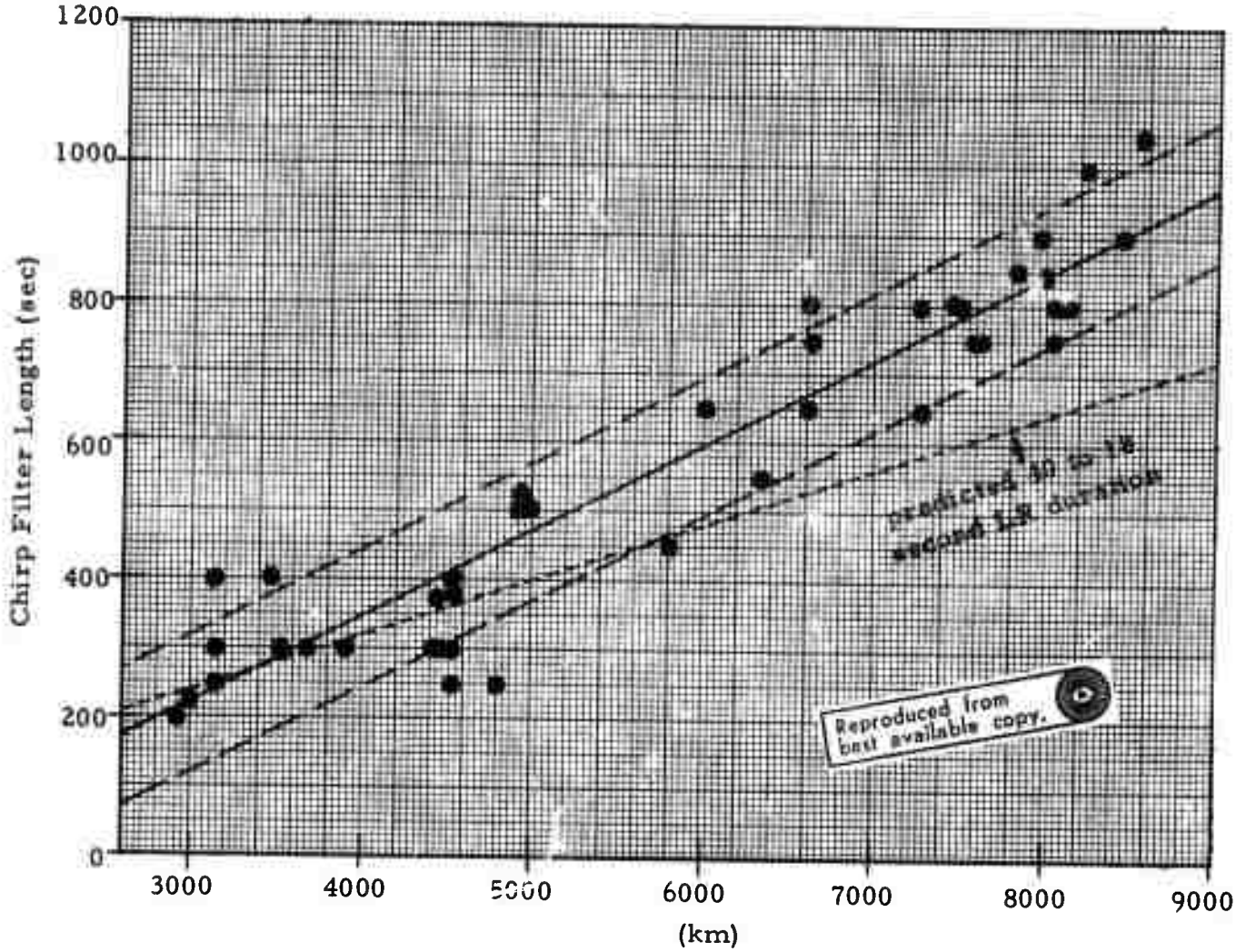

FIGURE VI-7

CHIRP LENGTH VS. DISTANCE-RADIAL COMPONENT

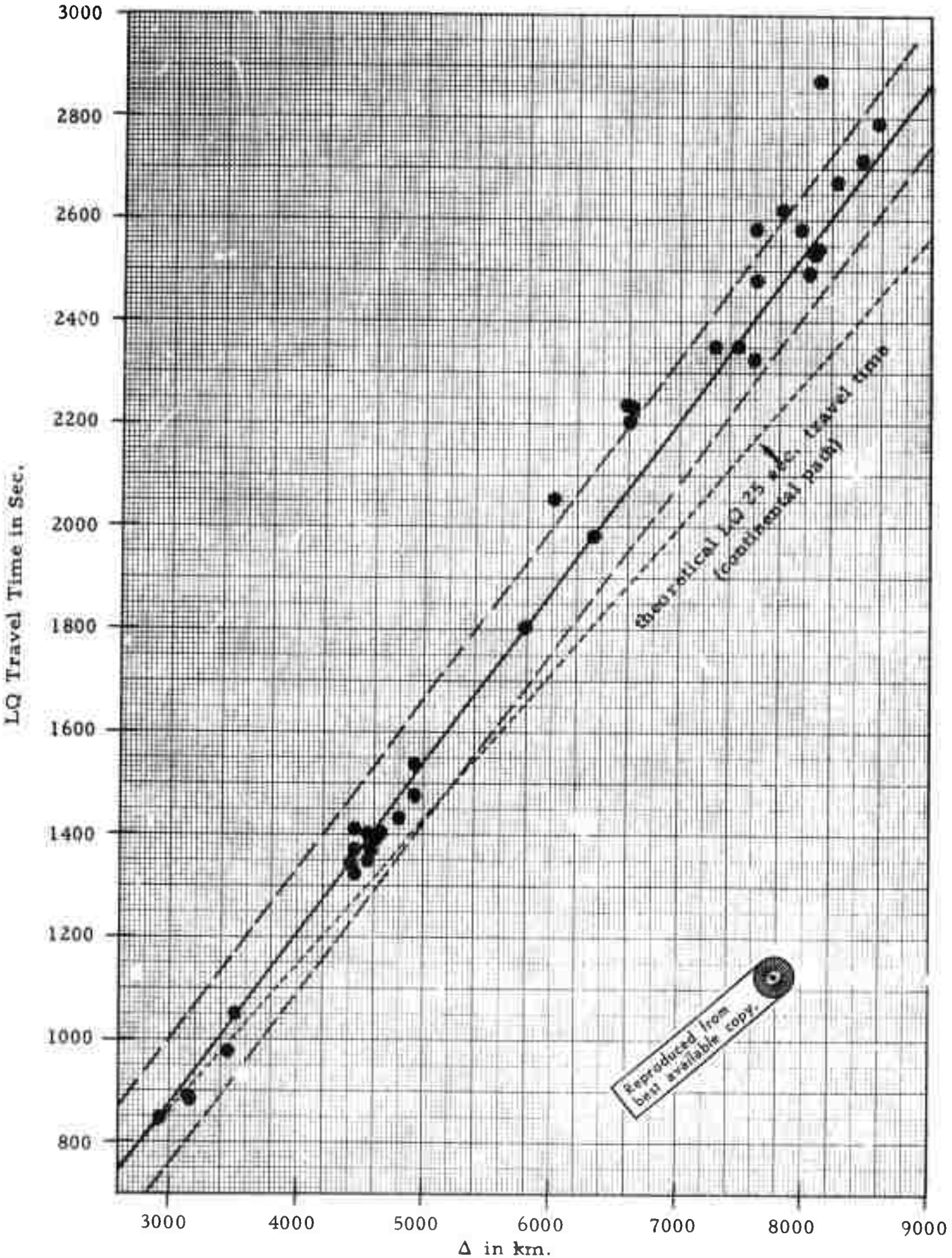

FIGURE VI-8

CHIRP PEAK TRAVEL TIME VS. DISTANCE-TRANSVERSE COMPONENT

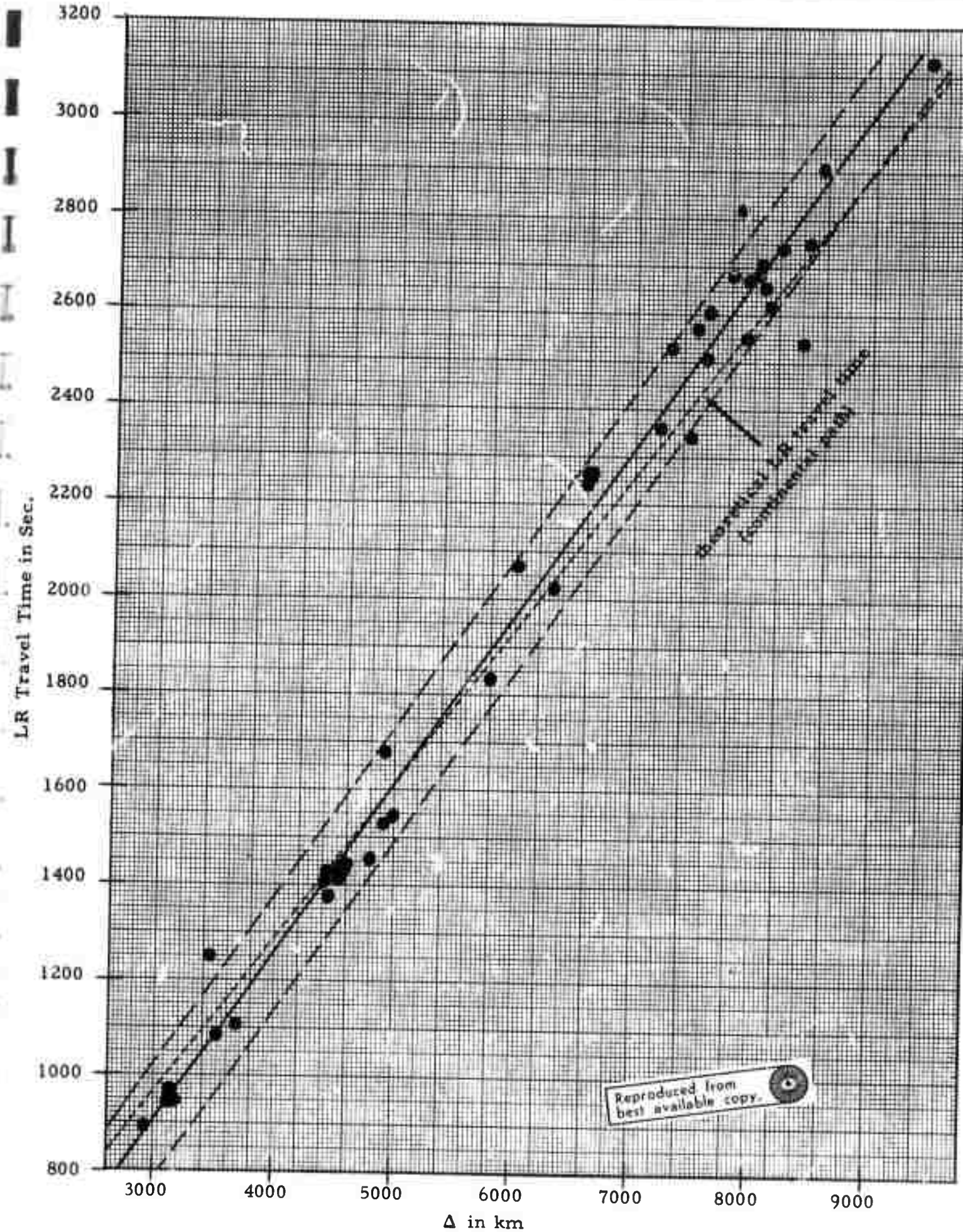

FIGURE VI-9

CHIRP PEAK TRAVEL TIME VS. DISTANCE-VERTICAL COMPONENT

(Oliver 1962). The effective chirp peak travel time curve agrees reasonably well with the theoretical travel time curve in the case of the transverse component data; the agreement is quite good in the case of the vertical component data.

D. TWO-COMPONENT MATCHED FILTER RESULTS

Matched filtering of the two-component output beam was attempted for 46 events. Both master waveform filters and chirp filters were applied. The master waveform filter applied in each case was the LR vertical component of the master event for the region in question; the lengths for the chirp filters were selected as described above. The results of the two-component matched filtering are presented in Table VI-2 for the master waveform processing and in Table VI-9 for the chirp filter processing. The two-component matched filter results for both types of matched filter are presented in terms of the difference in dB between the two-component matched filter output SNR and the SNR of the better of the vertical and radial matched filters. The figures thus represent the additional SNR improvement from two-component matched filtering over standard matched filtering.

The average two-component SNR improvement over the conventional matched filter SNR is 0.5 dB in the case of the master waveform matched filter and 0.7 dB in the case of the chirp matched filter. The two-component chirp results compared to the master waveform results appear to be more nearly correlated with the two-component beam SNR improvements; that is, the two-component chirp filter SNR improvement over the conventional chirp filter is closer in most cases to the observed two-component beamforming gain than is the two-component master waveform SNR improvement over the conventional master waveform filter. As noted in the case of the two-component beamforming results, substantially higher than average gains can be obtained in certain cases. For example, two-component matched filtering of the two events from the Tadzhik region yields more than two dB higher SNR than that of either form of conventional matched filter.

The conclusion of this study is that two-component matched filtering generally preserves the SNR improvement obtained from two-component beamforming.

SECTION VII

S WAVE PROCESSING RESULTS

Long-period S wave beams were formed for 73 of the events listed in Table II-1, using the apparent horizontal S-wave velocity appropriate to each epicentral distance. The curve for S-wave apparent horizontal velocity as a function of epicentral distance was taken from the Array Research Semiannual Technical Report No. 1 (Texas Instruments, 1964). Bandpass filtered (0.025 - 0.055 Hz) S-wave beams were formed for the rotated transverse, vertical, and radial component traces. The amplitude versus period data used in Figure VII-3 were taken from the component which showed the largest S wave amplitude.

A. LONG-PERIOD S-WAVE DETECTION THRESHOLD ESTIMATE FOR ALPA

The histograms in the upper portions of Figures VII-1 and VII-2 show the total number of events processed at each body wave magnitude for Kurile-Kamchatka and Central Asian earthquake populations, respectively. The lower graphs in Figures VII-1 and VII-2 show the detection percentages as a function of m_b. The scatter in the data makes the results difficult to interpret; however, 90 percent probability of S-wave detection appears to occur above $m_b = 5.0$ for the Kurile - Kamchatka events and above $m_b = 5.5$ for the Central Asian events.

B. DISCRIMINATION BY MEANS OF LONG-PERIOD S-WAVE

Figure VII-3 presents S-wave amplitude versus period data for a set of 28 events for which S-waves were detected. Of the events, one is a presumed explosion (designated by the solid triangle in Figure VII-3). The values in Figure VII-3 were normalized to a body wave magnitude of 5.0 and an epicentral

FIGURE VII-1

S-WAVE DETECTION DATA FOR KURILE KAMCHATKA AREA

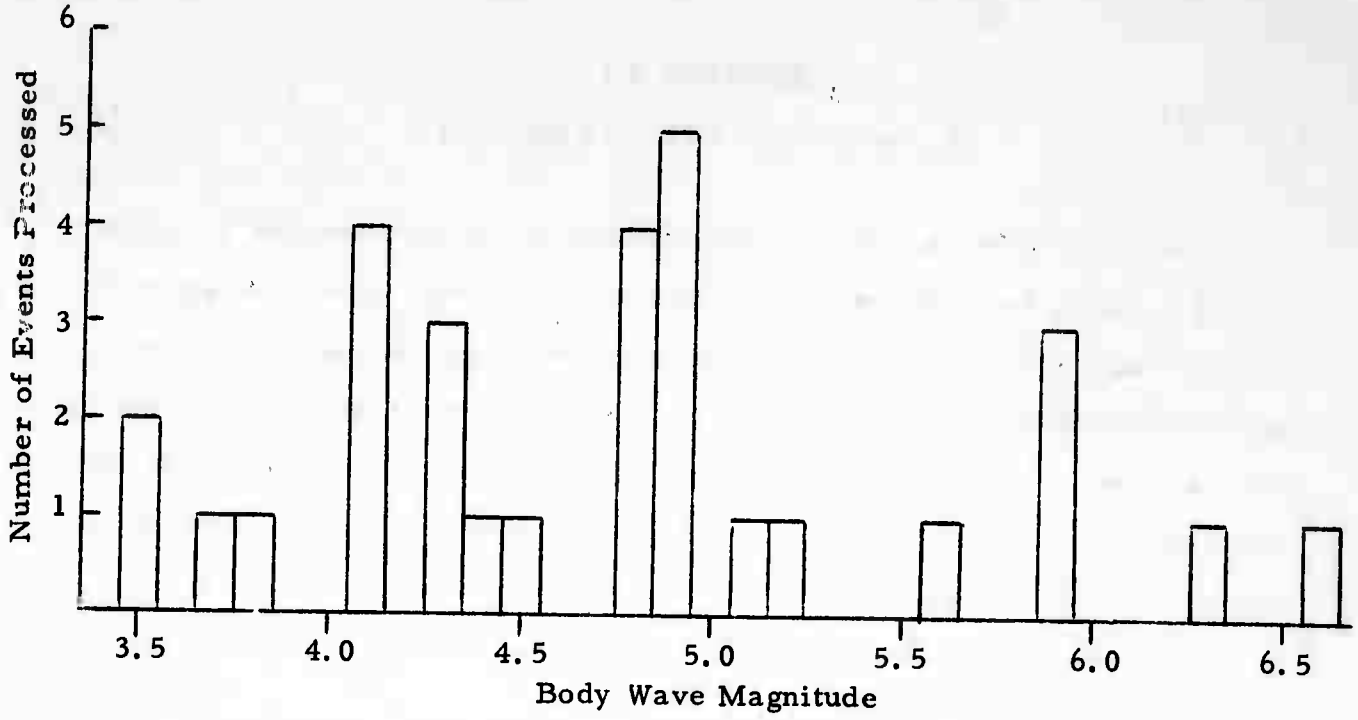

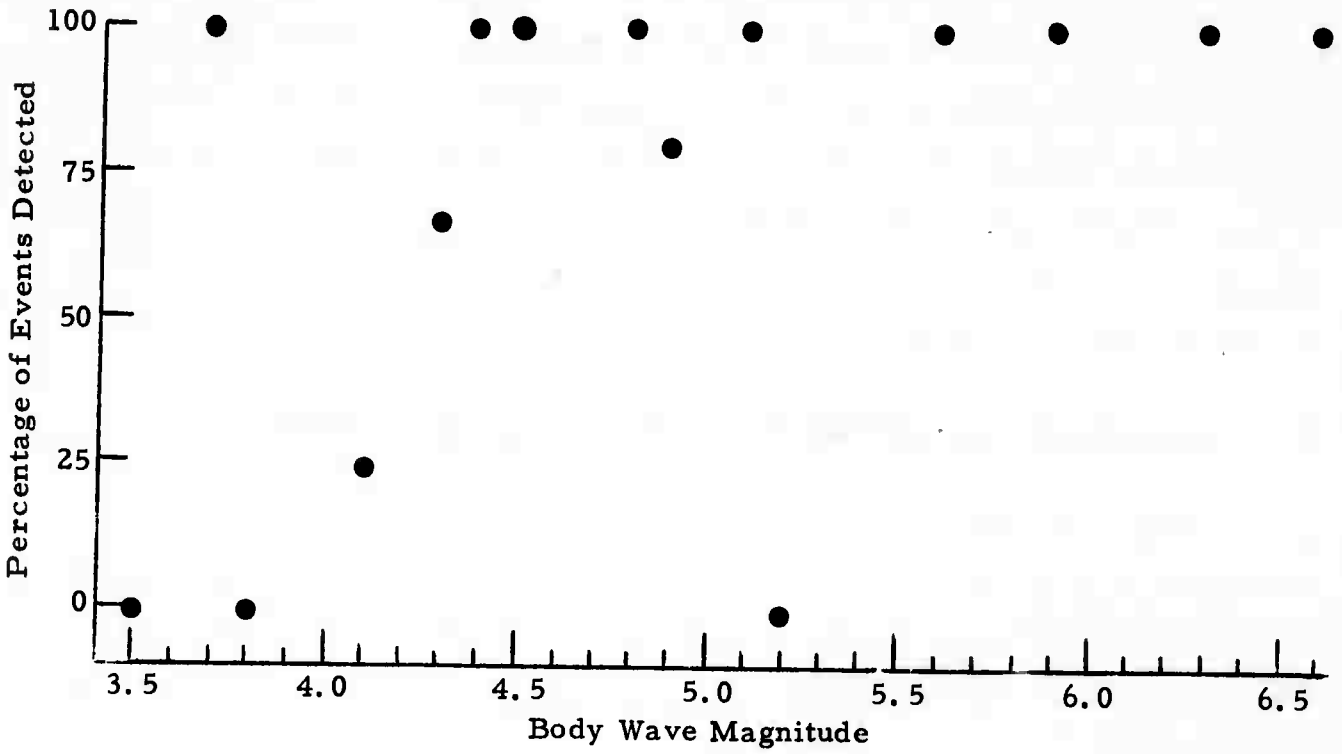

VII-2

FIGURE VII-2

S-WAVE DETECTION DATA FOR CENTRAL ASIA

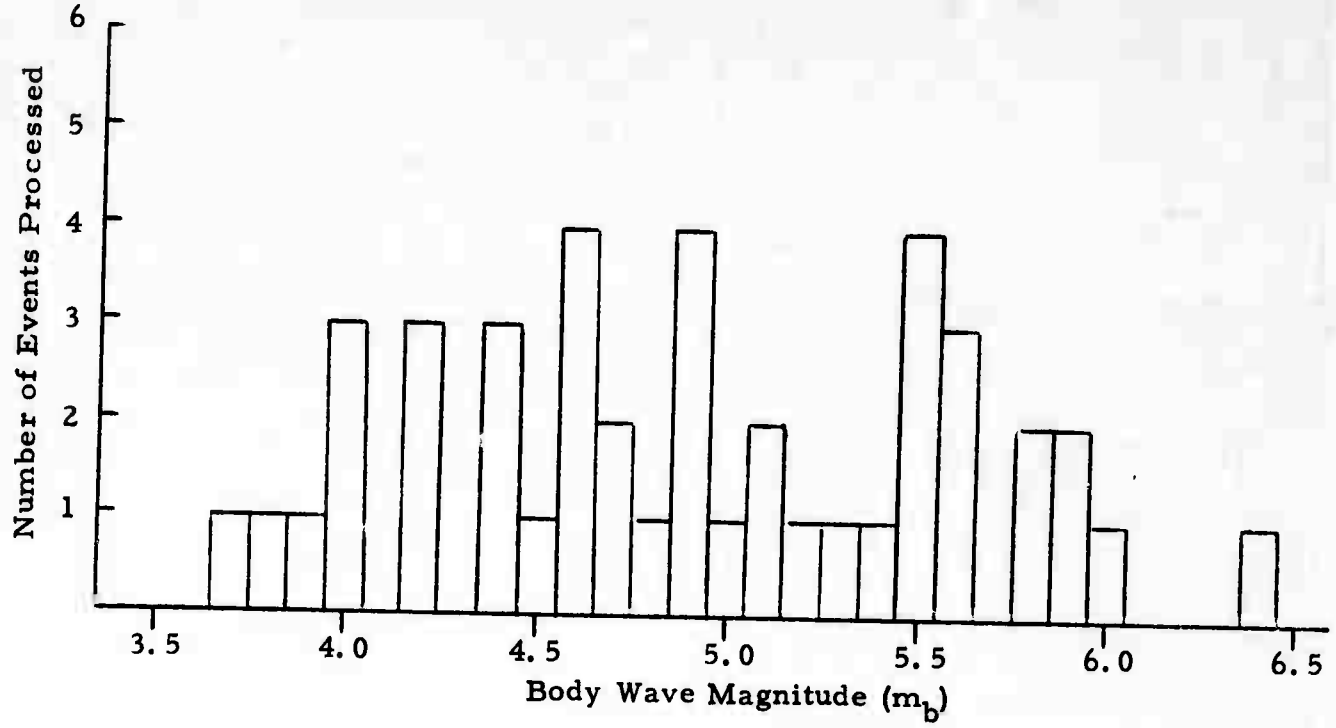

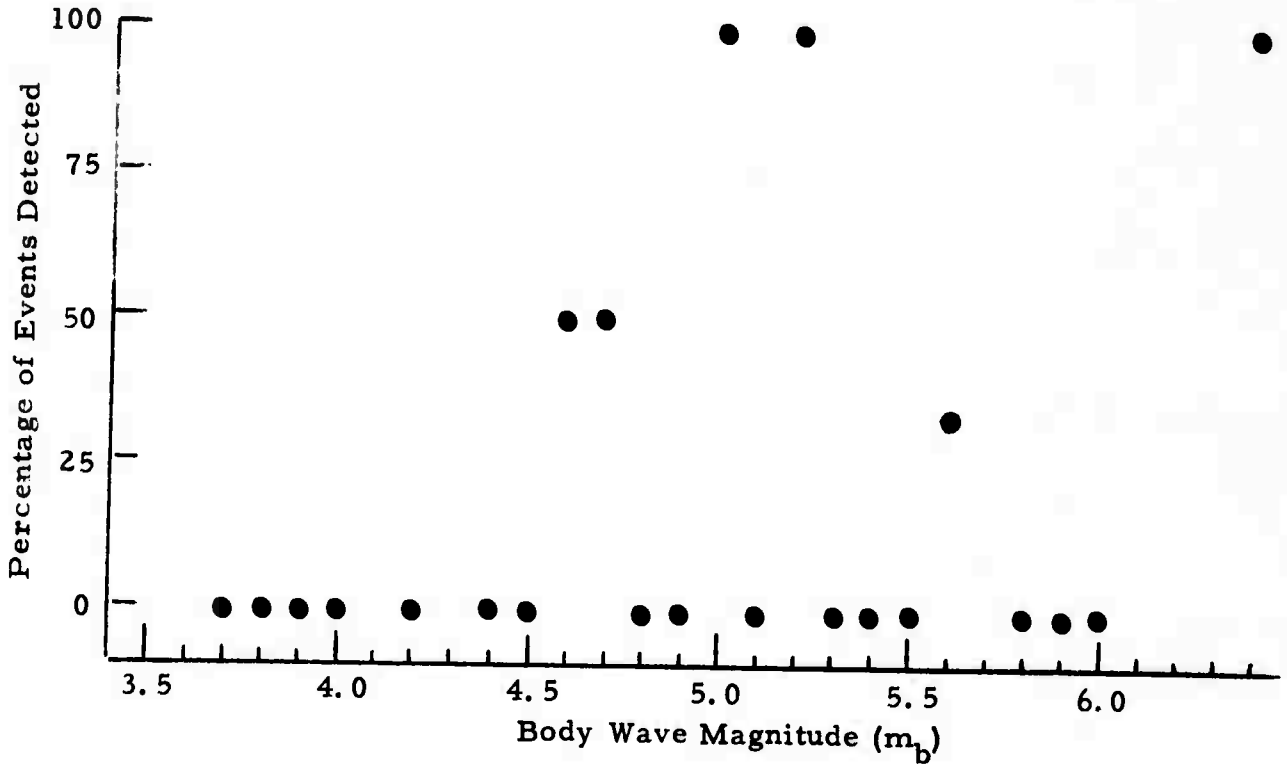

VII-3

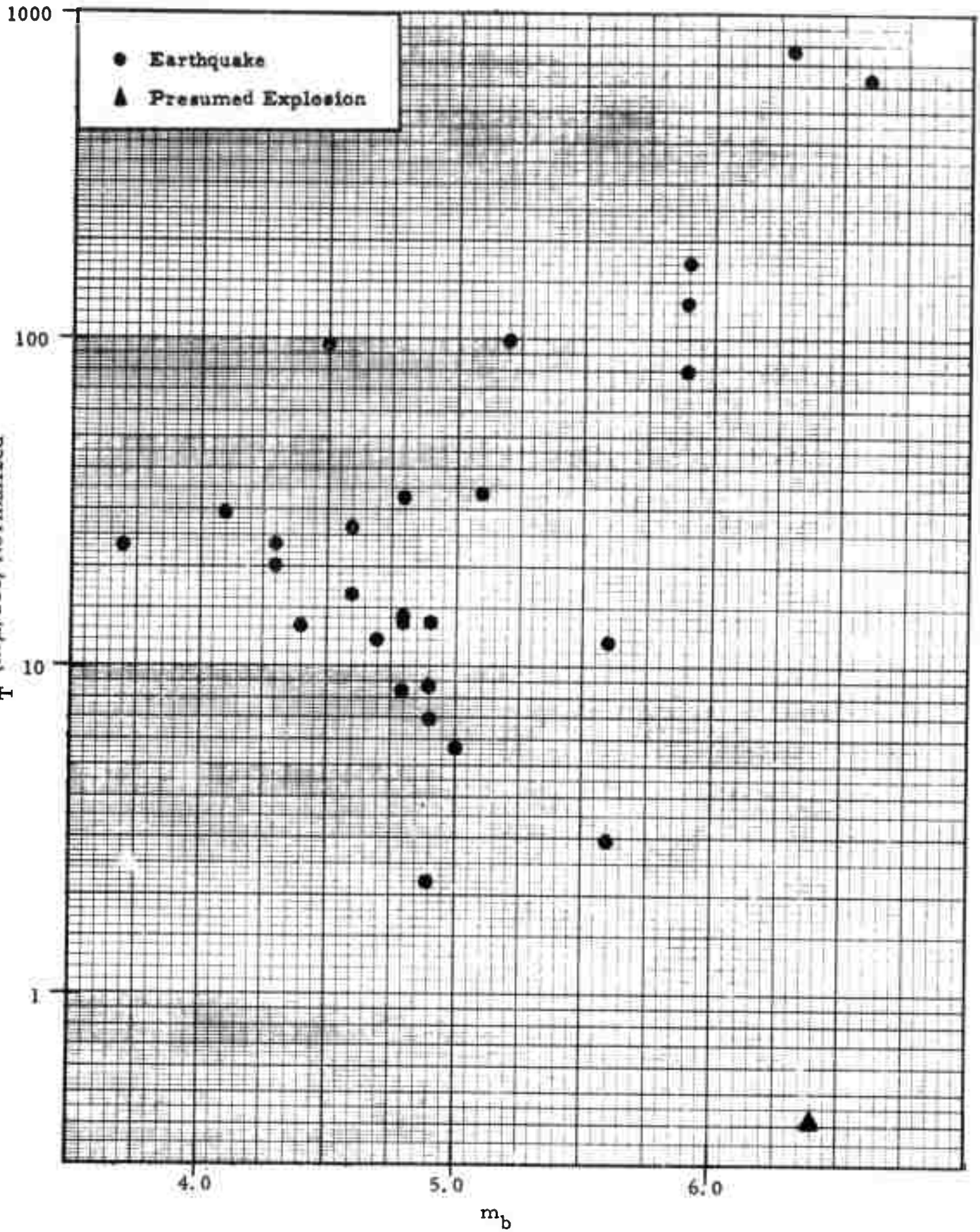

FIGURE VII-3

S-WAVE AMPLITUDE/PERIOD VS. m_b

stance of 20°, following the general procedure used by Evernden (1969). he normalizations were performed as follows:

1. Magnitude

The values of amplitude versus period (A/T) for S were rrected to a body wave magnitude (m_b) of 5.0 by multiplying each by the tio $1/10\ (m_b - 5)$.

2. Epicentral Distance

The m_b - normalized values of A/T were initially normalized an epicentral distance of 20° using Evernden's empirical relationship tween epicentral distance in degrees (Δ) and A/T:

$$\left(\frac{A}{T}\right)_{20^\circ} = \left(\frac{A}{T}\right)_{\Delta^\circ} \left(\Delta/20\right)^{0.7}$$

e resulting corrected data showed a factor of three difference in A/T between one presumed explosion for which S-waves were detected and the lowest rthquake value.

In an attempt to improve on this separation a least-mean square aight-line fit was made to a plot of $\log \left.\frac{A}{T}\right|_{m_b = 5.0}$ versus epicentral tance (Δ). The equation for this line is:

$$\log \left.\frac{A}{T}\right|_{m_b = 5.0} = -0.013\Delta + 1.437 \ .$$

normalize to 20°, the $\left.\frac{A}{T}\right|_{m_b = 5.0}$ values were multiplied by:

$$\left[10^{-0.013\,(20) + 1.437}\right] \Big/ \left[10^{-0.013\Delta + 1.437}\right] \ .$$

normalization computations may be summarized as:

$$\left.\frac{A}{T}\right|_{\text{norm.}} = \left[10^{0.013\Delta - m_b + 4.74}\right] \left[\frac{A}{T}\right] \ .$$

This normalized data showed a factor of five difference in A/T between the presumed explosion and the lowest earthquake value. The increase in separation was the result of a reduction in the scatter of the data when using the latter normalization. Upper bounds for the S-wave A/T normalized values were also computed for the two next largest presumed explosions (m_b's of 5.9 and 5.8), for which S-waves were not detected. The measurements were made on the component showing the largest excursion at the predicted S-wave arrival time. The normalized A/T value was 0.3 in the case of the larger (m_b = 5.9) presumed explosion and 0.1 in the case of the smaller (m_b = 5.8) presumed explosion. Because of their small values, they are omitted from Figure VII-3.

In the computation of the least squares fit, events with epicentral distances between 39° and 45° were omitted, since some of their A/T values seemed abnormally high. A possible explanation of these high values is that at 40° the travel times of the phases PS, S, and PcS are equal. Thus, the high amplitudes may be due to constructive interference of these phases.

On the basis of the observed data, it appears that the S-wave is a good earthquake - explosion discriminant for events for which an S-wave can be detected. However, since only large events generate S-waves of sufficient amplitude to be visible at teleseismic distances, the S-wave discriminant appears to be of little value in investigating most seismic events of interest.

SECTION VIII

ALPA EARTHQUAKE SURFACE WAVE DETECTION CAPABILITY

A. DIRECT METHOD

The direct estimate of ALPA surface wave detection capability was obtained by plotting the percentage of earthquakes for which surface waves were detected as a function of body wave magnitude. A suite of 78 Asian earthquakes was used to obtain the direct estimate. The histograms in the upper portions of Figures VIII-1 and VIII-2 describe respectively the Central Asian and Kurile/Kamchatka/Sakhalin portions of this earthquake population. These data are all for events processed using the full array. The events used are designated by the symbols D (detected) and ND (not detected) in Table II-1. In determining whether detection was achieved for any given event, the following detection criteria had to be met:

- A peak in any output trace (beamsteered, and bandpassed filtered; or beamsteered, bandpassed filtered, and matched filtered) 6 dB above any other peak in a 20 minute time gate centered at the expected peak occurrence time.
- A peak which occurs within $\pm$ 180 seconds of the expected peak occurrence time.

The histograms of Figures VIII-1 and VIII-2 were used to compute the incremental detection probabilities which appear in the lower portions of Figures VIII-1 and VIII-2. The detection percentage for Central Asian events show considerable scatter. The directly-estimated 90% detection probability for Central Asian events occurs near $m_b = 4.5$. The detection percentage for the Kurile/Kamchatka/Sakhalin events show somewhat less scatter; the directly-estimated 90% detection point occurs near $m_b = 4.3$.

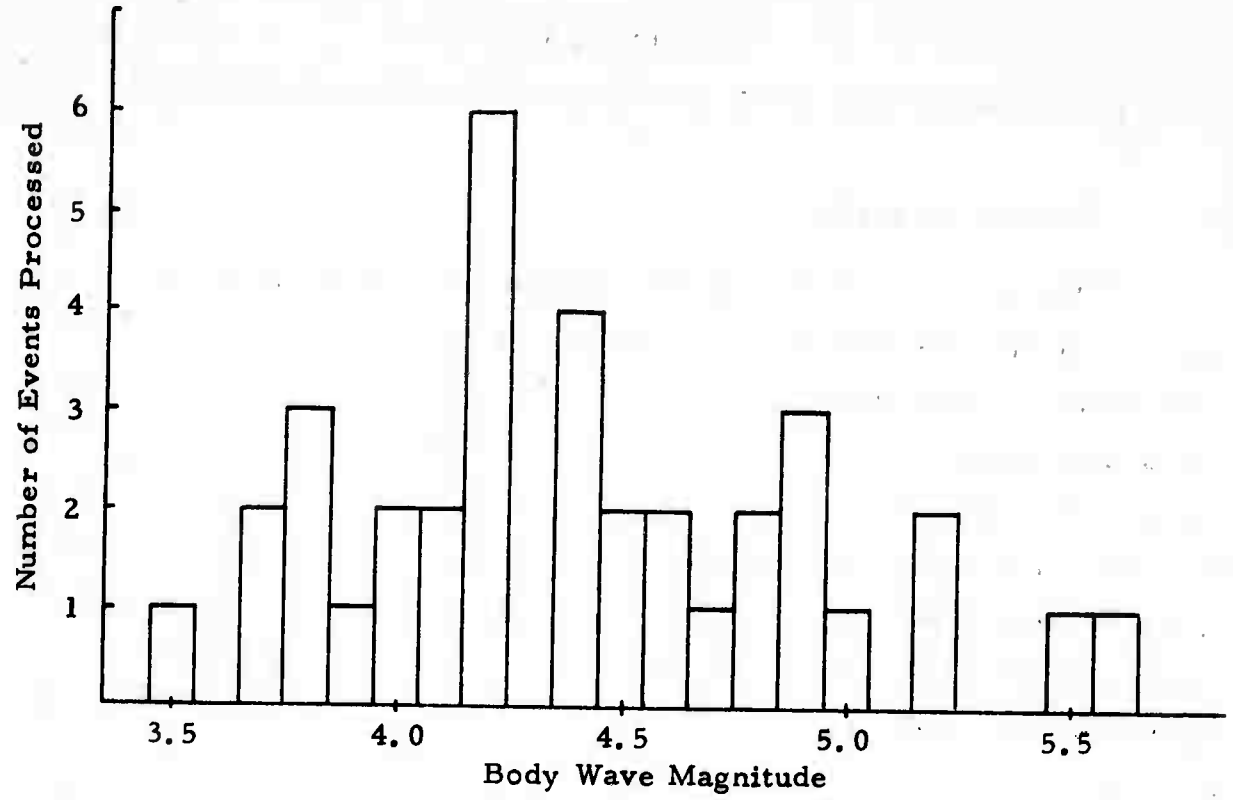

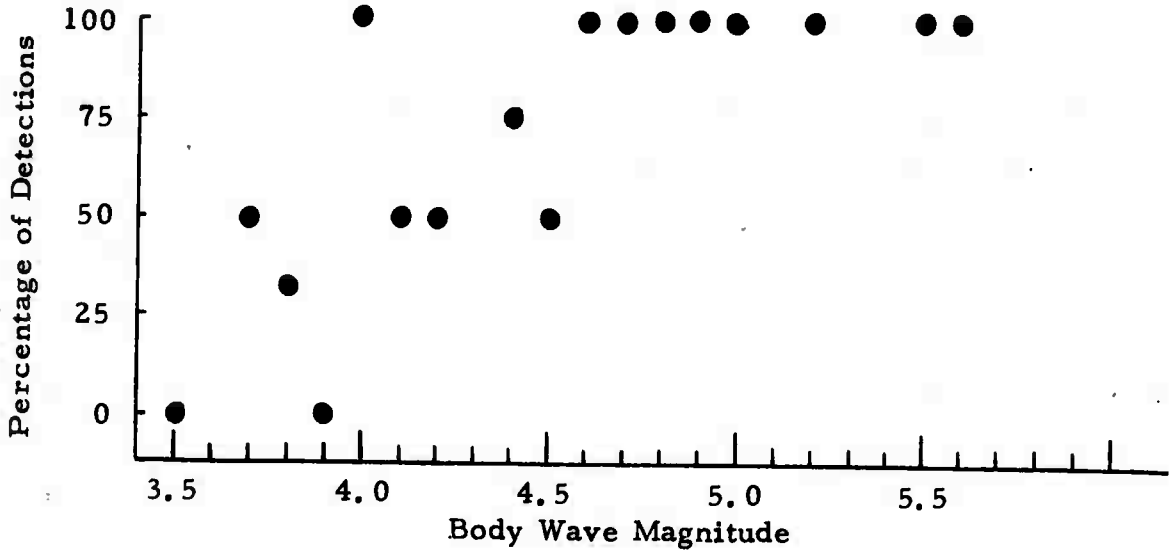

FIGURE VIII-1

SURFACE WAVE DETECTION DATA FOR CENTRAL ASIA

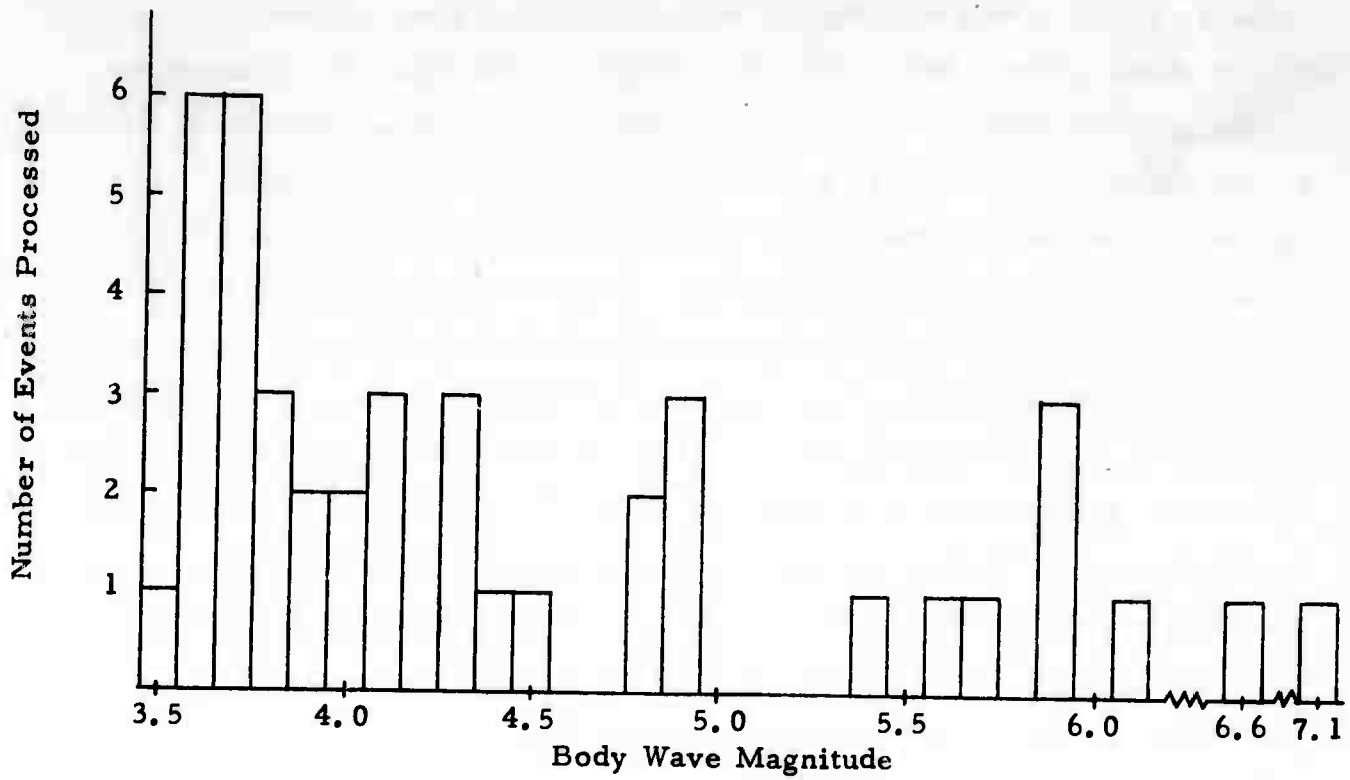

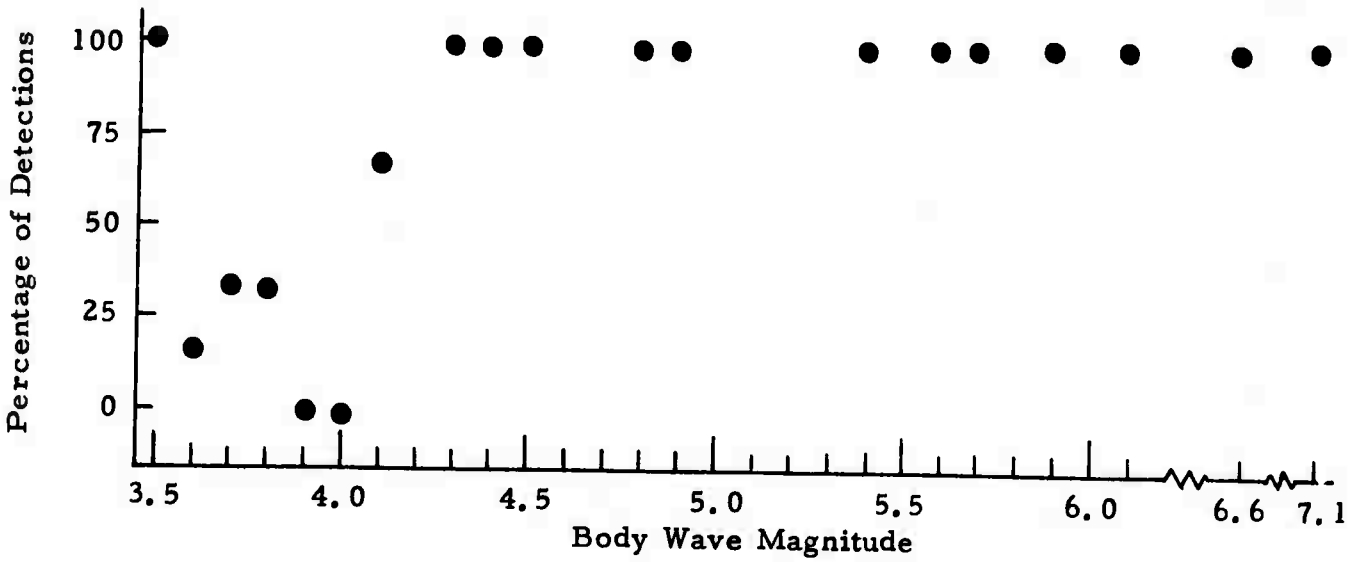

FIGURE VIII-2

SURFACE WAVE DETECTION DATA FOR KURILE-KAMCHATKA AREA

VIII-3

In order to reduce the scatter in the incremental detection probability values, figures similar to Figures VIII-1 and VIII-2 were constructed using all ALPA events processed up to the present time. The data base included the events reported earlier (Harley, 1971), all the events from Table II-1, and other events which were processed before the full array became available. To reduce the effect of distance on detection probability, the data were divided into two groups according to epicentral distance. Events with epicentral distances greater than 45° (representative of Central Asian events) are included in Figure VIII-3. Events with epicentral distances less than 45° (representative of Kurile Island, Kamchatka, and Sakhalin Island events) are included in Figure VIII-4. In each figure the upper portion is the histogram describing the data base; the lower portion is the plot of incremental detection probability versus m_b. The 90% detection probability for Central Asian events is not changed when all data, partial and full array, are included. It remains near $m_b = 4.5$. The 90% detection probability occurs at an m_b somewhat higher than 4.3 when all data are included; in this case it appears to be near $m_b = 4.5$.

B. INDIRECT METHOD

An indirect estimate of the detection threshold was made using a procedure discussed previously (Lacoss, 1969; Harley, 1971). Central to this method is the function relationship used to obtain the m_b for a given surface wave amplitude measurement. When reasonable values of the slope and intercept of the M_s versus m_b curve were used ($M_s = m_b - 0.73$), the indirect estimate of the detection capability was unrealistically low (90% detection probability at $m_b = 3.6$ and 50% detection probability at m_b 3.3 at $\Delta = 50^{\circ}$). The probable cause for this discrepancy is that the procedure fails to account for signal variance and hence is biased low. That is, a signal variance of 0.5 M_s units (which is typical) would shift the detection threshold curve obtained by the indirect estimate to significantly higher magnitudes. We plan to develop in the coming year a method for including signal variance in the indirect estimate of detection capability.

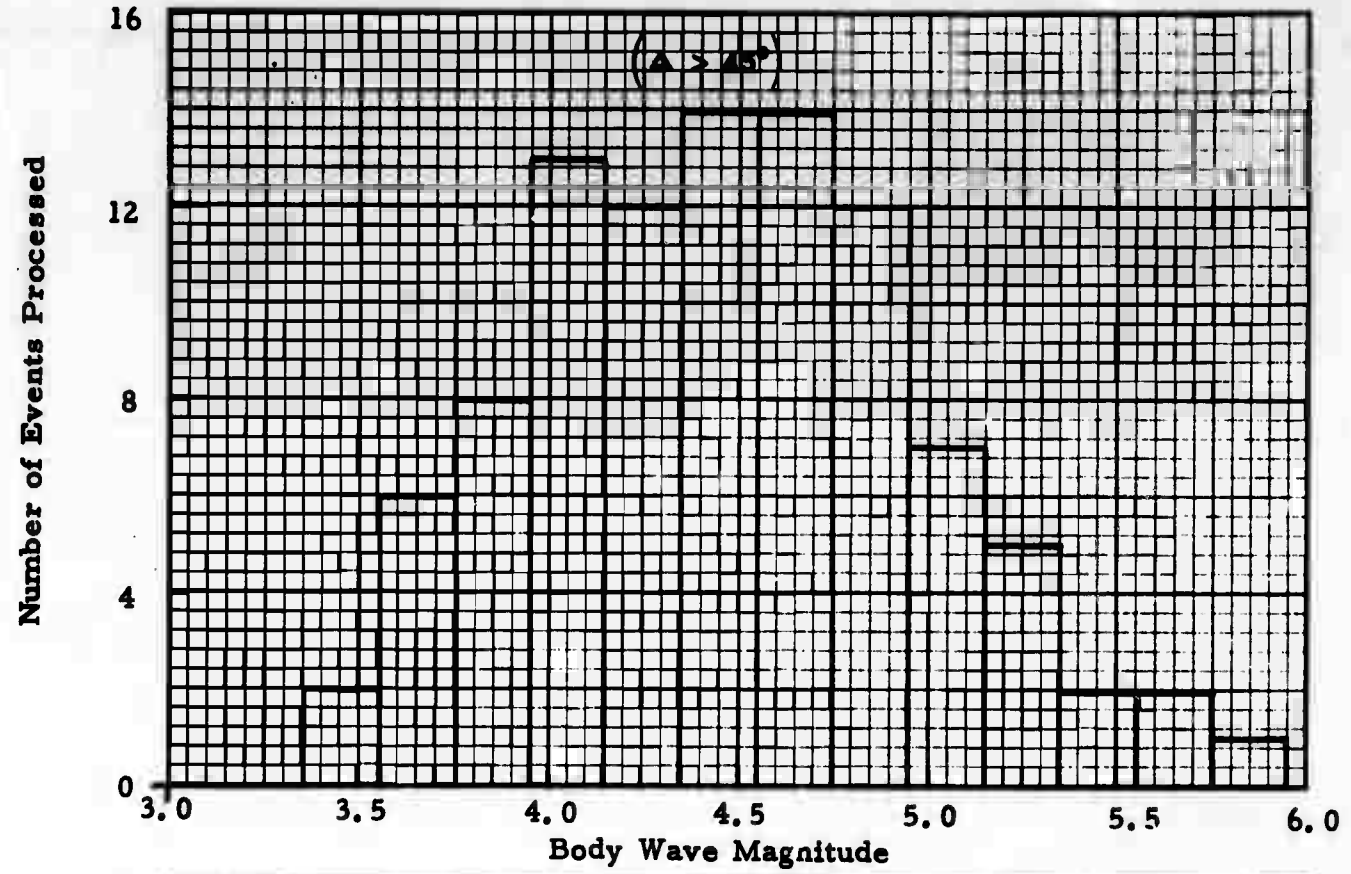

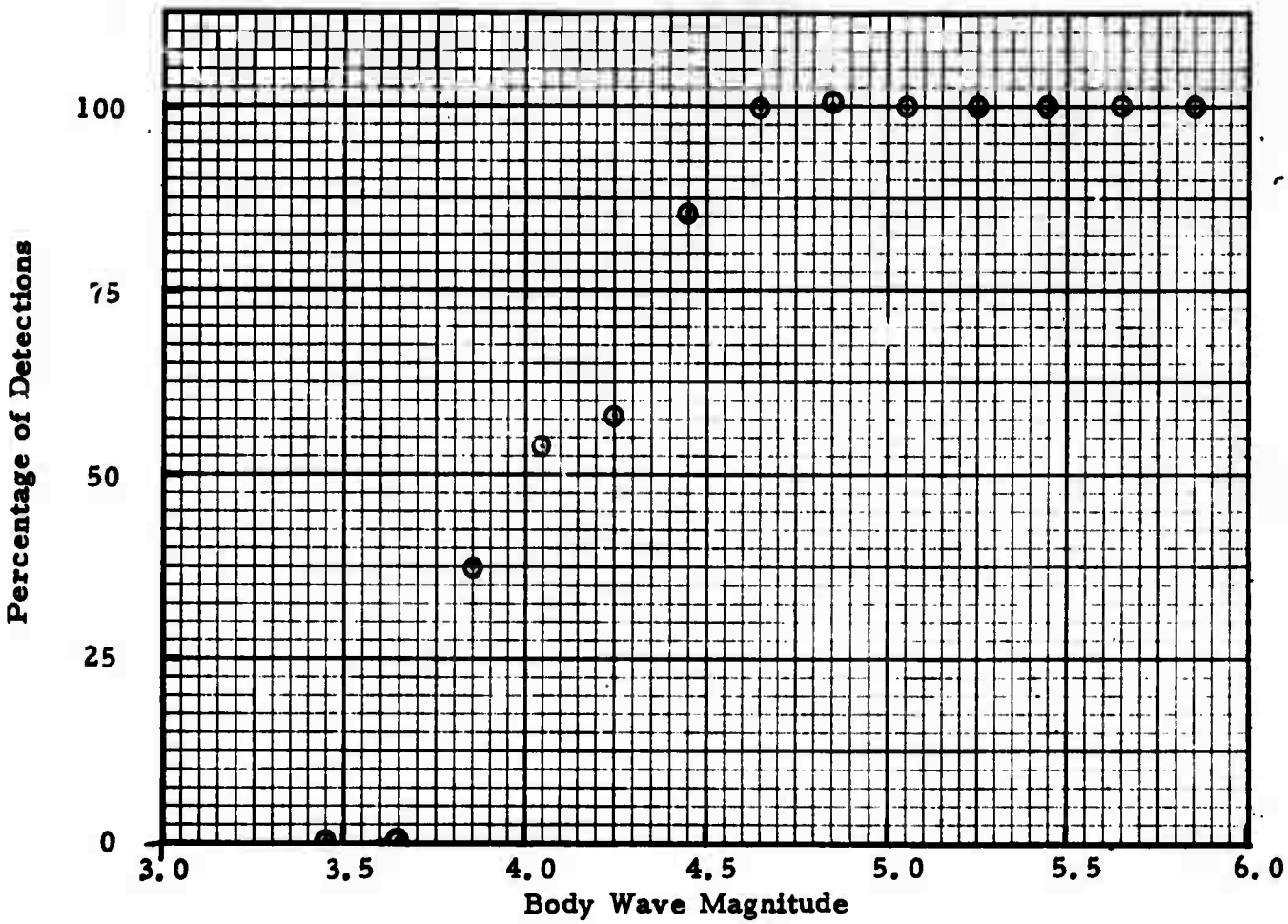

FIGURE VIII-3

ALPA LR INCREMENTAL DETECTION PROBABILITY - ALL DATA

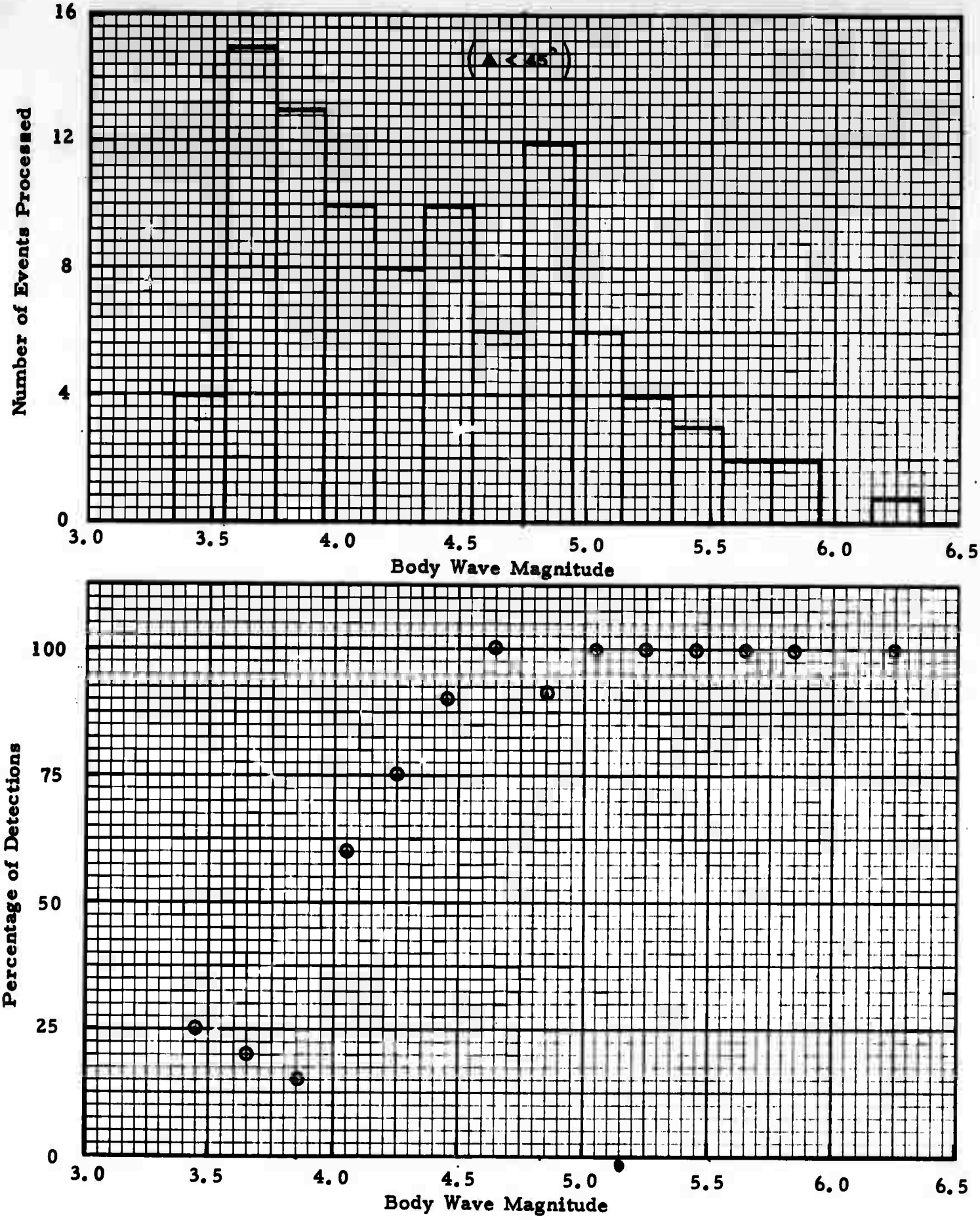

FIGURE VIII-4

ALPA LR INCREMENTAL DETECTION PROBABILITY - ALL DATA

SECTION IX

BEHAVIOR OF STANDARD DISCRIMINANTS

A. $M_s - m_b$

Surface wave magnitudes were computed for 92 of the events listed in Table II-1. In most cases surface wave magnitudes were computed for both the Rayleigh wave (vertical component) and the Love wave (transverse component). In some cases the event was not detected on a particular component; in these cases an upper bound was computed for the corresponding surface wave magnitude (M_s) from the largest peak-to-peak noise amplitude occurring during the signal gate. These upper bounds are designated by the symbol $\leq$ preceeding the M_s figure in Table II-1. The surface wave magnitude was determined for each event by the formula:

$$M_s = \log \frac{A}{T} + 1.66 \log \Delta$$

Where: A is the largest peak-to-peak value in millimicrons near twenty-five seconds

T is the period in the neighborhood of the peak in seconds

Δ is the epicentral distance in degrees

All measurements were made on beamsteered traces which had been bandpass filtered (0.025-0.055 Hz passband). The maximum peak amplitudes in the beams usually occurred near 25-second periods; no periods greater than 30 seconds or less than 20 seconds were used. $M_s - m_b$ plots for the Rayleigh wave energy are presented in Figures IX-1 and IX-2, for the Central Asia and Kurile/Kamchatka/Sakhalin areas respectively. Earthquake data are represented by the dots and presumed explosions by the open triangles. The Asian presumed explosions also are shown on Figure IX-2 for purposes of comparison with the Kurile/Kamchatka/Sakhalin earthquake data.

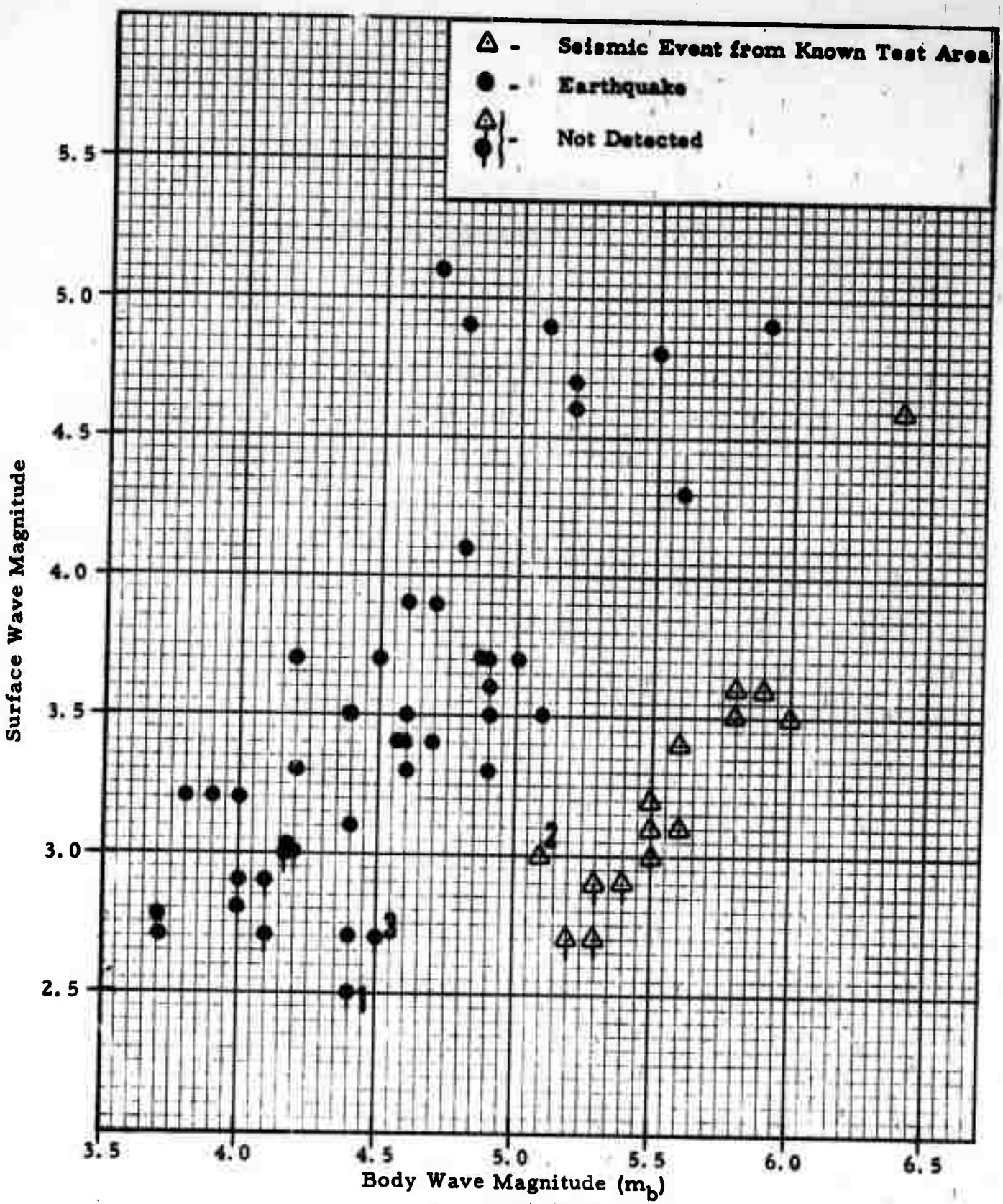

FIGURE IX-1

M_s VS. m_b FOR CENTRAL ASIA EVENTS (RAYLEIGH WAVE)

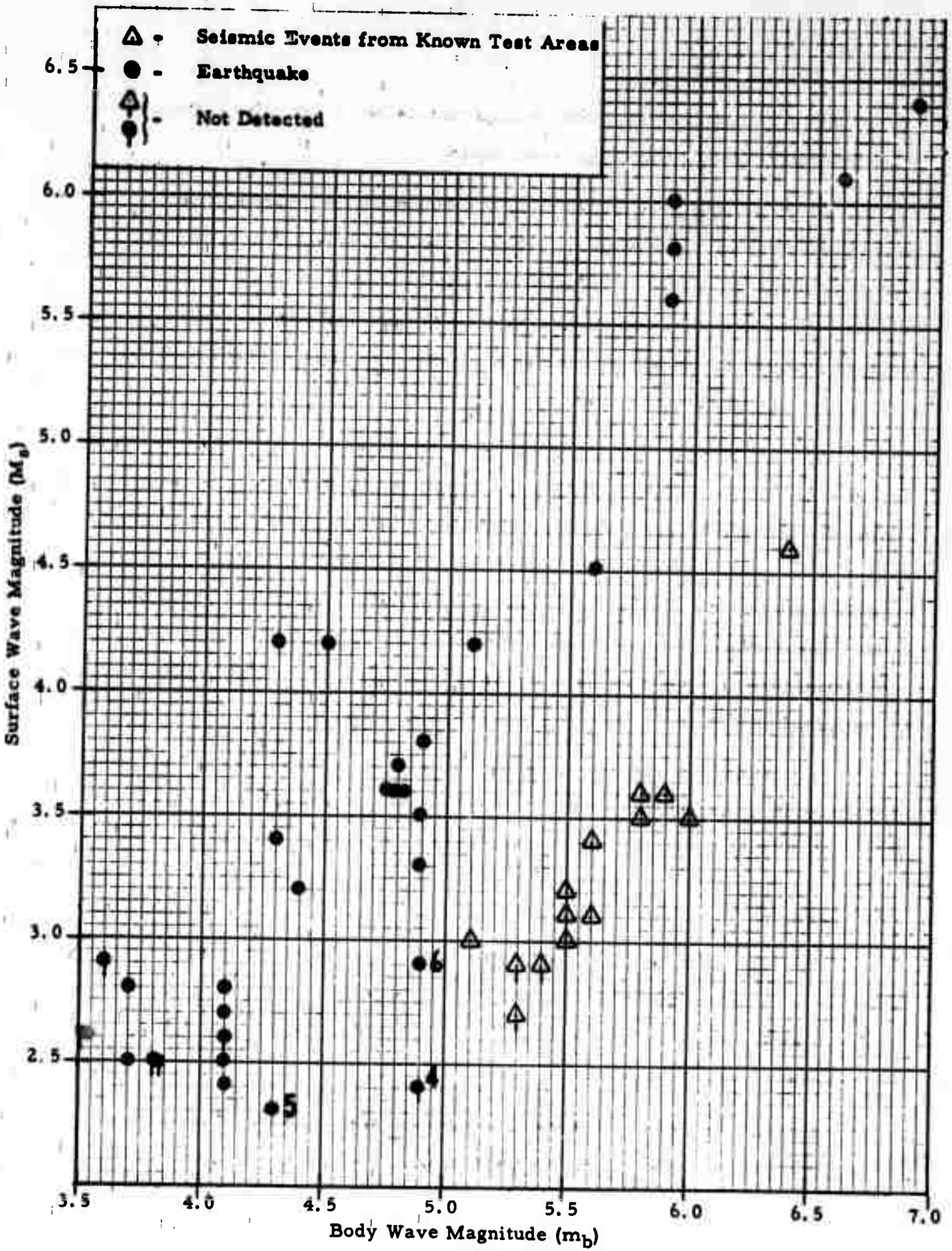

FIGURE IX-2

M_s VS. m_b FOR KURILE/KAMCHATKA/SAKHALIN EVENTS (RAYLEIGH WAVE)

For the events not detected, a vertical line below the point signifies that the corresponding M_s value is an upper bound.

The Asian data show the normal separation between earthquake and presumed explosion populations except for the events designated by the numbers 1, 2, and 3 in Figure IX-1. These events are discussed in detail later in this section. The Kurile/Kamchatka/Sakhalin events generally show good separation except for the events designated by the numbers 4, 5, and 6 in Figure IX-2; these events also are discussed below.

$M_s - m_b$ plots for the Love wave energy are presented in Figures IX-3 and IX-4 for the Central Asia and Kurile/Kamchatka/Sakhalin regions respectively. Again, the presumed explosion data from Asia has been included in both plots. In this case there is complete separation between the earthquake and presumed explosion populations for the Asian events. Separation is poor between the Kurile/Kamchatka events and the body of Asian presumed explosions. This poor performance results from the fact that for low magnitudes, there is more scatter in the Kamchatka/Kuriles.

Figure IX-5 shows least-squares straight line fits to each of the populations in Figures IX-1 through IX-4. These line fits tend to confirm that the Love wave $M_s - m_b$ is a better discriminant than the Rayleigh wave $M_s - m_b$.

B. AL and AR

The AR parameter is related to the total Rayleigh wave energy in a seismic event and was introduced by Brune, Espinosa, and Oliver (1963). It has been used by Evernden (1969), who also studied AL (the corresponding parameter for Love wave energy).

The AL and AR parameters used here are computed by summing the absolute values (in millimicrons) of the data points within the appropriate signal

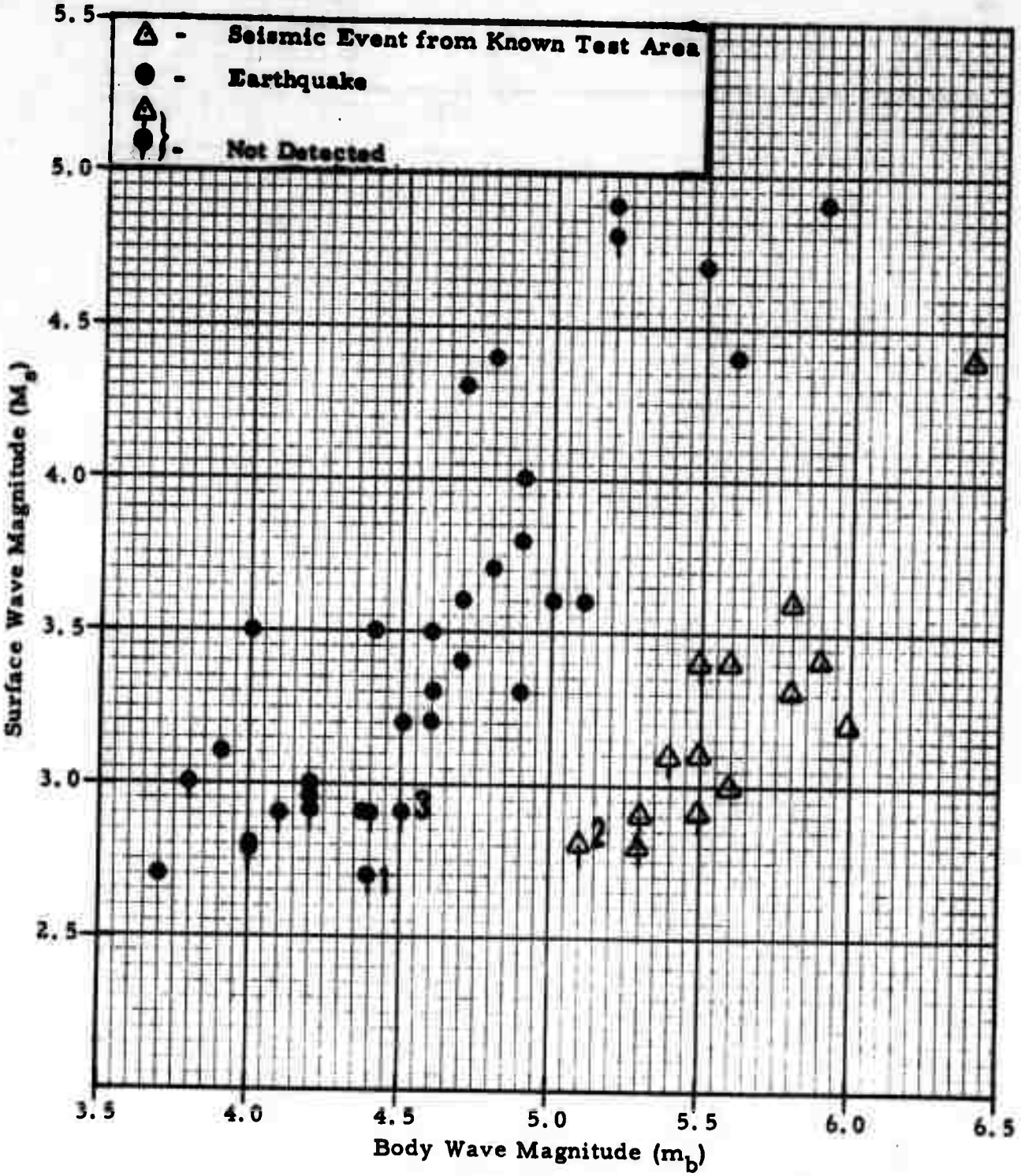

FIGURE IX-3

M_s VS. m_b FOR CENTRAL ASIA EVENTS (LOVE WAVE)

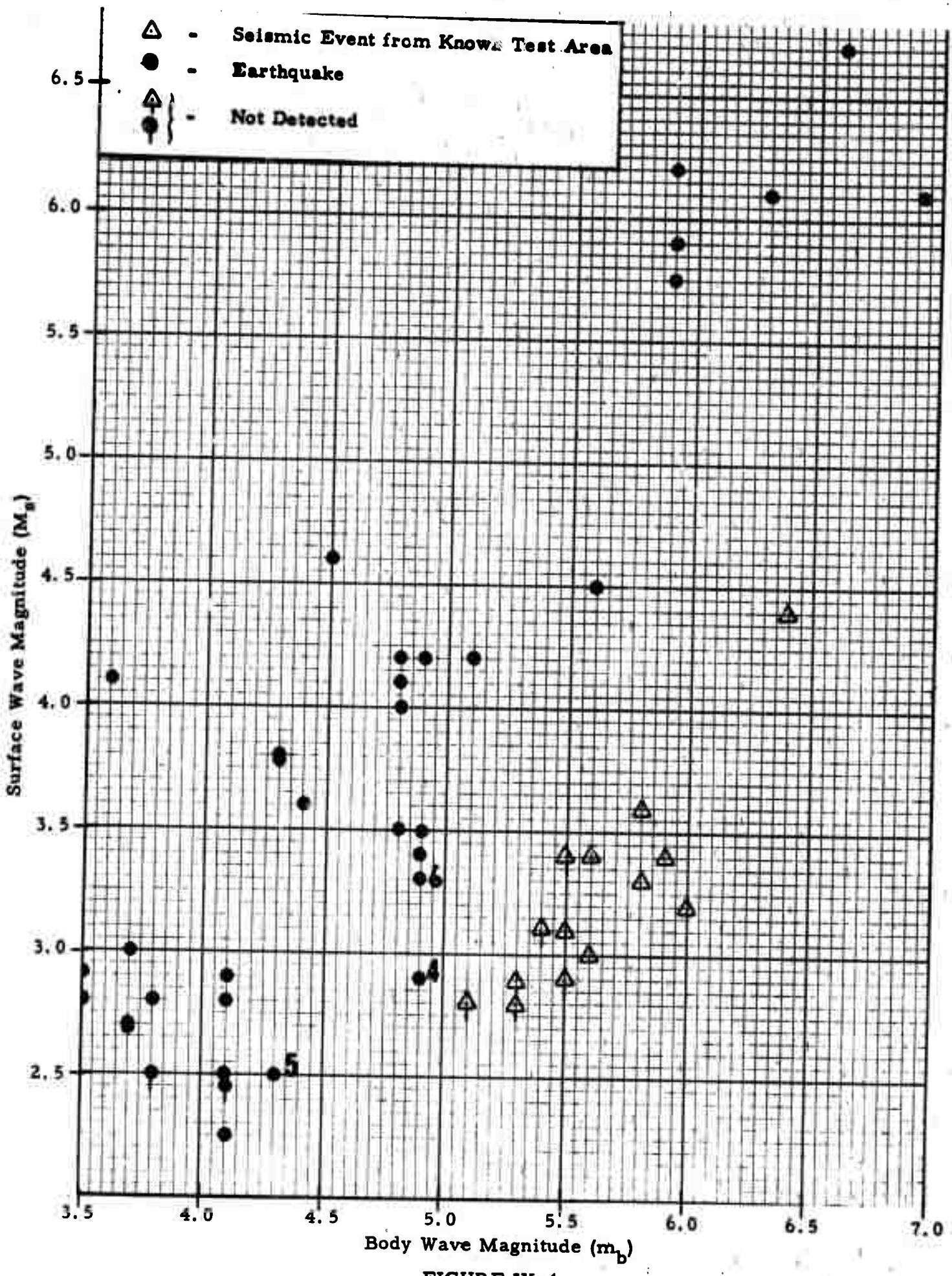

FIGURE IX-4

M_s VS. m_b FOR KURILE/KAMCHATKA/SAKHALIN EVENTS (LOVE WAVE)

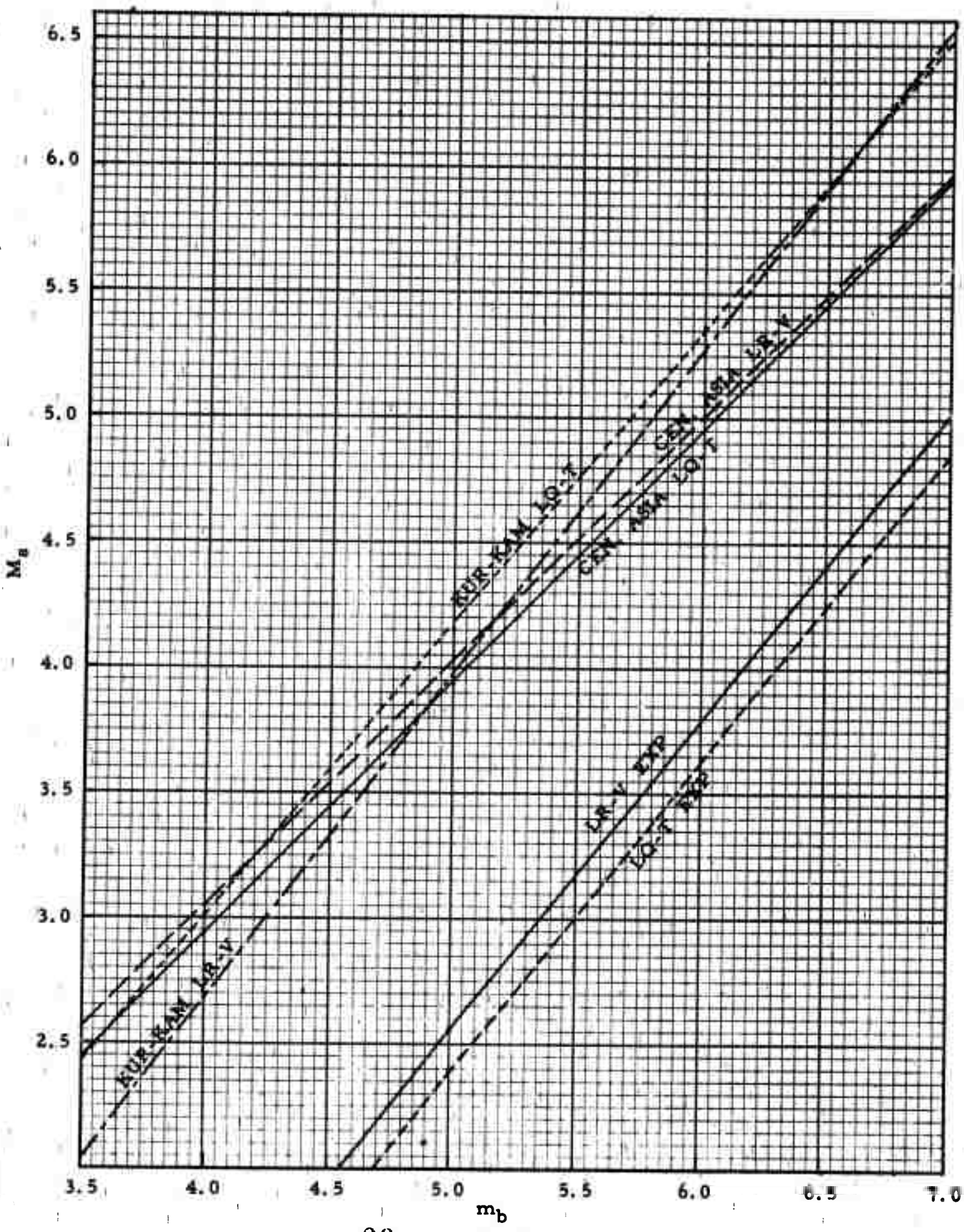

FIGURE IX-5

LEAST SQUARES STRAIGHT LINES FITTED TO THE M_s VS. m_b DATA

time gate. The results are scaled as described earlier (Harley, 1971) to correspond to the parameters as defined by Evernden. This scaling of AL and AR values includes a factor which normalizes the measured values to an m_b of 5.0. This normalization previously was accomplished by a multiplicative factor of $1/10^{(m_b - 5.0)}$. When this normalization was applied to the current data, there remained a skew which tended toward large AL and AR values for large m_b values. Evernden used a factor of $1/10^{1.75(m_b - 5.0)}$, but this factor over-corrects our data and introduces a negative average slope. It appears that a factor of $1/10^{1.3(m_b - 5.0)}$ is correct for our 1971 data. When this factor was applied to our 1970 data (Harley, 1971), it did not introduce a noticeable slope or materially affect the conclusions reached there. It is concluded, therefore, that the exponent $1.3(m_b - 5.0)$ works best for ALPA data. Accordingly, this was used for magnitude normalization in the following. Plots of AR vs. m_b and AL vs. m_b are given in Figures IX-6 and IX-7, respectively. In earlier ALPA results, AL and AR appeared to be fair discriminants, the smallest earthquake AL value being 2.5 times greater than the largest presumed explosion AL value. In the present study there is poorer separation of the earthquake and presumed explosion populations on the basis of either AL or AR differences. In fact event number 4, which is believed to be an earthquake, overlaps the explosion population. As discussed below, there is some question as to the validity of the m_b value for this event. Even if this event is ignored, however, the separation between minimum earthquake AR and maximum explosion AR is only a factor of 1.7. The corresponding AL separation is 3.0.

In order to arrive at an estimate of the lower limit of application of the AL and AR parameters, representative AL and AR values were selected from values computed over noise gates. Two gate lengths were employed, one corresponding to the expected duration of an event from Central Asia and the other corresponding to the expected duration of an event from the Kurile-Kamchatka area. These values then were normalized using various m_b's, and the resulting values yielded the lines in Figures IX-6 and IX-7.

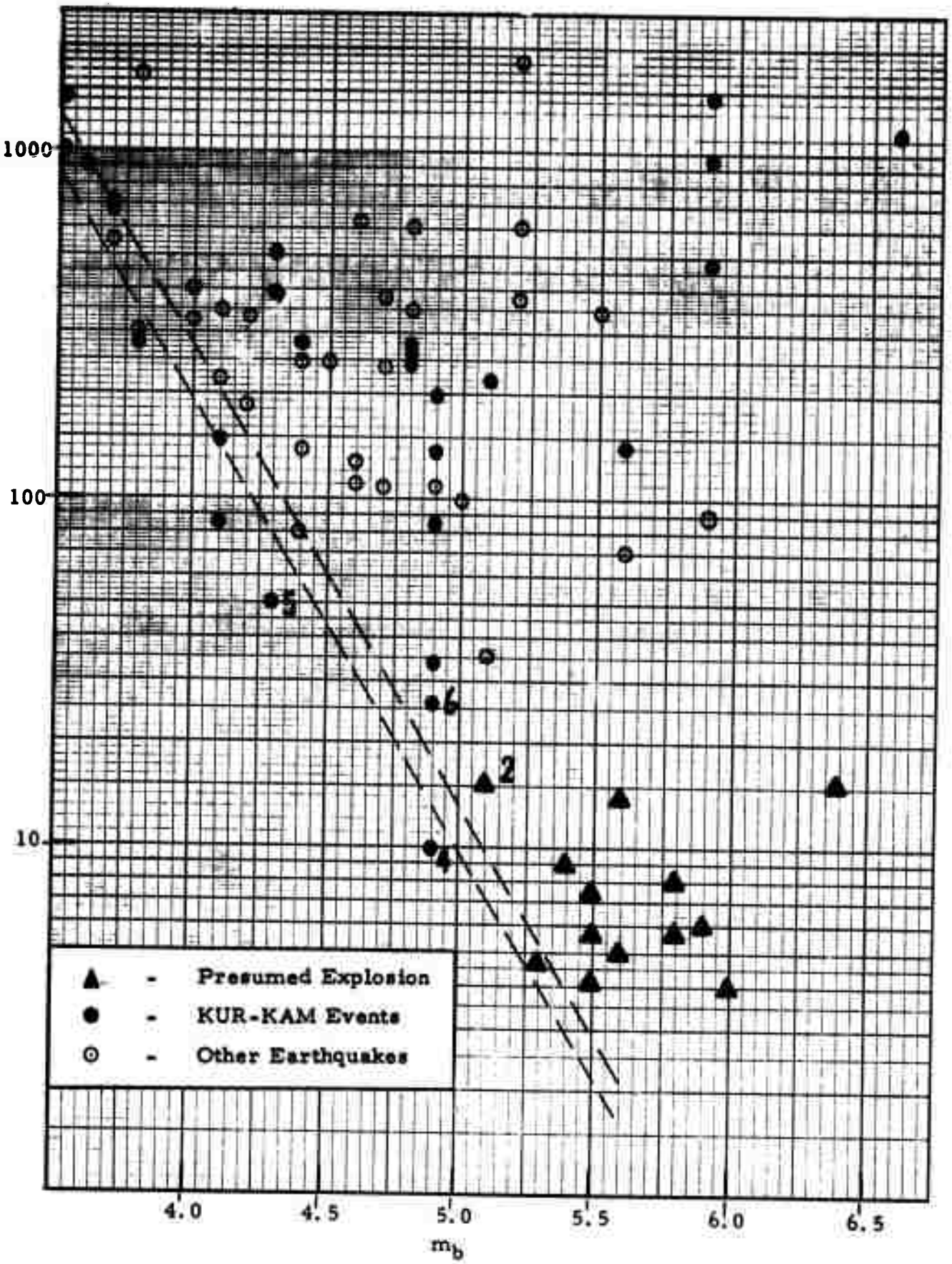

FIGURE IX-6

AR VS. m_b - COMPOSITE PLOT

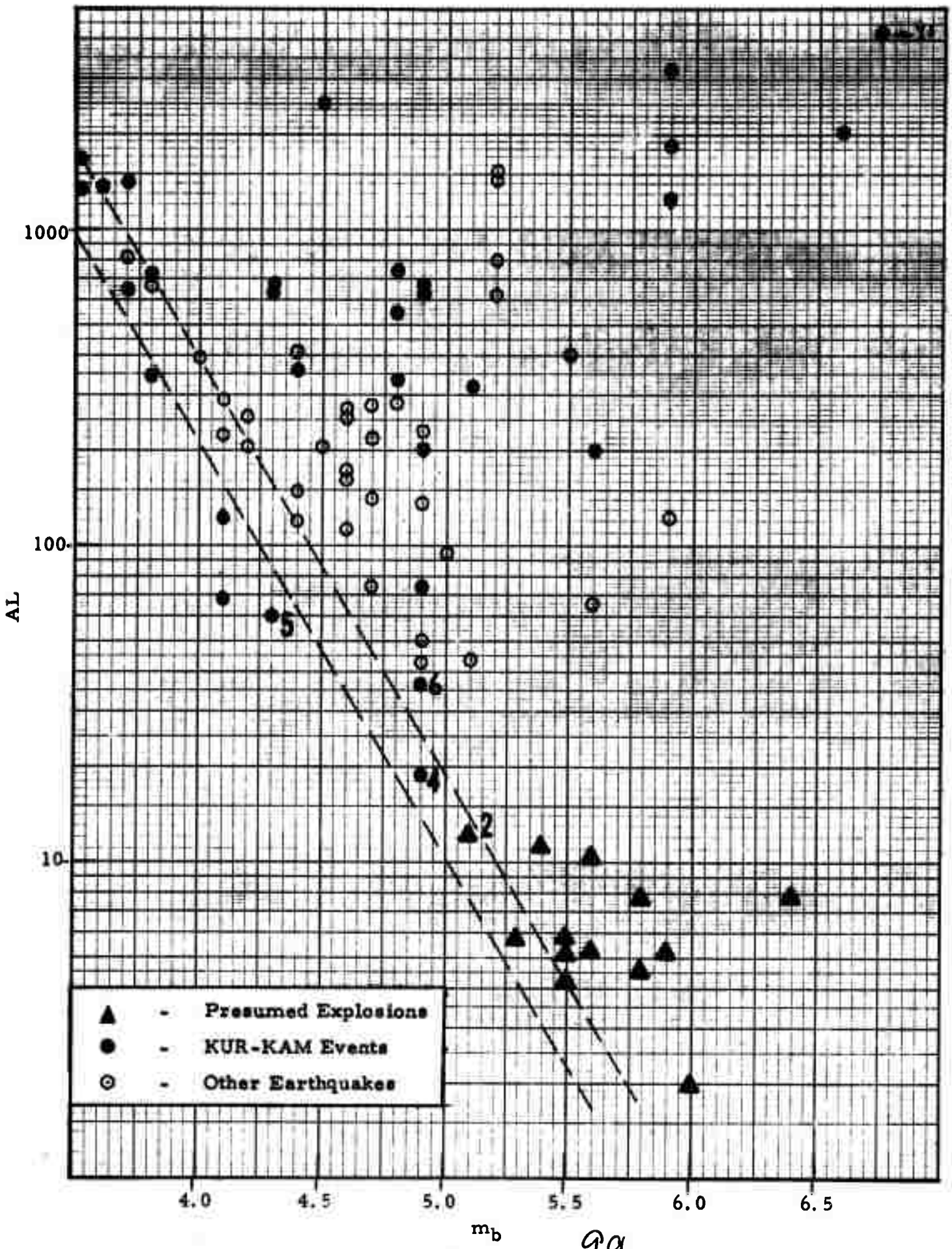

99

FIGURE IX-7

AL VS. m_b - COMPOSITE PLOT

The upper lines in each figure represent approximate limiting AL or AR values imposed by the noise for Kurile/Kamchatka/Sakhalin region events recorded on a noisy day. The lower lines represent approximate limiting values for Central Asian events recorded on a relatively quiet day. Thus, values below these lines represent cases of AL and AR measured in exceptionally quiet periods. These lines show that the AL and AR values measured from noise alone usually will reach the lowest earthquake values at a body wave magnitude of about 4.5. Therefore, the threshold for application of AL and AR as discriminants lies above an m_b of 4.5.

The events which gave poor discrimination results from one or more of the above methods are listed in Table IX-1, along with the discriminant values and depths. The performance of each discriminant is rated by the symbols G or P (good or poor) beside each discriminant value. The number to the left of each event is the number identifying that event in Figures IX-1 through IX-4, IX-6, and IX-7 above.

The G or P rating of the discriminants in Table IX-1 is subject to an assumption as to the true nature of the event in question. In the absence of conclusive a priori information, the procedure is to examine all discriminants for the purpose of tentatively classifying the event. Then each discriminant is evaluated relative to this tentative classification.

Events 1 and 3 were not detected, as was the case with a number of other events. In such cases it is customary to measure the largest peak-to-peak value occuring during the signal time gate, and to assign a corresponding upper bound to M_s. In these two cases, these upper bounds are at best on the lower side of the earthquake range, and an element of uncertainty arises. Since the true values of M_s cannot be measured, the events cannot be classified.

The M_s (LR-V) value for event number 2 does not clearly classify this

TABLE IX-1

EVENTS WITH POOR DISCRIMINATION RESULTS

No.	Event Name	m_b	M_s (LR-V)	M_s (LQ-T)	AL	AR	Depth & Source
1	CAU*262*06	4.4	≤ 2.5P	≤2.7	-	-	U*, L**
2	WRS*277*10	5.1	3.0P	≤2.8G	12G	15G	13 km, C***
3	WRS*262*11	4.5	≤ 2.7P	≤2.9	-	-	N****, C
4	SAK*182*14	4.9	≤ 2.4P	2.9P	19P	10P	33 km, L
5	KUR*199*12	4.3	2.3P	2.5G	60G	50G	33 km, L
6	KUR*168*09	4.9	2.9P	3.3G	37P	26P	N, C

*U = Unknown

**L = LASA Bulletin

***C = National Earthquake Information Center Data

****N = "the depth was restrained at 33 km for earthquakes whose character on seismograms indicate a shallow focus but whose depth is not satisfactorily determined by the data"

event. The upper bound on M_s (LQ-T) is sufficiently low to suggest that this event is an explosion. This suggestion is also present in the AR and AL values. The conclusion is that this event is an explosion, but that M_s (LR-V) was not useful in classification.

In the case of event number 4, all discriminants are either indeterminate or suggest that the event is an explosion; but the epicenter makes this conclusion questionable. It is noted that a 37 event subset of the Sakhalin earthquake swarm of September 6, 7, and 8, 1971, has been processed. The twelve events of that subset which the LASA bulletin reported as having body wave magnitude 4.5 or greater, were all reported by PDE. It might be expected that event number 4, which LASA reported at $m_b = 4.9$, would also be reported by PDE. Since it was not, the magnitude is considered questionable. If the true m_b is 4.5 or less, the M_s (LQ-T) and AL discriminants would tend to classify the event as an earthquake.

If event number 5 is an earthquake, the M_s(LR-V) value is anomalously low. AL and AR would marginally classify it as an earthquake and M_s (LQ-T) confirms this more strongly.

Event number 6 is questionable in the case of AR, AL, and M_s (LR-V) but seems to be clearly identified as an earthquake using M_s (LQ-T).

To summarize, six events of the total population considered yielded one or more discriminants that would not be useful in classification or would lead to a wrong classification. In three of these cases it is probable that, by considering all the possible discriminants, a correct identification could be made. In two cases where only an upper bound could be estimated for M_s, these upper bounds were slightly low if the events are earthquakes, and the question could not be resolved. The last event, an $m_b = 4.9$ from Sakhalin would probably be mis-identified using the discriminants considered here. There is a question

regarding the correctness of the m_b value for this event, however, and it is not considered to be a clear case of mis-identification.

The conclusion from the discrimination results is that the most powerful discriminant is the Love energy M_s - m_b relationship, but all the discriminants studied are useful when used in combination.

SECTION X
CONCLUSIONS AND FUTURE ANALYSIS PLANS

A. CONCLUSIONS

Summarized below are the major results from each of the areas of evaluation discussed above:

1. Signal Analysis

- Signal similarity across the full 19 element ALPA array is less than that across the limited nine element array studied earlier. Average signal correlation coefficient for the vertical component is 0.84 for the full array and 0.93 for the limited array.
- Average beamsteer signal attenuation for the transverse component is approximately the same for both the full array as for a seven site hexagonal subarray, about 1.4 dB. For the vertical and radial components the full array beam causes about two dB attenuation, as opposed to about one dB for the small array beam.

2. Noise Analysis

- The anomalous long-period noise problem observed at ALPA during 1970 has been apparently alleviated.
- During the period day 240 to day 320 in 1971, ALPA experienced occasional days with high RMS noise levels (up to 26 $m\mu$ site average RMS vertical ground motion amplitude in the 0.025 - 0.055 Hz frequency band); however, the noise levels were only slightly above normal summer levels (≈ 9 $m\mu$ site

average RMS vertical ground motion amplitude in the 0.025-0.055 Hz band) for the day 320 to day 360 period.

- Azimuths of strong directional noise sources rarely coincide with azimuths of areas of interest.
- The RMS value of beamsteered noise in the 0.025-0.055 Hz band ranges from 1.5 to 3.0 mμ.
- On the average the 19 site array will provide no more than 0.1 M_s units of increased signal detectability over the nine-site array.

3. Two-Component Beamforming

- SNR gains of one to two dB in the bandpassed output beam may be expected from two component beamforming, but gains of more than three dB are observed on occasion.

4. Matched Filter Studies

- Overall SNR improvements from master waveform matched filtering of the transverse, vertical, and radial components average 2.1 dB, 3.5 dB, and 2.7 dB, respectively. The true values are probably slightly higher. Signal measurements used in arriving at these figures were actually measures of signal plus noise. The presence of noise will, particularly in the case of small events, bias the observed SNR improvements low.
- Instances of SNR improvements of more than seven dB were observed. These gains might be exceeded in some instances if more nearly optimum master waveform lengths were used, and if, in certain regions, more than one master waveform matched filter were tried.

- Chirp filter improvements from the transverse, vertical, and radial components average 2.0 dB, 3.9 dB, and 3.0 dB, slightly better overall than master waveform improvements. Large gains (greater than five dB) were observed in the same percentage (17%) of cases for both forms of matched filter.
- Two component matched filtering appears generally to preserve the SNR gains obtained from two component beamforming.

5. S-Wave Processing Results

- The 90 percent S-wave detection probability appears to lie above an m_b of 5.5 for Central Asian events.
- Since S-waves are detected only for the largest earthquakes in areas of interest, the S-wave discriminant appears to be of little practical value.

6. ALPA Earthquake Surface Wave Detection Capability

- The directly-determined 90% detection probability for surface wave occurs near $m_b = 4.5$ for Central Asian events and near $m_b = 4.3$ for events from the Kurile/Kamchatka region.

7. Behavior of Standard Discriminants

- The M_s-m_b relationship determined from Love wave energy is a better discriminant than the same relationship determined from Rayleigh wave energy.
- AL and AR were not fully successful as discriminant methods and were clearly inferior to the M_s-m_b discriminants.
- No discrimination method achieved a complete separation of earthquakes and presumed explosions, although the Love wave M_s-m_b discriminant failed clearly in only one case.

B. FUTURE ANALYSIS PLANS

The following areas will be emphasized in future analysis of ALPA.

- Continued monitoring of the ALPA noise field, and a detailed analysis of anomalous noise samples.
- Analysis of complicated signals in an attempt to understand multipath structure, etc.
- Further investigation of the effects of master waveform matched filter length on performance, and more detailed study of the utility of multiple master waveforms for each region.
- Comparison of simple phases shift-and-sum two component processing with more sophisticated techniques such as two component multi-channel filtering.
- Extended comparison of the array processing capabilities of the optimum seven element array and the full 19 element array.
- Region-by-region estimation of the ALPA detection threshold utilizing matched filtering regional differences, etc.

In addition to these ALPA studies, ALPA evaluation results will be integrated with those obtained from the Norwegian Seismic Array, and the stations of the Long Period Experiment in order to obtain a preliminary estimate of the detection and discrimination capability of the existing long period network.

SECTION XI
REFERENCES

Evernden, J. F., 1969, Identification of Earthquakes and Explosions by Use of Teleseismic Data; Journal of Geophysical Research, Vol. 74, pp 3828-3886, July.

Harley, T. W., 1971, Long Period Array Processing Development; Final Report AFTAC Project No. VT/9707, Contract F33657-69-C-1063, Texas Instruments, Incorporated, Dallas, Texas May.

Harley, T. W., 1967, Long Period Signal Waveform Similarity at LASA; ARPA Special Report No. 9, Texas Instruments, Incorporated, Dallas, Texas.

Lacoss, R. T., 1969, A Large Population LASA Discrimination Experiment, Lincoln Laboratory, Technical Note 1969-24, April.

Oliver, J., 1962, A Summary of Observed Seismic Surface Wave Dispersion, B. S. S. A., Vol. 52, No. 1, p 81-86.

Texas Instruments Incorporated, 1964, Array Research Semiannual Technical Report No. 1, AFTAC Project No. VT/4053, Contract AF33(657)-12747, Dallas, Texas, May.

Texas Instruments Incorporated, 1970, Long Period Array Processing Development, Quarterly Reports Numbers 4,5,6,7, AFTAC Project No. VT/9707, Contract F33657-69-C-1063, Dallas, Texas.